Dyer County Seismic and Liquefaction Hazard Maps
(HUD Grant Year One Products)

Chris H. Cramer, Roy B. Van Arsdale, Rene Reichenbacher, David Arellano, Hamed Tohidi,
Shahram Pezeshk, Stephan P. Horton, Roshan Bhattarai, Nima Nazemi, and Ali Farhadi

Abstract

A five-year seismic and liquefaction hazard mapping project for five western Tennessee counties began in 2017 under a Disaster Resilience Competition grant from the U.S. Department of Housing and Urban Development to the State of Tennessee. The project supports natural hazard (flood and earthquake) mitigation efforts in these five counties. The seismic hazard maps for Dyer County in northwestern Tennessee were completed in 2020. Additional geological, geotechnical, and geophysical information has been gathered in Dyer Co. to improve the base northern Mississippi Embayment hazard maps of Dhar and Cramer (2018). Information gathered includes additional geological and geotechnical subsurface exploration logs, water table level data collection and measurements, new measurements of shallow and deep shear-wave velocity (Vs) profiles, and the compilation of existing Vs profiles in and around the county. Improvements were made in the 3D geological model, water table model, the geotechnical liquefaction probability curves, and the Vs correlation with lithology model for Dyer Co. Resulting improved soil response amplification distributions on a 0.5 km grid were combined with the 2014 U.S. Geological Survey seismic hazard model (Petersen et al., 2014) sources and attenuation models to add the effect of local geology for Dyer Co. Resulting products are an improved 3D-geology, geotechnical, seismic hazard, and liquefaction hazard models and maps for Dyer Co. Seismic hazard maps at PGA and 1.0 s show a 30-70% decrease in hazard at short periods and a 10-100% increase at long periods compared with USGS NSHMP maps.

Introduction

As part of the 2015 Disaster Resilience Competition, the State of Tennessee received funds from the Department of Housing and Urban Development (HUD) for several grants for flood hazard mitigation efforts. The University of Memphis received one of the grants for flood and seismic hazard mapping efforts in five western Tennessee counties (Figure 1) covering a five-year period starting in 2017. The second-year seismic hazard mapping effort is for Dyer County seismic and liquefaction hazard maps (this report).

The goal for the seismic hazard mapping project is to develop seismic and liquefaction hazard maps for use in flood hazard mitigation efforts in other portions of the HUD grant effort via the University of Memphis. The hazard maps will also be useful for other earthquake hazard mitigation efforts in the five western Tennessee counties.
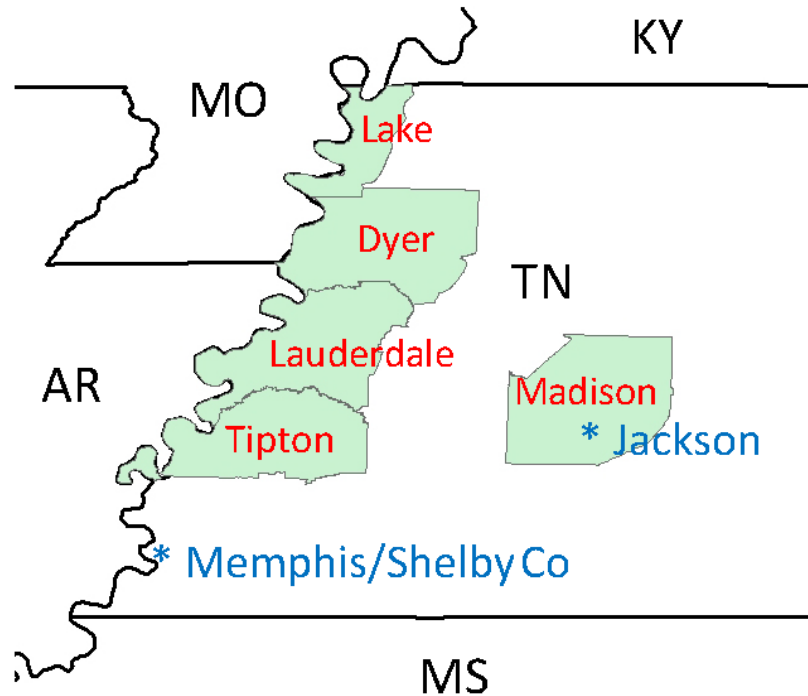
Figure 1: Five western Tennessee counties of the HUD grant supported seismic hazard study. AR – Arkansas, KY – Kentucky, MO – Missouri, MS – Mississippi, and TN – Tennessee.

The major elements to the seismic and liquefaction hazard mapping in this project are (1) geological 3D model development, (2) geotechnical (soil response to ground motions) model development, (3) seismological data gathering, and (4) hazard maps generation. The 3D geological model of sediments above bedrock involves the gathering and interpretation of boring logs, entering geological information into a geographic information system (GIS), and developing maps of the depth to the tops of key geological sediment layers. The accompanying geotechnical model involves the gathering of geotechnical information (sediment properties and water table levels) from boring logs, and modeling liquefaction potential of the shallow sediments. Seismological data gathering includes collecting published sediment velocity profiles with depth, and making new measurements of sediment velocity with depth in the study area. The final step is to integrate the geological, geotechnical, and seismological data into a county wide hazard model and maps that included the effects of local geology (sediments).

Geological Model

Introduction

Dyer County in western Tennessee was mapped as part of a five-county earthquake hazard mapping program (Figure 2) (Cramer et al., 2018; Weathers and Van Arsdale, 2019). Located immediately east of the New Madrid seismic zone, Dyer County is vulnerable to both earthquake ground shaking and liquefaction in the event of future large earthquakes (Chiu et al., 1992; Cramer, 2006; Csontos and Van Arsdale, 2008; Cramer and Boyd, 2014; Cramer et al., 2018a and b).

The topography of Dyer County consists of lowland floodplains of the Mississippi, Obion, and Forked Deer rivers and loess covered terraces of these rivers (Figure 3). Beneath the near-surface geology are Eocene (~34 Ma) sediments that overlie older Paleogene, Late Cretaceous, and Paleozoic strata (Hardeman, 1966; Weathers and Van Arsdale, 2019). Structurally, the county overlies Cambrian age Reelfoot rift faults (Csontos et al., 2008), which have Quaternary reactivation in adjacent Obion, Lake, and Lauderdale counties (Figure 4) (Kelson et al., 1996; Cox et al., 2001; 2006; Weathers and Van Arsdale, 2019). The surface and subsurface geology of a region influences how the landscape will react during a large earthquake. In this study we present geologic maps of Dyer County that provide important information for companion seismologic and liquefaction hazard modeling studies.

Methods

Subsurface lithologic boring logs were acquired from North American Coal Company, US Army Corps of Engineers, Tennessee Department of Transportation, petroleum exploration wells, Tennessee Department of Environmental Control, and the Center of Applied Earth Science and Engineering Research at the University of Memphis. The lithologic boring logs were geologically interpreted and recorded in Excel Spread sheets. A Lidar based 1-meter digital elevation model (DEM) of Dyer county was the base map upon which surface and near-surface geology was mapped from 1,115 bore holes (Figure 2). River terraces along the Obion and Forked Deer rivers in Figure 3 were derived from previously published maps (Saucier, 1994; Rodbell, 1996). Deep bedrock mapping was conducted down to the top of the Paleozoic strata, which is at an average depth of 700 m below Dyer County.

The top of the Eocene was mapped using 968 borings. The contact between the fine-grained Eocene sediment and the overlying alluvium is identified by the basal conglomeratic facies of the alluvium. The underlying top of the Cretaceous and top of the Paleozoic were mapped primarily from DOW Chemical seismic reflection lines (e.g. Figure 4B) (Parrish and Van Arsdale, 2004) and a few oil-exploration wells.

Structure contour maps were made of the elevation of the tops of the Eocene, Cretaceous, and Paleozoic beneath Dyer County and within a boundary zone (Figs. 5A-7A). These maps were

made using the Natural Neighbor contouring algorithm. Bedrock faults have been mapped beneath Dyer County (Parrish and Van Arsdale, 2004; Martin and Van Arsdale, 2017). These previously mapped faults (Figure 4) and their extensions in Dyer County were used in our mapping to produce faulted structure contour maps of the tops of the Eocene, Cretaceous, and Paleozoic using the Spline with Barriers contouring algorithm (Figs. 5B-7B).

Isopach (unit thickness) maps were made of the Lowland river floodplain alluvium and the silt/clay uppermost portion of the floodplain alluvium (Figure 8).

Results

Near Surface Geologic Map

The near-surface geology of Dyer County was geologically differentiated into three mapping units (Lowlands, Intermediate, Uplands) that differ in their elevation and near-surface geology (Figure 3). The Figure 3 cross section does not represent a particular place on the map but is a general depiction of the near-surface geology. Unit surface elevations and unit thicknesses in Figure 3B are averages from values measured throughout the county.

The Lowlands are at an elevation of < 82 m and consists of Holocene (< 12 ka) river floodplain alluvium (Saucier, 1994; Rittenour et al., 2007). In general, the alluvium consists of surface silt and clay overbank sediment that overlies laterally accreted sand and gravel sediment. Between elevations of 82 m and 107 m are the Intermediate units. Intermediate units are differentiated into river terraces of the Obion and Forked Deer rivers and areas where loess (wind-blown silt) overlies Eocene strata. The terraces have been mapped from topographically highest to lowest as the Humboldt, Hatchie, and Finley terraces (Saucier, 1987; Rodbell, 1996). All Intermediate units are covered with Peoria loess that is less than 20 ka. Except for the Finley terrace, the rest of the Intermediate surfaces have older loess units beneath the Peoria loess (Rodbell, 1996) that have not been mapped in this study because our data do not provide this information. Beneath the loess, the terrace strata consist of silt and clay overbank sediment and underlying laterally accreted sand and gravel sediment that is ~ 22 ka (Finley) and > 65 ka (Hatchie and Humboldt). The Upland unit is at an elevation > 107 m and is a loess-covered high-level terrace of the ancestral (~ 3.6 Ma) Mississippi/Ohio river system (Van Arsdale et al., 2007; Odum et al., in review). This high-level terrace alluvium, called the Upland Complex, consists of sand and gravel that is regionally a major source of aggregate (Van Arsdale et al., 2012; Lumsden et al., 2016).

The area mapped as uplifted floodplain in Figure 3 is 1-2 m higher than the adjacent Lowlands alluvium. It may be a low-level Pleistocene terrace of the Mississippi River or it could have been tectonically uplifted by Holocene displacement on the Lake County uplift (Figure 4).

Structure Contour Maps

The top of the Eocene strata is presented as an un-faulted surface and as a faulted surface (Figure 5). There is a lot of subsurface relief on the top of the Eocene because the Eocene has been eroded by the Mississippi, Obion, and Forked Deer rivers and because it has undergone structural deformation. When inserting the bedrock faults into this data set and contouring it with the Spline with Barriers contouring algorithm, fault displacement is apparent. Two structures are visible in the top of the Eocene structure contour maps. The Lake County uplift and its Tiptonville dome culmination appear to pass from Obion County into Dyer County and underlie Dyersburg. East of Dyersburg is a southwest-trending depression in the top of the Eocene that may be a paleochannel or more likely a graben that formed during post-Eocene reactivation of the eastern faults of the Reelfoot rift (Figure 4).

The less well constrained tops of the Cretaceous strata and Paleozoic strata were contoured without faults (Figures 6A and 7A). These surfaces slope westerly. When inserting the faults, the tops of Cretaceous and Paleozoic reveal fault displacements (Figures 6B and 7B).

Isopach Maps

The Quaternary floodplain alluvium, in general, consists of two layers. A surface silt and clay layer that averages 8 m thick and an underlying sand and gravel layer that averages 30 m thick. The isopach map of the thickness of the entire Quaternary floodplain alluvium reveals variation in thickness due to rivers of different sizes and scour depths (Figure 8A). Thickness of the uppermost silt and clay layer is also variable (Figure 8B).
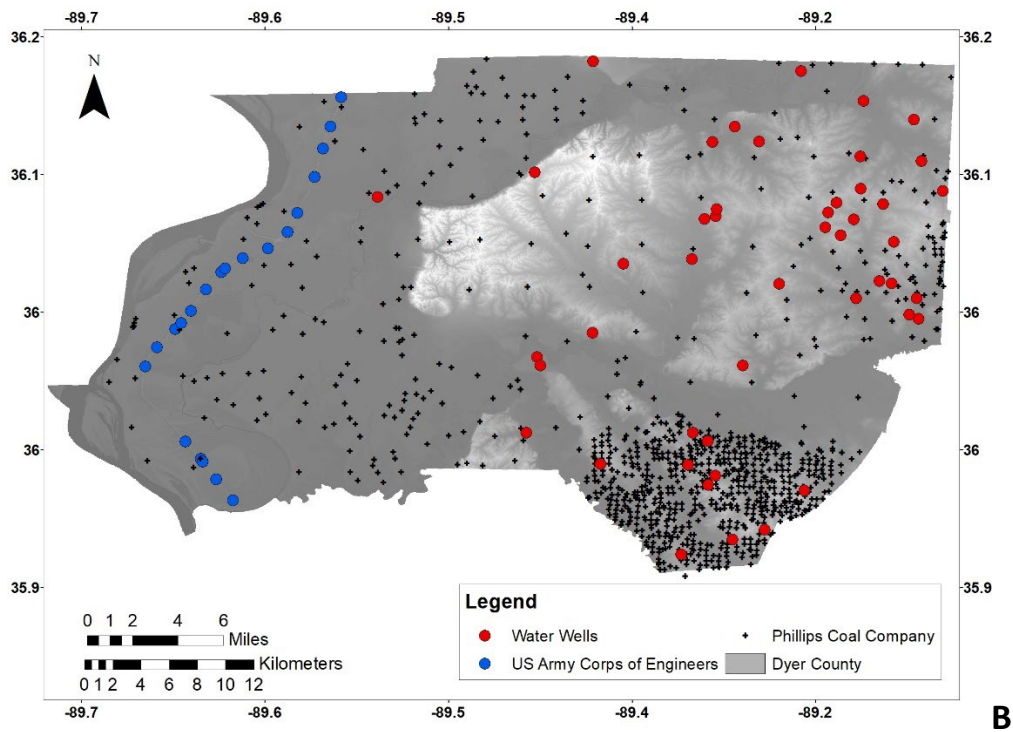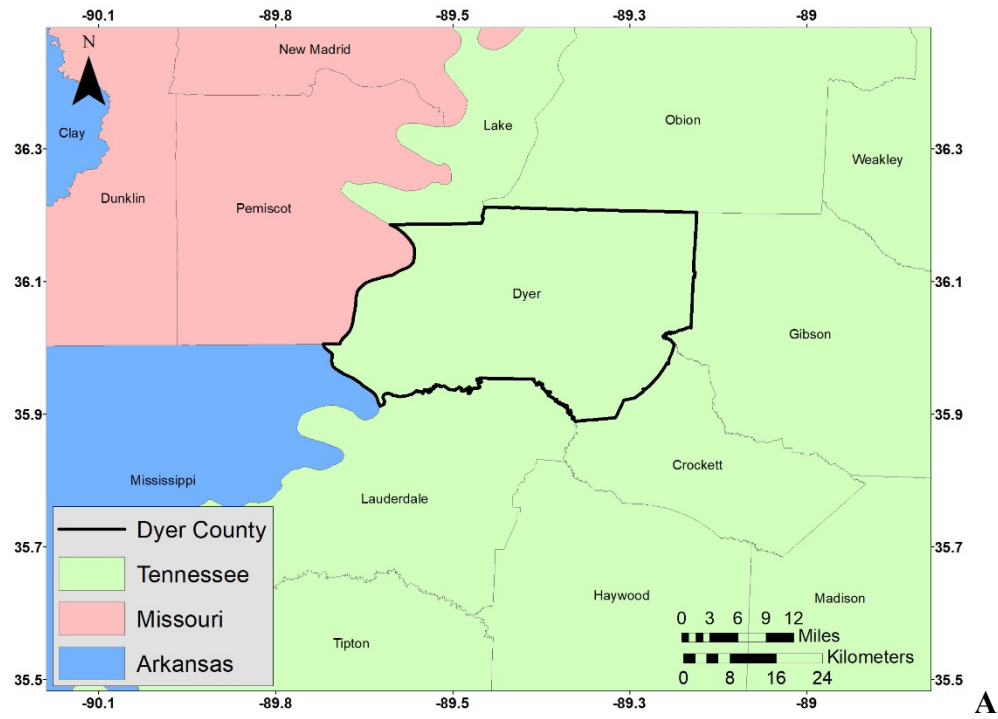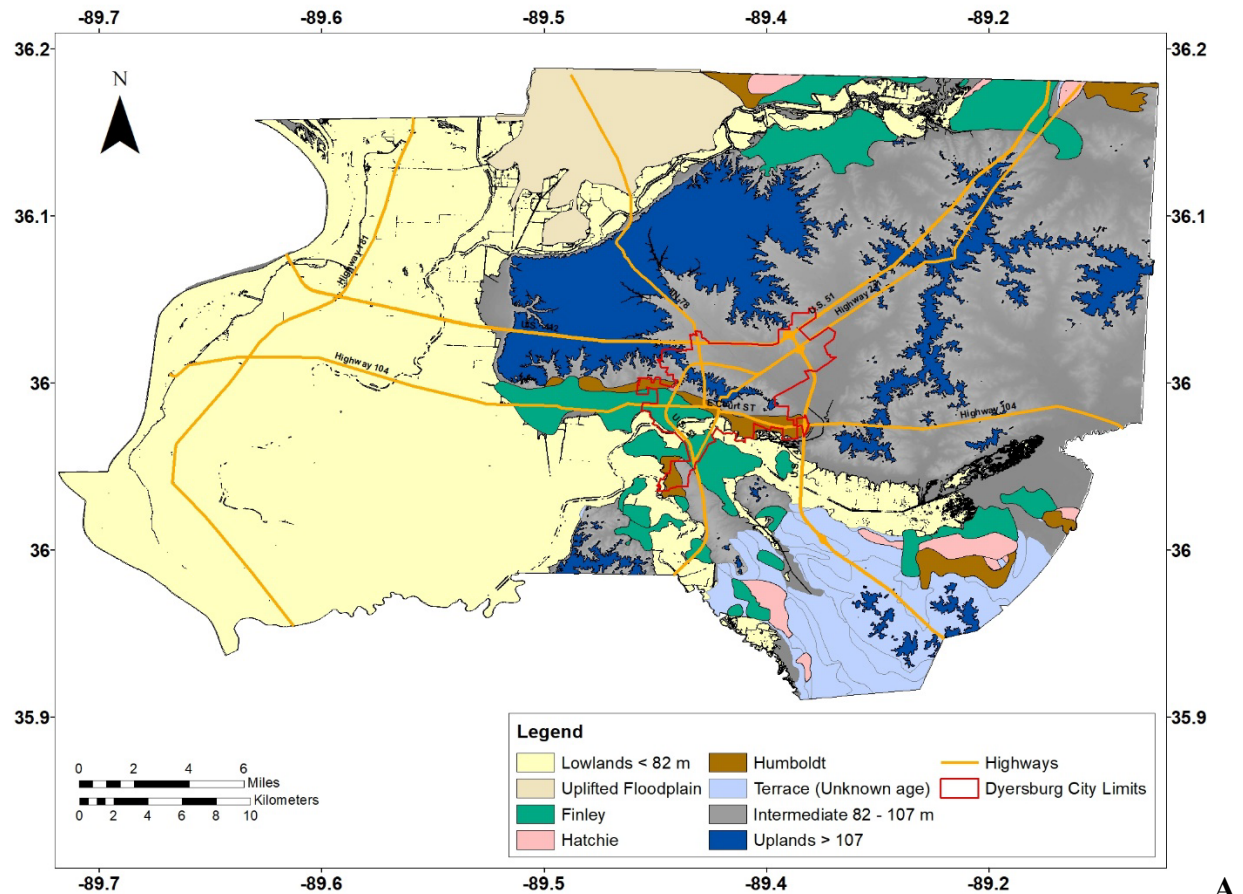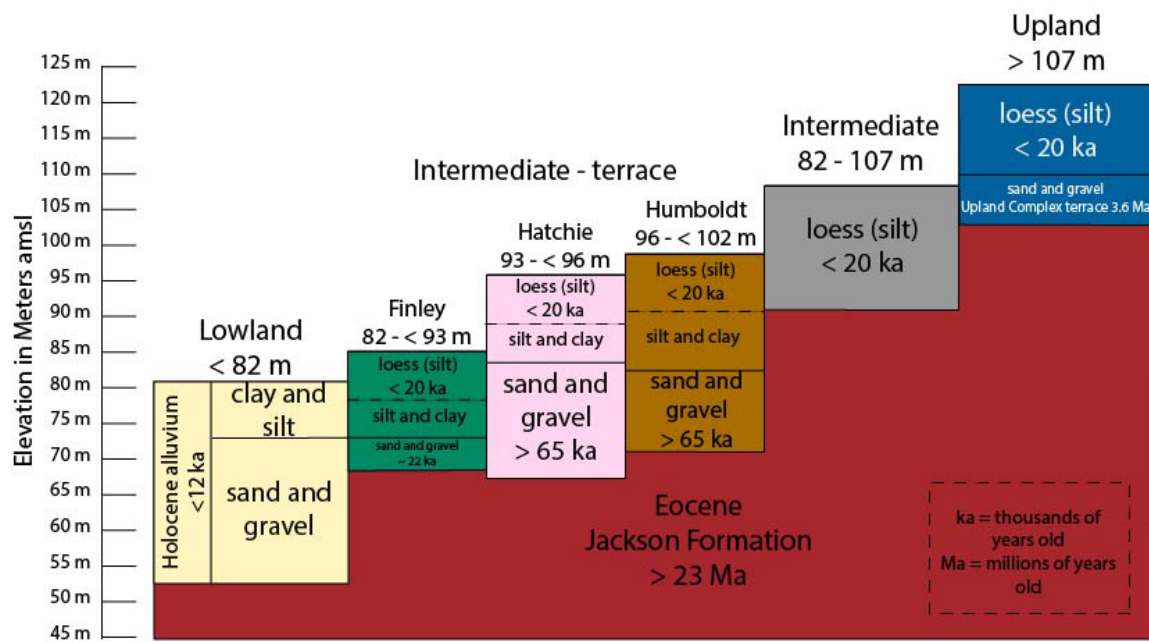
Figure 2: A) Dyer County in western Tennessee in bold. B) Dots show 1,014 geologic drill holes used in surface mapping of Dyer County.

Figure 3: A) Geologic map of Dyer County. B) General geologic cross section illustrating the near-surface geology beneath the Lowland, Intermediate, and Upland surfaces in Dyer County.
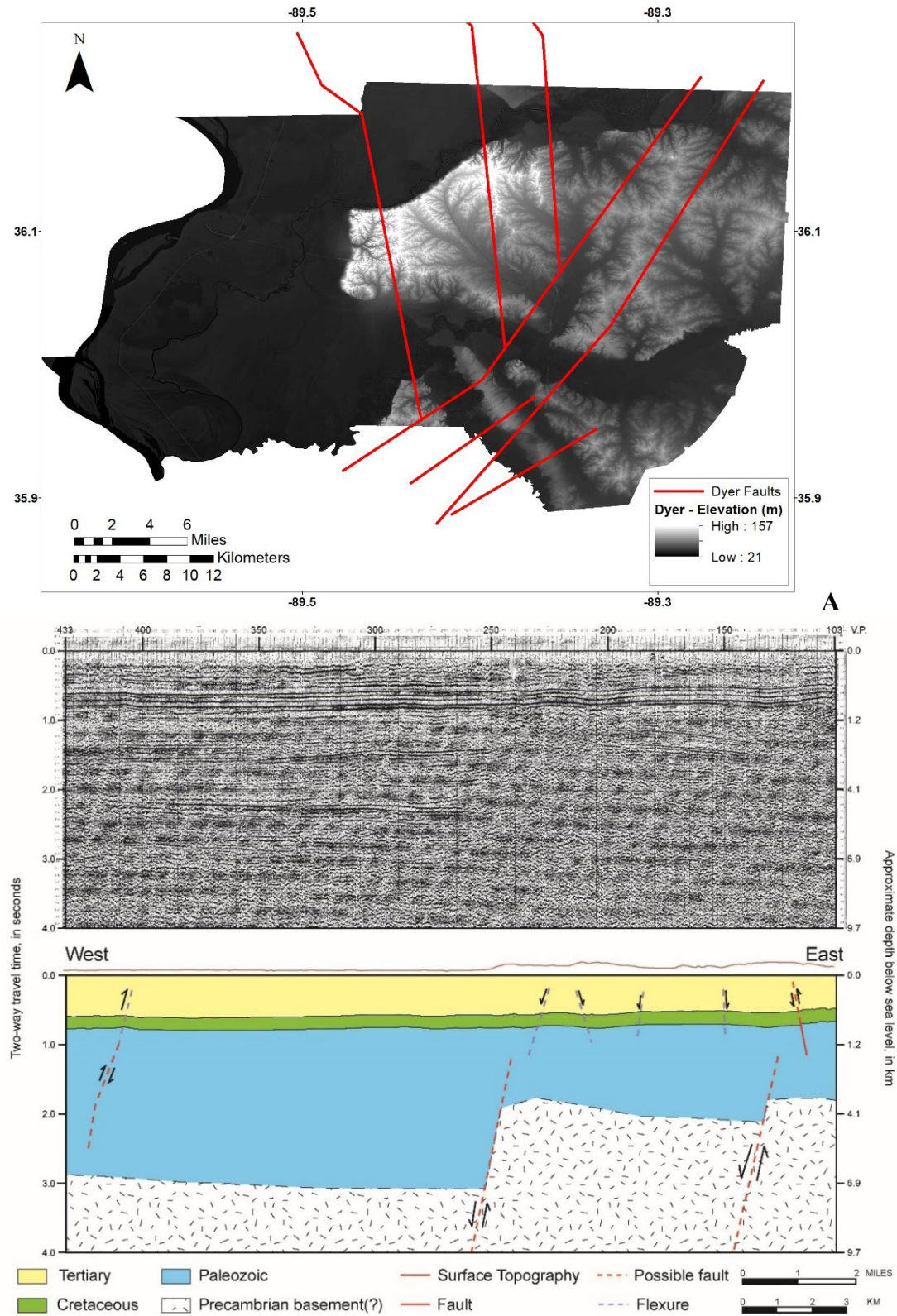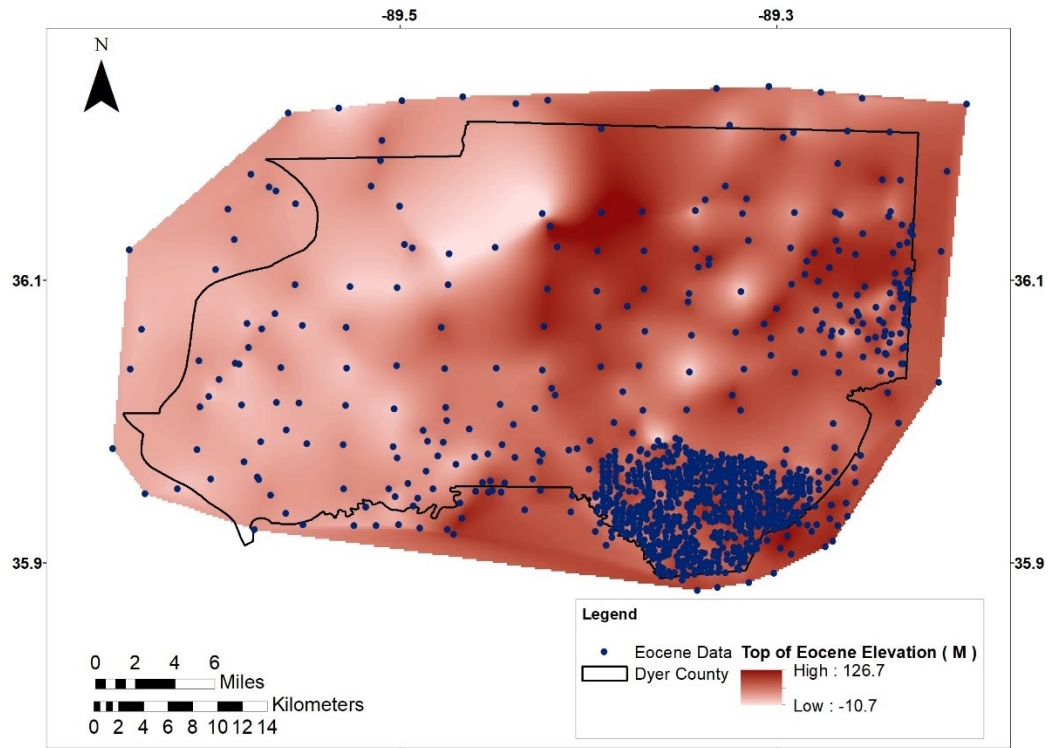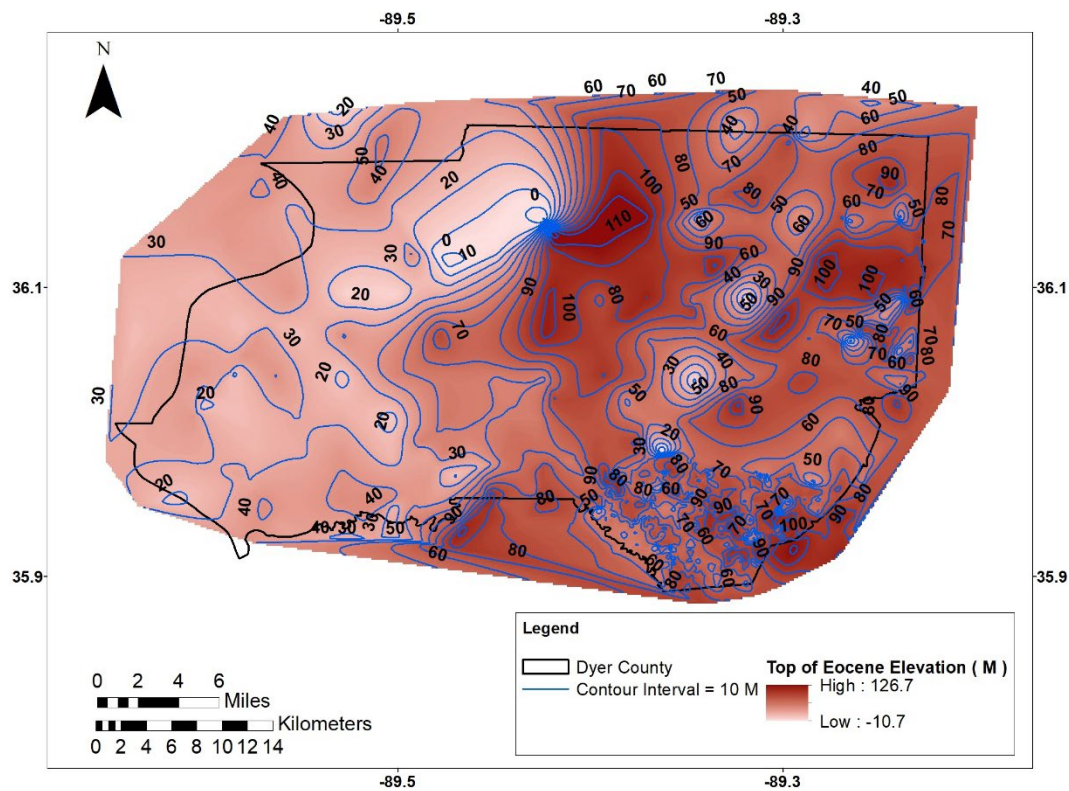
Figure 4: A) Faults mapped in the subsurface of Dyer County. B) Example of a seismic line and its interpretation used in fault mapping.
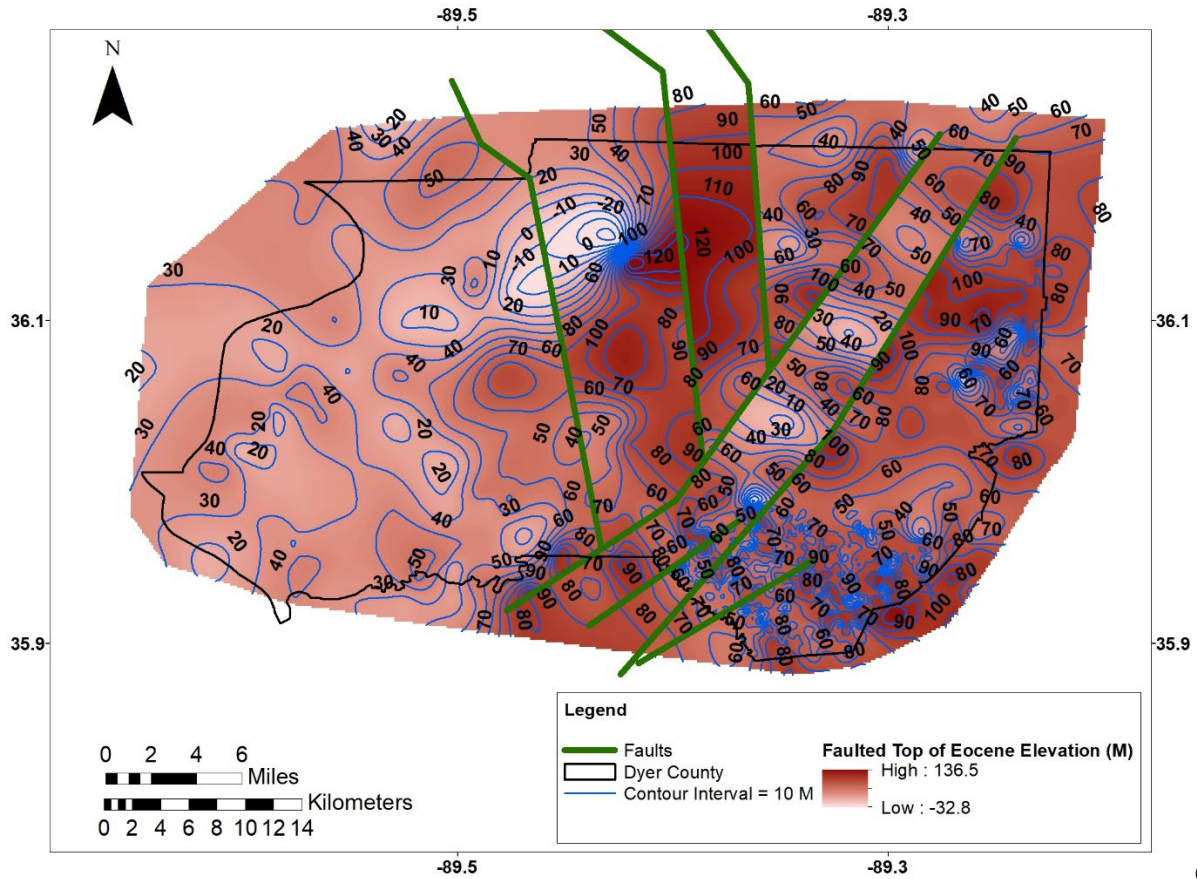
A

B

9

Figure 5: A) Top of Dyer County Eocene with drill hole locations as dots. (B) Un-faulted and (C) faulted structure contour maps of the top of the Eocene strata in Dyer County.
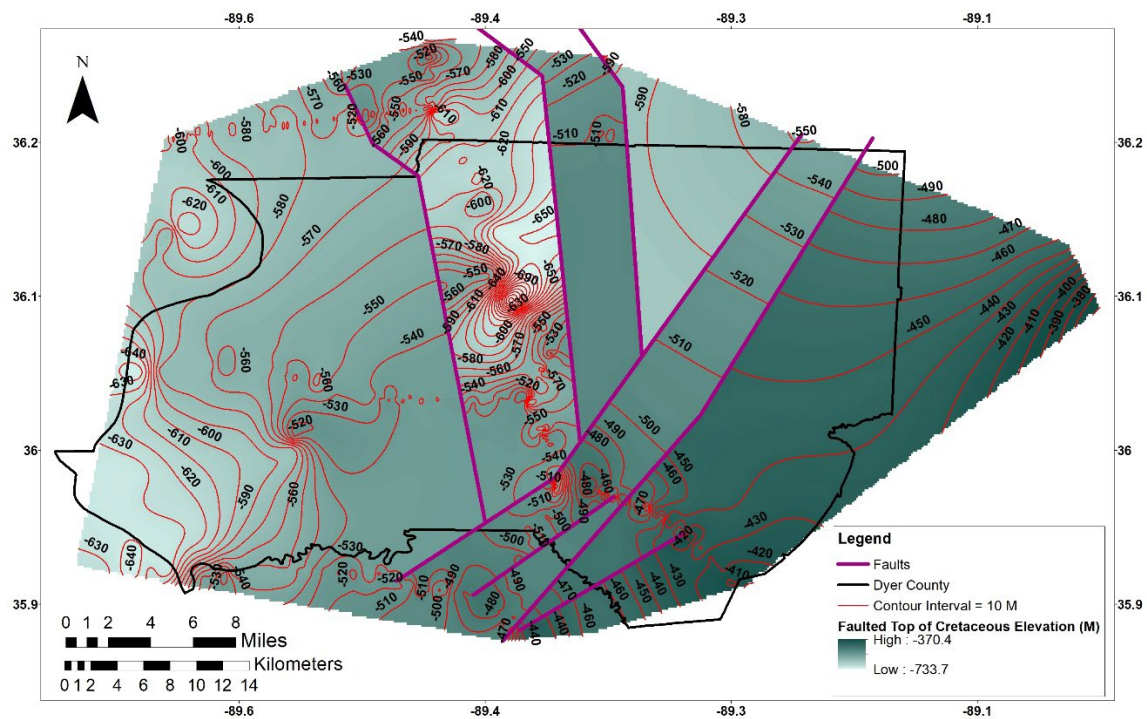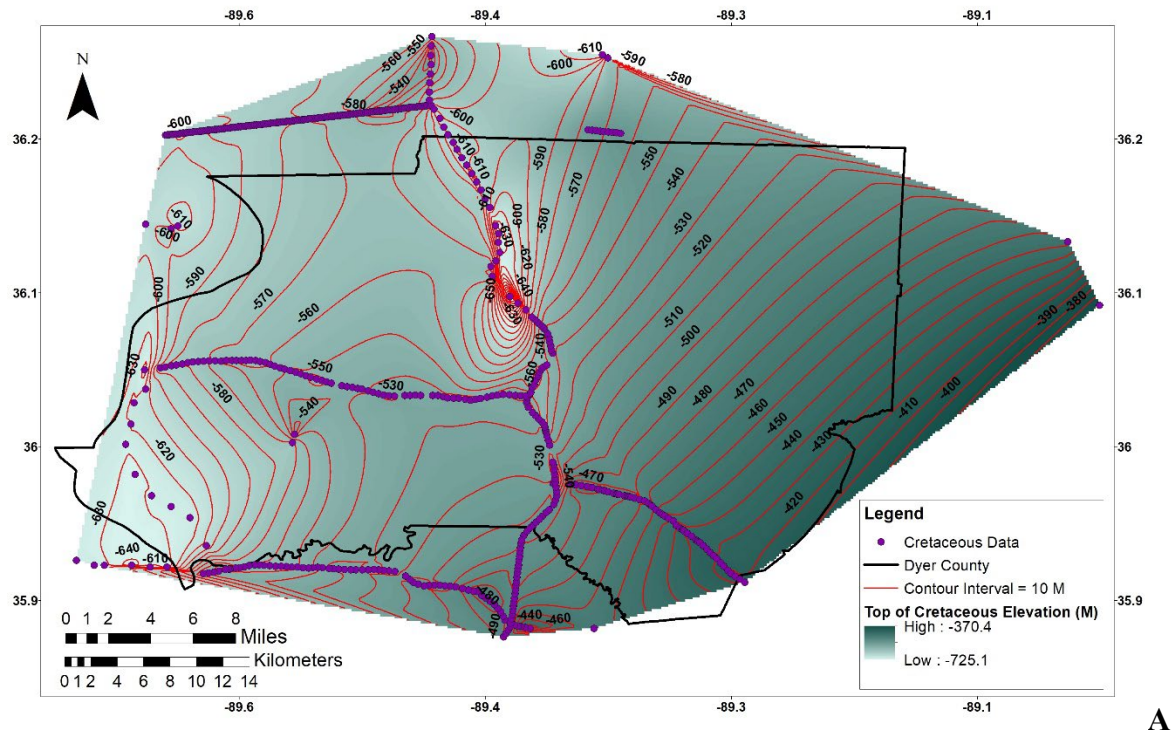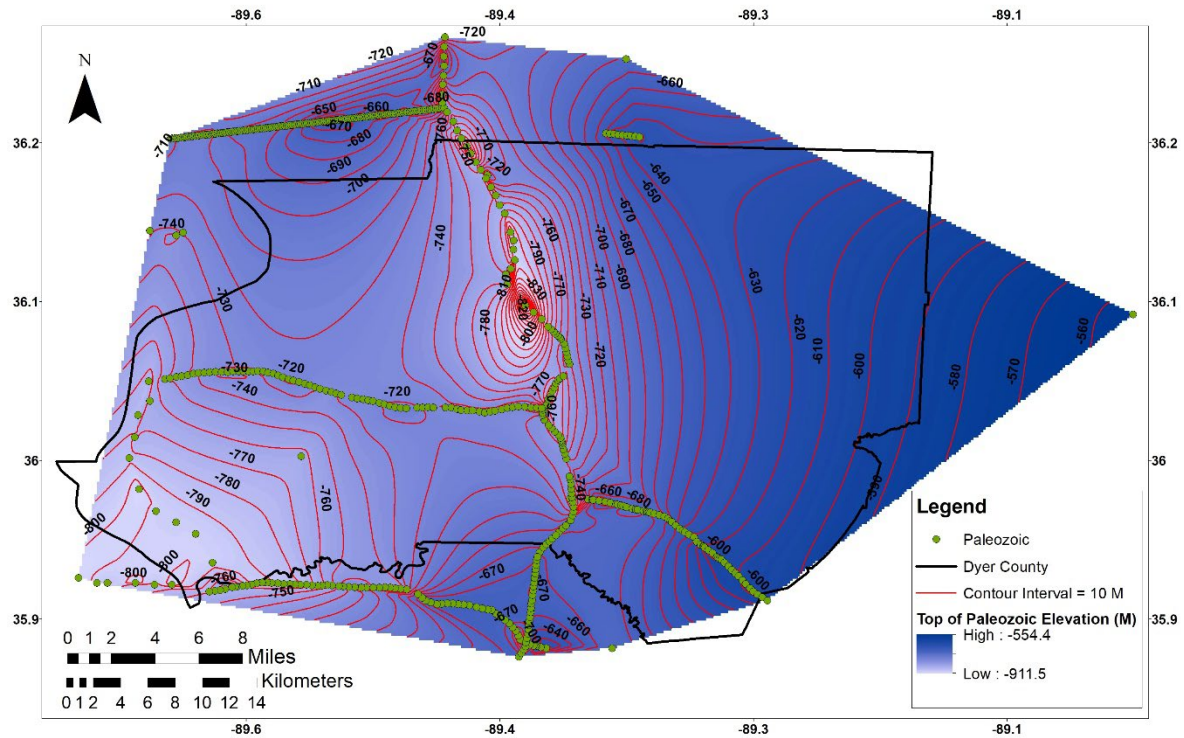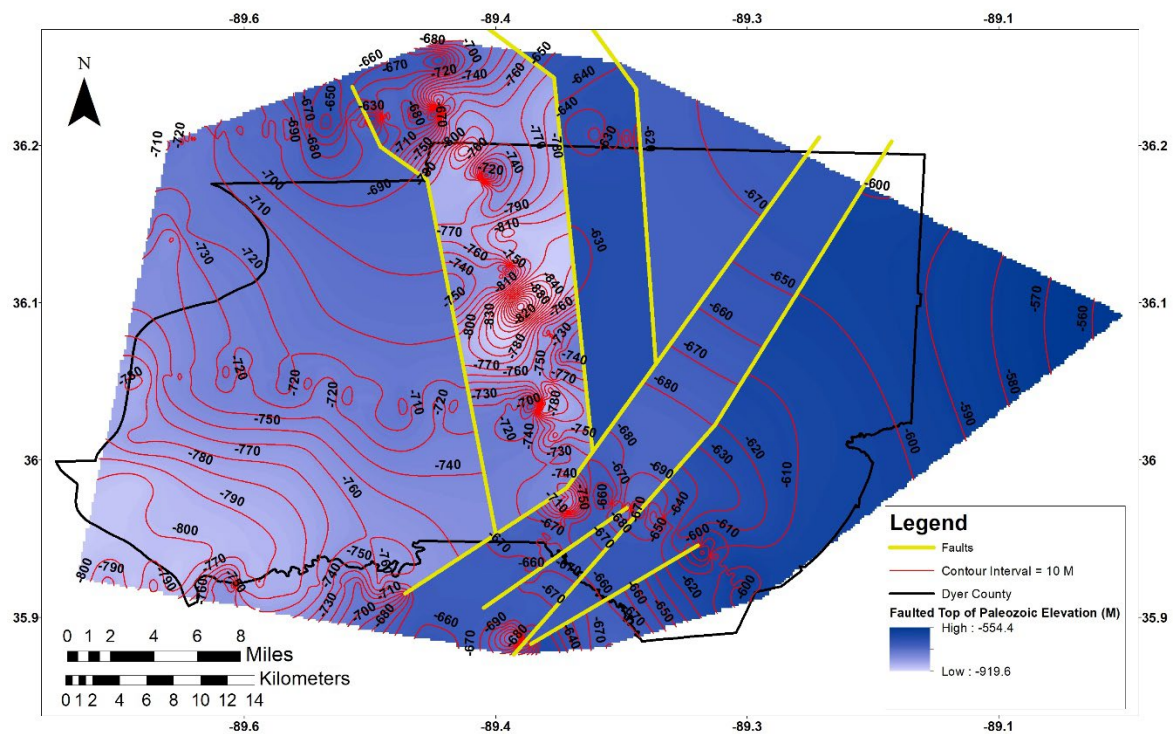
Figure 6: Un-faulted (A) and faulted (B) structure contour maps of the top of the Cretaceous strata in Dyer County with dots illustrating seismic reflection shot points and drill holes used to make the map.

Figure 7: Un-faulted (A) and faulted (B) structure contour maps of the top of the Paleozoic strata in Dyer County with dots illustrating seismic reflection shot points and drill holes used to make the map.
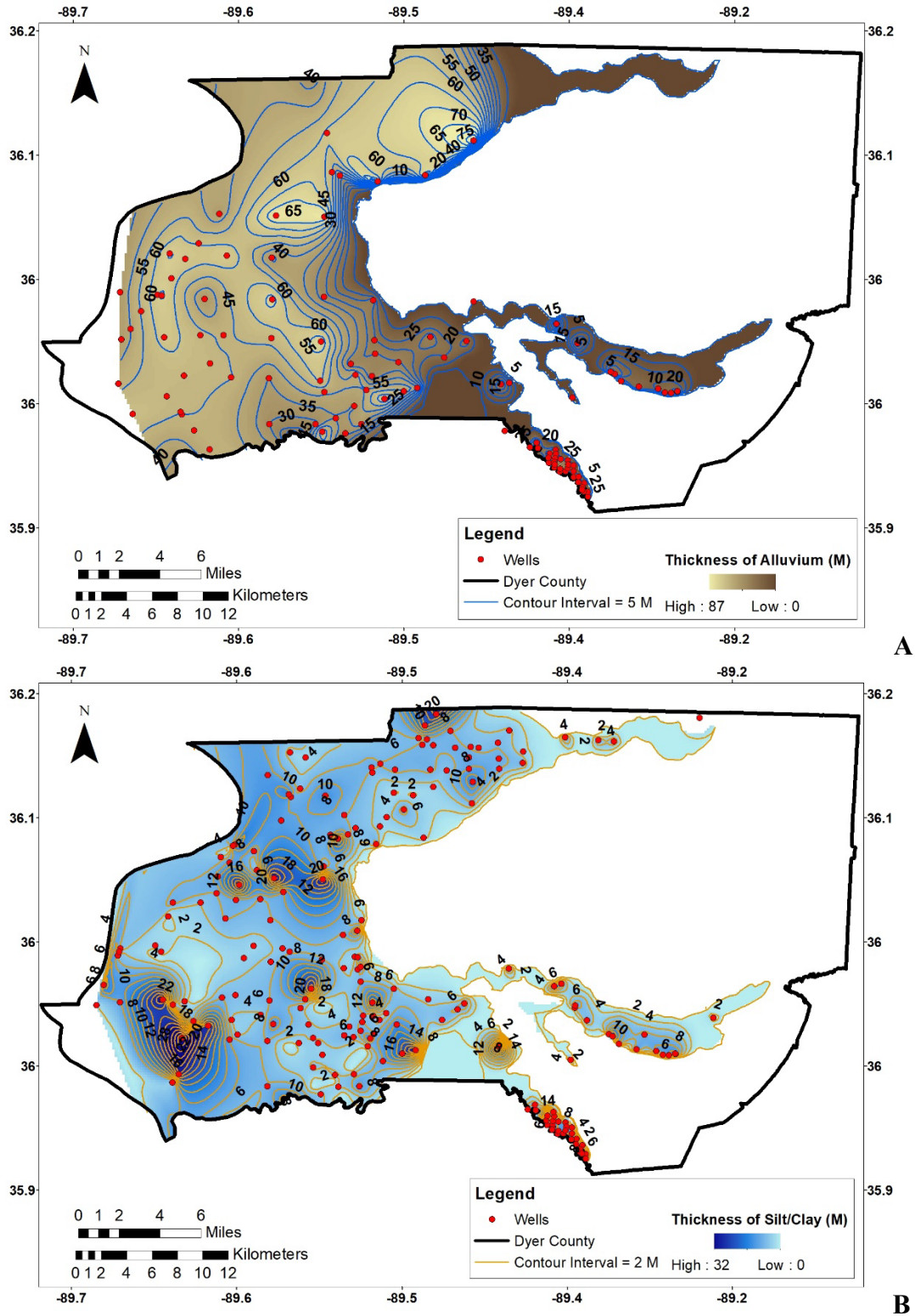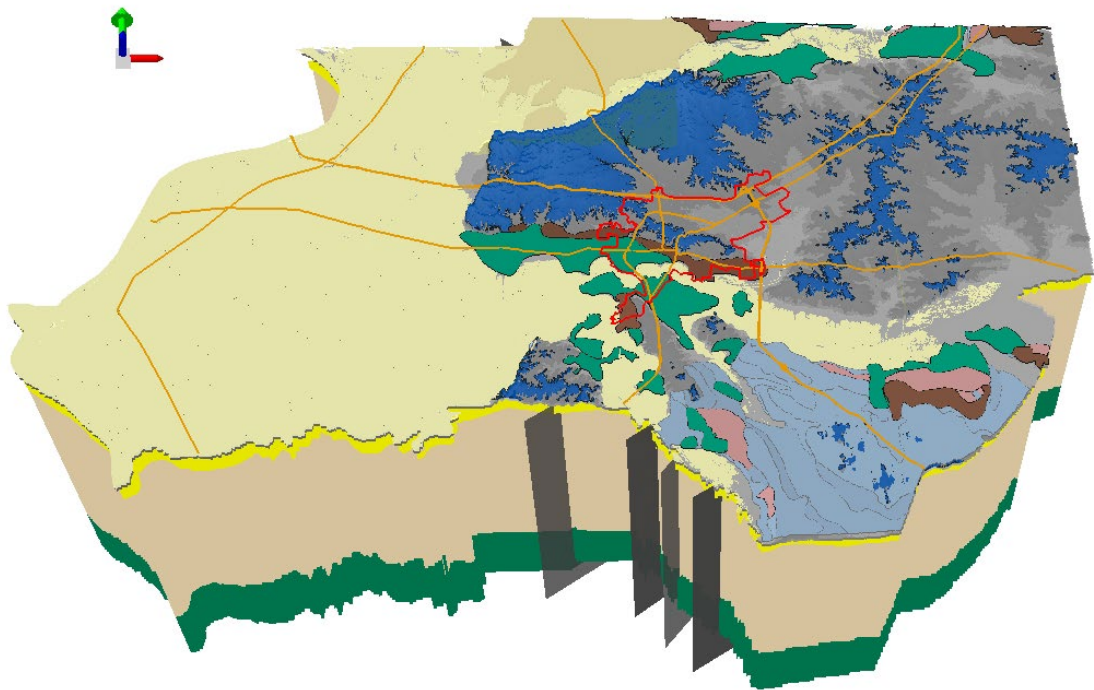
Figure 8: A) Isopach of the Quaternary alluvium in Dyer County. B) Isopach map of the uppermost silt and clay portion of the Quaternary alluvium in Dyer County.
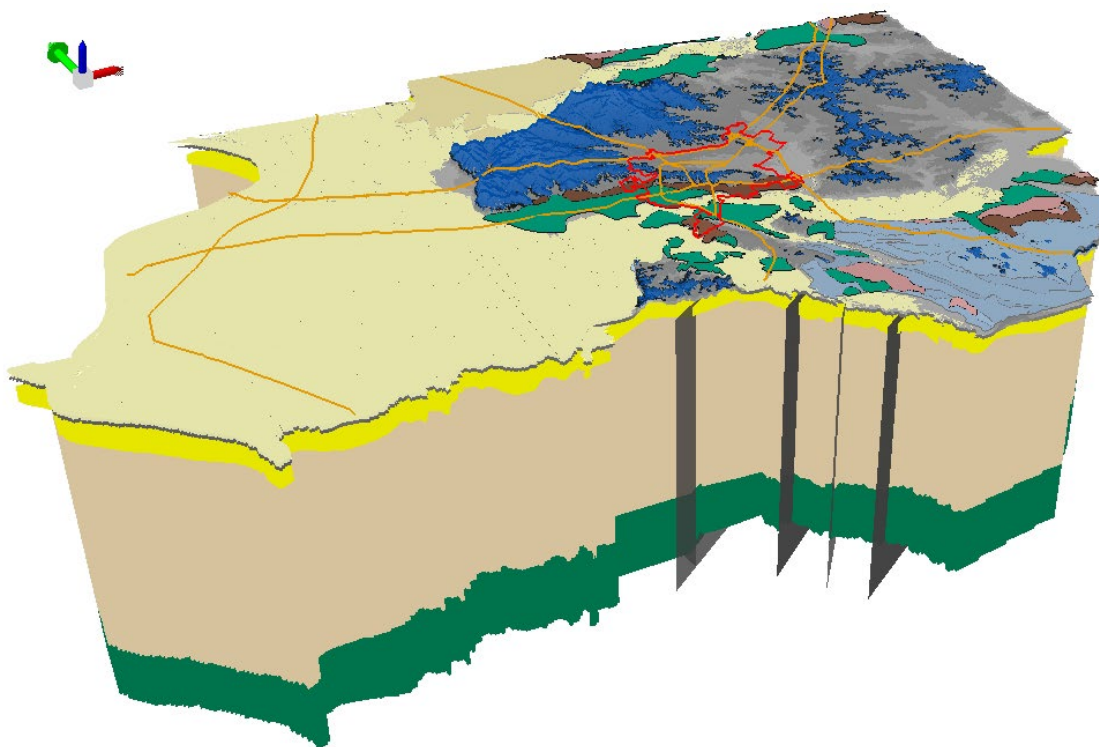
Geological Summary

The near-surface geology reveals the incision of the ancestral Mississippi/Ohio river system through time. Approximately 3.6 Ma the ancestral Mississippi/Ohio river system (Upland Complex) flowed across a vast floodplain surface that extended beyond Dyer County (Van Arsdale et al., 2007; Cupples and Van Arsdale, 2014; Cox et al., 2014). Incision through the Upland Complex throughout the lower Mississippi/Ohio river system began in the early Pleistocene with growth of continental ice sheets and resultant lower sea levels (Saucier, 1994; Van Arsdale et al., 2007). During the Pleistocene, up to four layers of loess were deposited in western Tennessee (Markewich et al., 1998). In Dyer County, Rodbell (1996) identified Peoria loess (< 20 ka) covering the Upland and Intermediate surfaces with underlying Roxanna silt (loess) that is > 65 ka on top of the floodplain alluvium of the Humboldt and Hatchie terraces. Based on these observations in Dyer County we know the ancestral Mississippi/Ohio river system and its tributaries entrenched > 65 ka because the Humboldt terrace alluvium is overlain by the > 65 ka loess (Figure 4). Subsequently, the Mississippi/Ohio river system and its tributaries further intrenched to form the Hatchie (also > 65 ka) and then Finley (~ 22 ka) terrace levels. The final entrenchment of the Mississippi River and its Obion and Forked Deer river tributaries in Dyer County occurred within the last 22 ka resulting in most of the Lowlands being underlain by floodplain alluvium that is < 12 ka.

Structures underlying Dyer County include the Lake County uplift, Tiptonville dome, and the eastern margin of the Reelfoot rift. Each of these structures have been active post 34 Ma since they appear to displace the top of the Eocene. Whether they have Quaternary fault displacement in Dyer County requires further research, but it must be noted that the Tiptonville dome in adjacent Lake County (Kelson et al., 1996; Greenwood et al., 2016; Weathers and Van Arsdale, 2019) and a fault within the eastern margin of the Reelfoot rift in adjacent Lauderdale (Porters Gap fault) and Obion (Union City fault) counties have Quaternary displacement (Cox et al., 2001; 2006).

Surface and subsurface geologic mapping of Dyer County has provided insight into the three-dimensional geology (Figure 9) and the Quaternary geologic history of the county. Of importance to the county's earthquake hazards are the seismic velocity structure of the underlying geologic strata, the recurrence intervals of Reelfoot rift faults (Tuttle et al., 2002), and the liquefaction potential of the Holocene floodplain sediments of the Mississippi, Obion, and Forked Deer rivers.
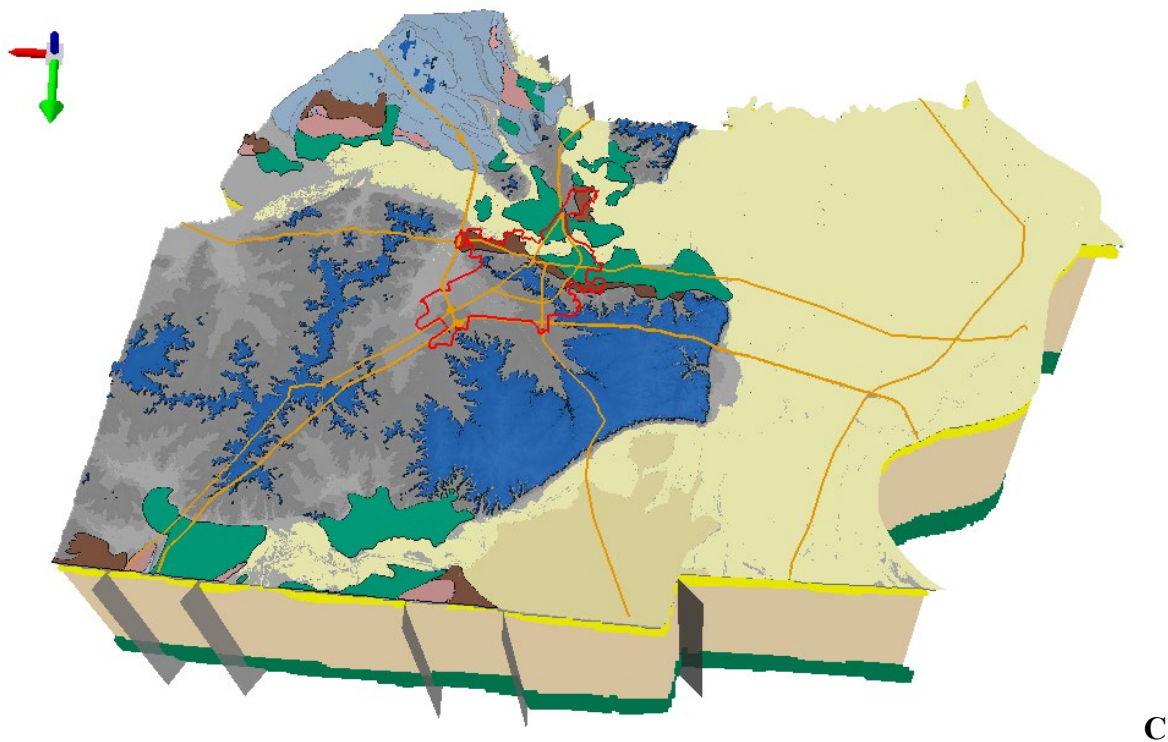
A

B

C

Figure 9: Three-dimensional model of Dyer County subsurface geology looking north (A), northeast (B), and south (C). Also see attached animation of the 3D geology of Dyer County (Appendix).

Geotechnical Model

Introduction

A summary of the geotechnical engineering analyses performed to develop liquefaction probability curves for Dyer County is presented in this section. Background information on the subsurface data collection procedures is initially presented followed by a summary of the methodologies used to generate liquefaction probability curves (LPCs).

Data Collection

The collected subsurface data within Dyer County consisted of Standard Penetration Test (SPT) resistance or "N-value", shear wave velocity (Vs), and groundwater level (GWL) data. The procedure of collecting each set of data is summarized in the next sections.

SPT Data

Soil boring logs containing soil classifications based on Unified Soil Classification System (USCS) and SPT-N values were obtained from the U.S Army Corps of Engineers (USACE) and Tennessee

Department of Transportation (TDOT). Table 1 shows the total number of soil boring logs that were received from each organization.

Table 1: Summary of the total number of borings

Organization	Number of Boring Logs
USACE	993
TDOT	140
Total	1133

USACE SPT Data

Initially, the USACE soil boring logs were selected based on the following selection criteria used in developing the liquefaction probability curves (LPCs) for the Lake County seismic and liquefaction hazard maps (Cramer et al., 2019):
- Borings must be at least 20 m (66 ft) deep.
- Borings must include N-values and USCS classifications to a depth of 20 m (66 ft).
- The boring locations must have latitude and longitude coordinates.

The above selection criteria yielded data only from 30 borings because many boring logs did not include N-values to a depth of 20 m (66 ft). Therefore, to include additional boring data in the development of LPCs, the screening criteria was revised to accept boring logs with most N-values included to a depth of 15 m (50 ft) instead of 20 m (66 ft) based on the following procedure:
- Missing N-values for any depth at a given boring location was estimated by using the same N-value for a given N-value above or below the depth of the missing N-value if the overlying and underlying soil had the same soil classification.
- If the soil layers above and below the layer of missing N-value did not have the same classification or did not have N-value in a given boring, the N-value was extracted from closest boring for the same classification and the same depth as classification and depth of the missing N-value.

The modified boring log screening criteria added 54 boring locations to the 30 boring locations that met the initial screening criteria. Thus, the total number of USACE borings selected for development of LPCs is 84. As shown in Figure 10, most boring locations are along the Mississippi River located along the western edge of Dyer County.
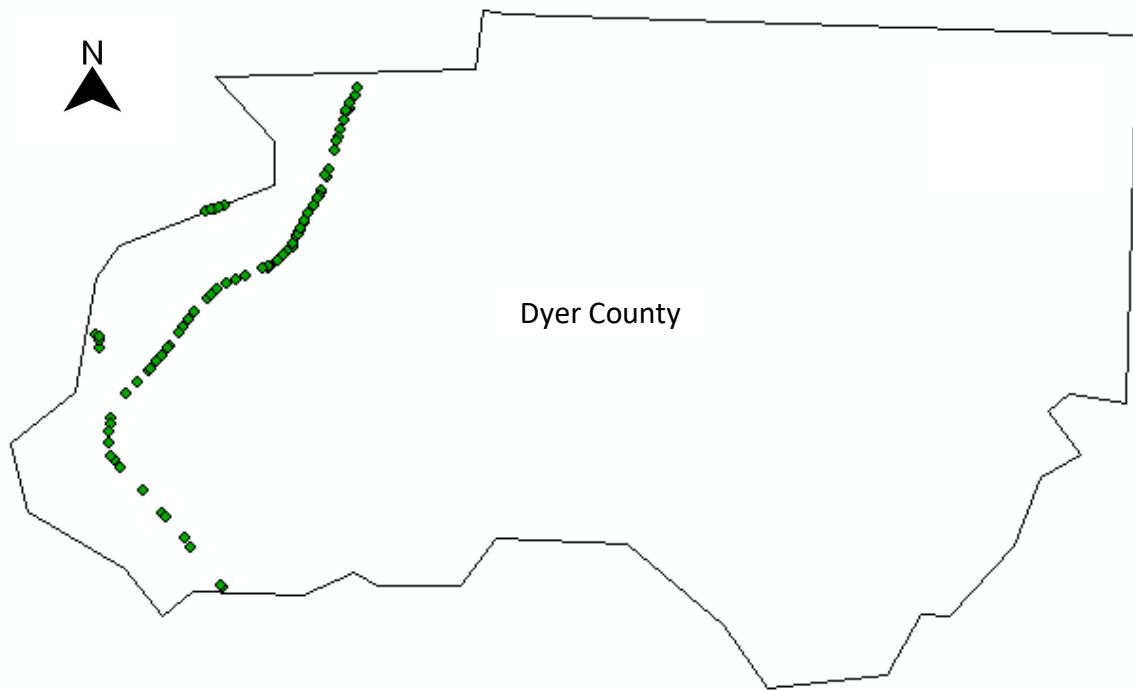
Figure 10: Locations of selected USACE SPT borings.

Dyer county consists of three primary geologic units: lowland, intermediate, and upland. Intermediate includes Terrace, Hatchie, Finley, and Humboldt. Figure 11 shows the distribution of the geologic units and the USACE boring locations in relation to these geologic units. As shown by Figure 11, all 84 USACE boring locations are located within the lowland geologic unit of Dyer County.
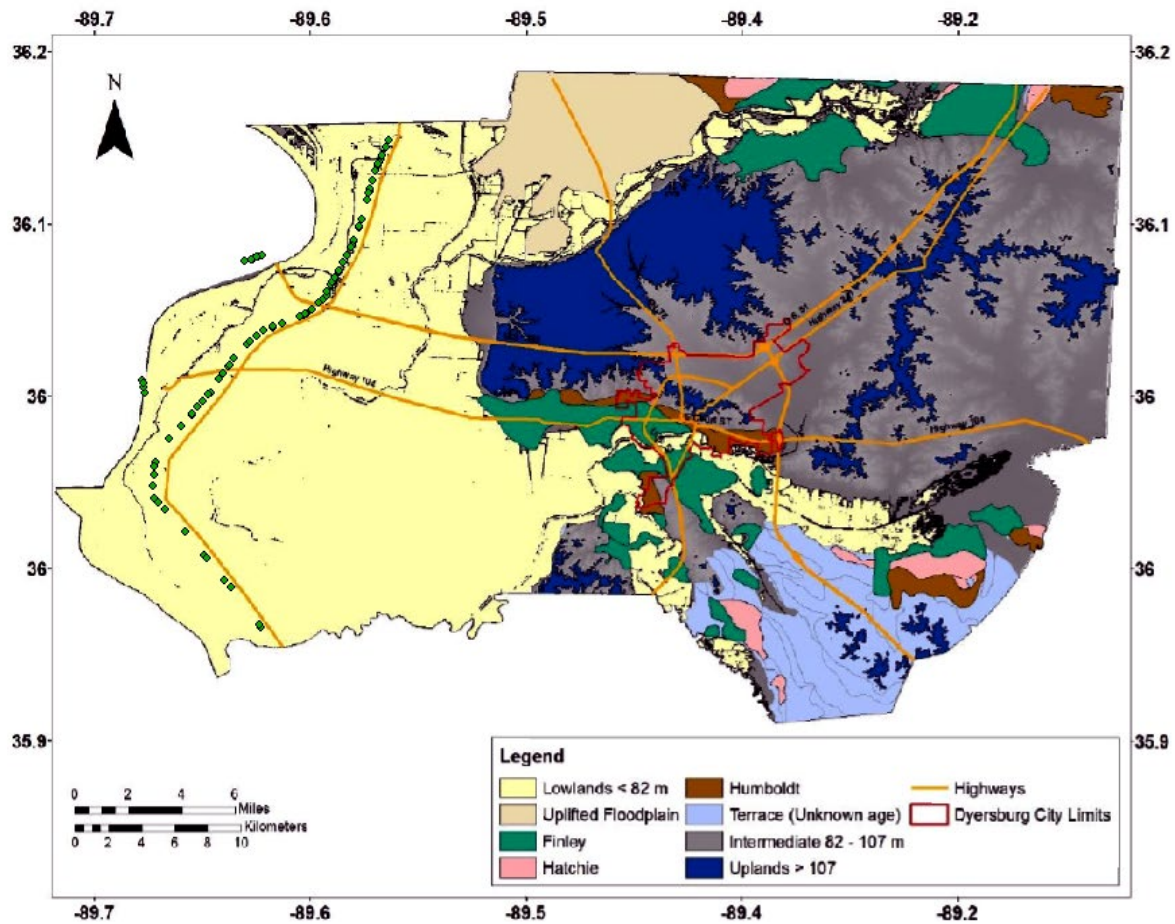
Figure 11: Locations of USACE selected borings on the geology map.

TDOT SPT Data

As shown in Table 1, a total of 140 soil boring logs were received from TDOT. The same screening criteria utilized in the selection of USACE boring logs were used to select TDOT boring logs for use in the development of LPCs. The TDOT boring logs did not provide a coordinate location of where the boring was obtained. We were only provided with a project location map (without scale) or a general project location description. Using Google Earth and Google Map, we estimated the location of the projects and used the project location for all soil borings of a project to find the geologic unit of the borings and to interpolate the GWL of each boring using the GWL contour map described later in this report. Figure 12 shows the 17 TDOT project locations in relation to the distribution of the geologic units of Dyer County.
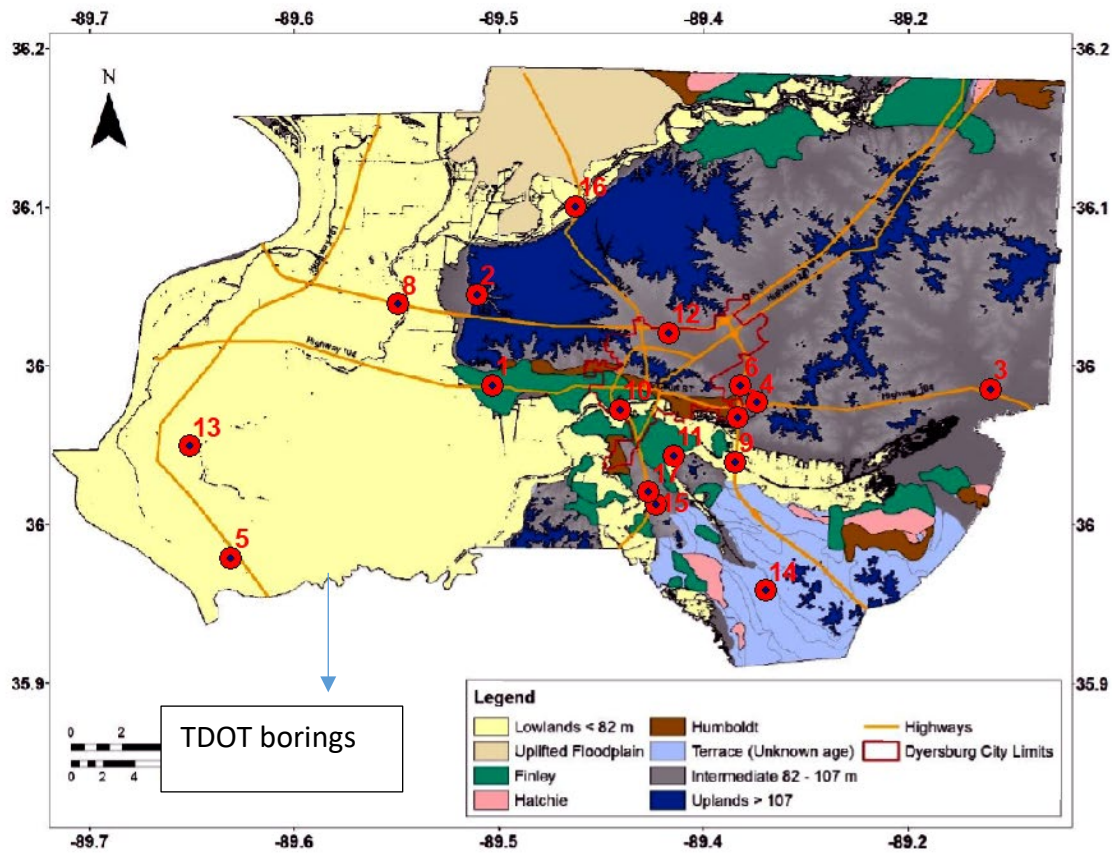
Figure 12: TDOT project locations.

Table 2 provides the distribution of the 54 boring locations in relation to the geologic units for the 17 project locations shown in Figure 12.

Table 2: Summary of the soil borings of TDOT based on geology

Geology	Number of Borings	Project No. on Map
Lowland	34	5-8-9-10-13-16
Intermediate	22	1-3-4-6-7-11-12-14-15-17
Upland	2	2

Table 3 summarizes the total number of borings selected for use in developing LPCs within the Dyer County based on geologic unit.

Table 3: Summary of the total number of SPT borings for each geologic unit

Geology	Organization	USACE	TDOT	Total
Lowland		84	34	118
Intermediate		0	22	22
Upland		0	2	2

Shear Wave Velocity Data

A total of 11 *Vs* profiles with a minimum depth requirement of 20 m (66 ft) were obtained within Dyer County. Figure 13 shows the locations of the *Vs* profiles in relation to the distribution of the geologic units of Dyer County and Table 4 provides the number of *Vs* profiles within each geologic unit type.
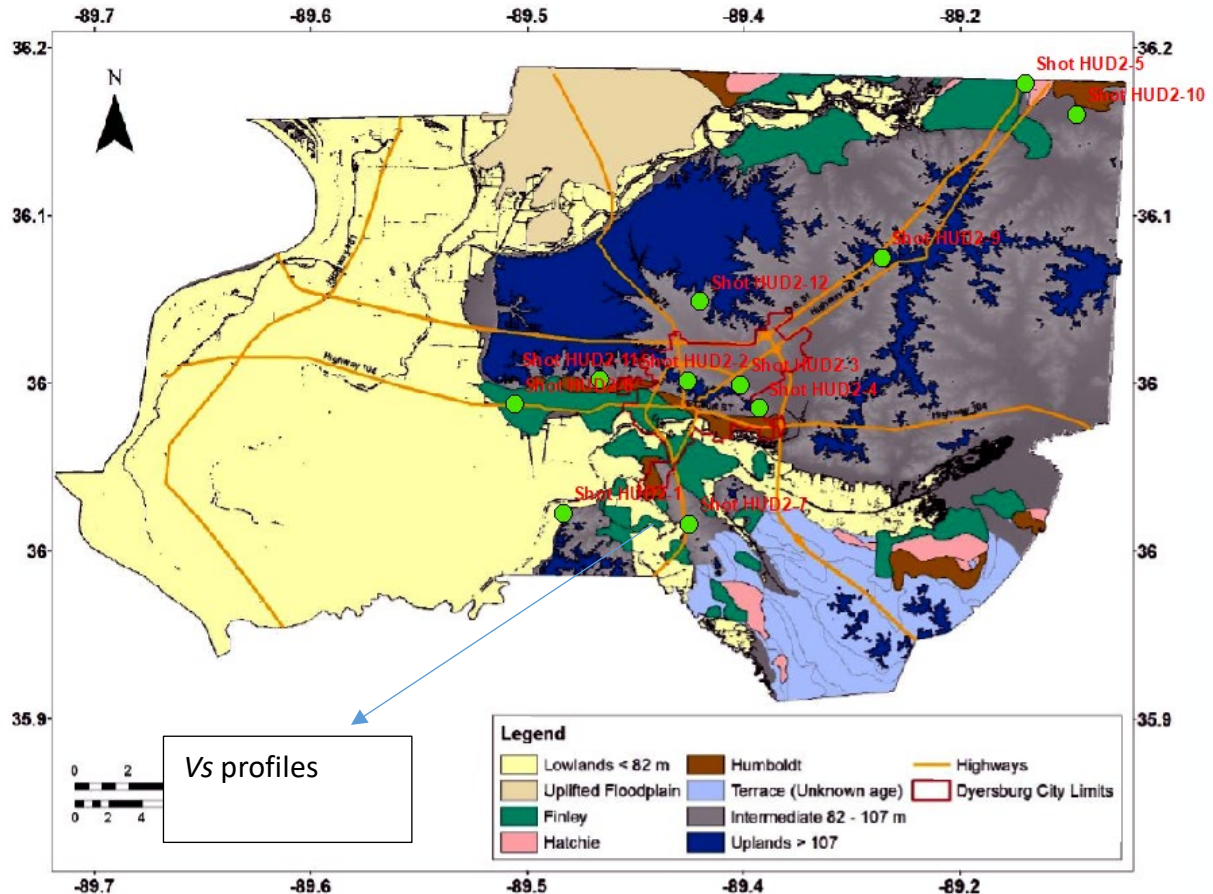

Figure 13: *Vs* profile locations.

Table 4: Summary of the *Vs* profiles based on geology

Geology	Number of *Vs* profiles
Lowland	0
Intermediate	9
Upland	2

Groundwater Data

To develop the GWL contour map of Dyer County, we used a similar procedure we used to develop the water level contour map of Lake County (Cramer et al., 2019). The primary source

of establishing the GWL contour map for Dyer County was the GWL contour map shown in Figure 14 that was developed by Schrader (2008).
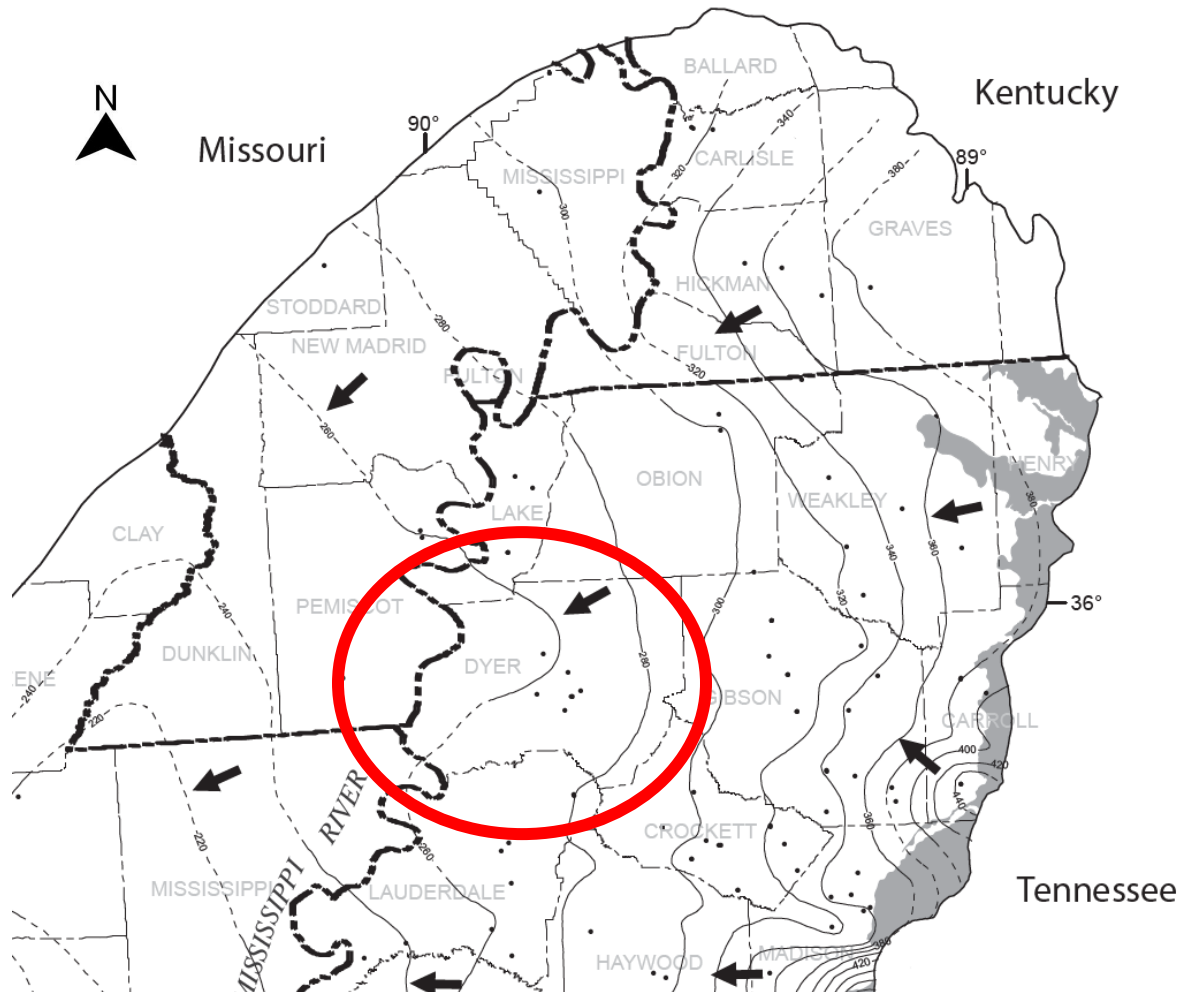

Figure 14: USGS groundwater level contour map (Schrader 2008).

To establish the contour map of Dyer County, we also interpolated the contour lines from Gibson, Lake, Obion, and Lauderdale counties provided by Figure 14. Using ArcMap, we digitized the contour lines on a shapefile boundary of Dyer County and the contour map was developed by the Inverse Distance Weighting (IDW) method. Figure 15 shows the GWL contour map of Dyer County that was used to develop the LPCs.
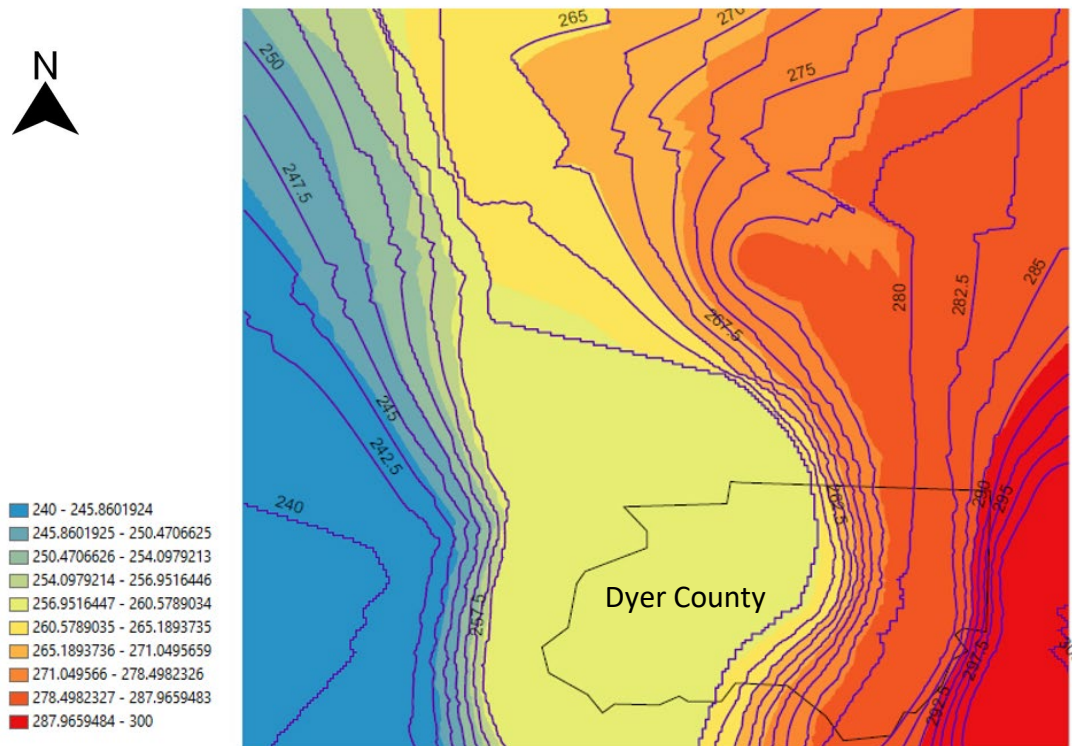
Figure 15: Groundwater level contour map for Dyer County.

We obtained additional groundwater data for eight wells within Dyer County from the United States Geological Survey (USGS) groundwater data website (https://maps.waterdata.usgs.gov). Wells are all periodic, meaning that water levels are recorded in a specific time of a year. As shown in Figure 16, all eight USGS water wells are in the lowest elevation areas of the GWL contour map.
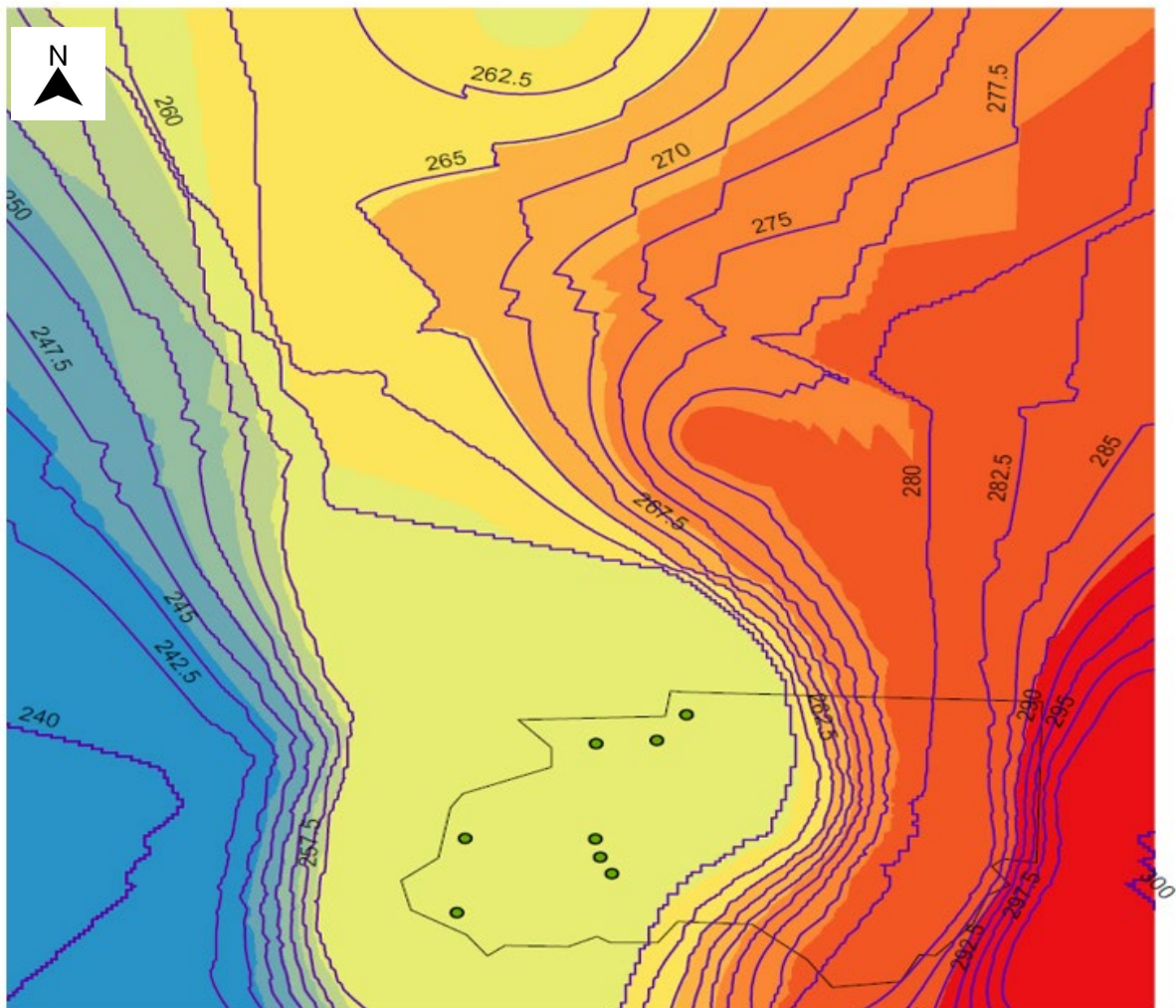
Figure 16: Location of USGS wells on the contour map.

Because the wells had periodic readings and a various number of recorded water level data, we calculated an average of lowest and highest readings of each well. For each USGS well, the GWL was interpolated from the contour map and the interpolated level was compared with the computed average of lowest and highest GWL of each well. As it is provided in Table 5, for four wells the average is slightly higher than the interpolated GWL from the contour map, and for four wells the average is slightly lower than the contour map level for each specific well. We also compared the overall average of lowest and highest readings of wells with overall average GWL obtained from the contour map for wells. As shown by the last row of Table 5, the difference between the average readings of all wells and the average interpolated levels from the contour map is 0.75 ft. (0.2 m).

Table 5: Comparison of contour map level for USGS wells and the average of lowest and highest readings of wells

Well NO.	Average Readings (ft-NGVD of 1929)	Contour Map (ft-NGVD of 1929)	Difference between contour map and wells readings (ft)
1	257	249	8
2	257	258	-1
3	257	255	2
4	257	255	2
5	257	254	3
6	260	268	-8
7	260	265	-5
8	260	267	-7
Overall average	258.125	258.875	0.75

Because there is no water well data available within higher elevation parts of the county, and there is a good agreement between USGS wells data and contour map, therefore, we utilized the GWL contour map shown by Figure 15 to interpolate the GWL at each soil boring location.

Methodologies Used to Develop Liquefaction Probability Curves

We used the same general procedure to develop LPCs that we used to develop the Lake County LPCs (Cramer et al., 2019). The procedure consists of the following three steps:
- Calculating the factor of safety (FS) against liquefaction at a given depth in the soil profile of each soil boring using the simplified procedure (Seed and Idriss, 1971).
- Calculating the liquefaction potential index (LPI) of each soil boring location using the Iwasaki et al. (1978, 1982) method.
- Developing LPCs for the probability of exceeding LPI of 5 and 15 for each primary surficial geologic unit.

We developed the LPCs for Dyer County based on SPT-N and *Vs* profile data using the methodologies that are subsequently described.

Liquefaction Probability Curves Based on the Standard Penetration Test (SPT)

We used the same methodology to include equations that we used to develop the LPCs for Lake County. Therefore, only changes made to the Lake County methodology are summarized herein.

For Lake County, the LPI was determined at each boring location for peak ground acceleration (PGA) values of 0.1, 0.2, 0.3, 0.4, and 0.5g and earthquake magnitudes (M_w) of 6, 6.5, 7, 7.5, and

8. For Dyer County, additional peak ground accelerations of 0.6, 0.7, 0.8, 0.9, and 1.0 were added because the predicted ground motions within Dyer County are higher than Lake County. Green and Bommer (2019) investigated the smallest earthquake magnitude that needs to be considered in assessing liquefaction hazard and they concluded that the moment magnitude 4.5~5 can be a magnitude threshold below which the liquefaction probability is negligible. Therefore, we added M_w values of 5 and 5.5 to the analysis. In summary, the LPI was determined for each soil boring location for PGA values of 0.1, 0.2, 0.3, 0.4, 0.5, 0.6, 0.7, 0.8, 0.9 and 1.0 and M_w values of 5, 5.5, 6, 6.5, 7, 7.5, and 8. The distribution of LPI was determined for each of the 70 possible combinations of PGA and M_w using the same procedure we utilized for determining the distribution of LPI in the Lake County study. Additionally, we utilized the same procedure as Lake County to calculate the probability of exceeding LPI values of 5 and 15, which are the lower bounds of "moderate" and "severe" liquefaction, respectively, based on the results of Iwasaki et al. (1978,1982) and Toprak and Holzer (2003).

As mentioned previously, the surficial geology of Dyer County consists of lowland, intermediate, and upland geologic units. Based on the methodology used to develop liquefaction hazard maps of Shelby County, TN (Cramer et al., 2015; Cramer et al., 2018b), LPCs can be developed to represent each geological unit. However, as shown by Table 3, most boring data available is from the lowland and insufficient boring data to develop LPCs is available from the intermediate, and upland units. Therefore, we combined the boring data from the intermediate and uplands geologic units to represent the non-lowland parts of Dyer County. Thus, LPCs were developed for lowland and non-lowland parts of Dyer County.

For the lowland part of Dyer County, we developed the LPCs using data of 118 SPT borings. Figures 17 and 18 provide the LPCs for the probability of exceeding LPI of 5 and 15 denoted as P[LPI>5] and P[LPI>15], respectively. As shown in Figure 17, LPCs are plotted as a probability range ([0,1]) of exceeding the target LPI value versus the ratio of PGA over magnitude scaling factor (MSF).
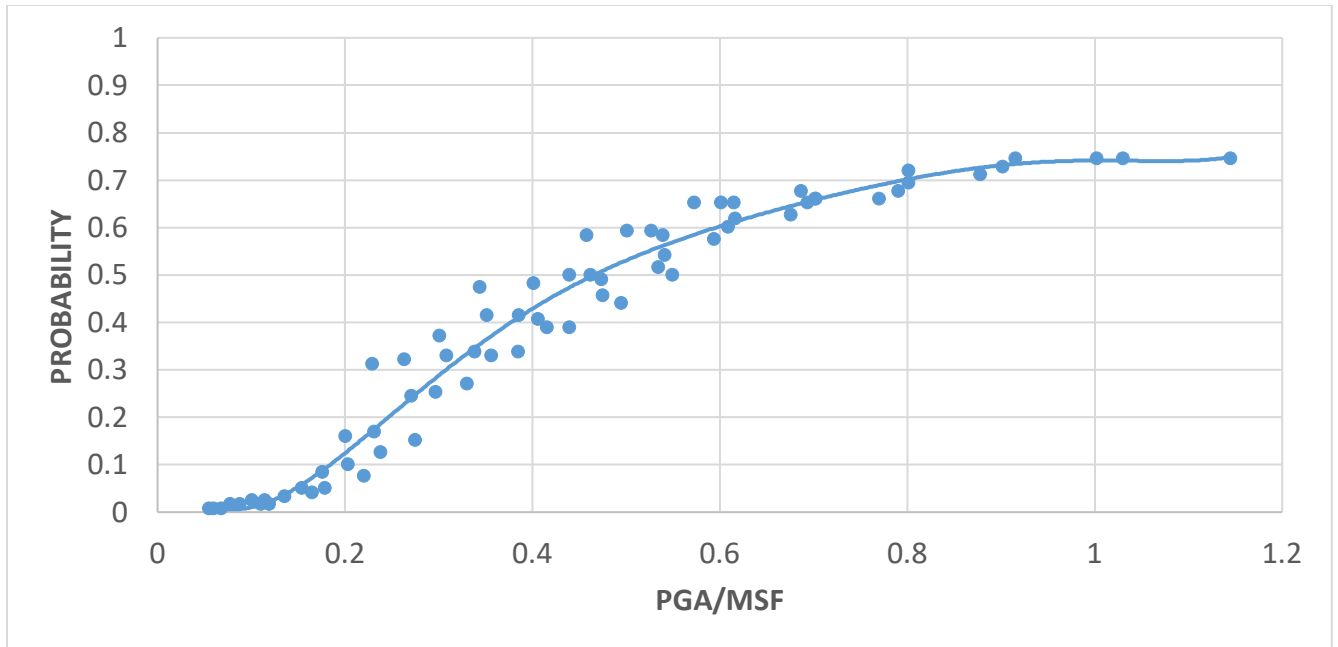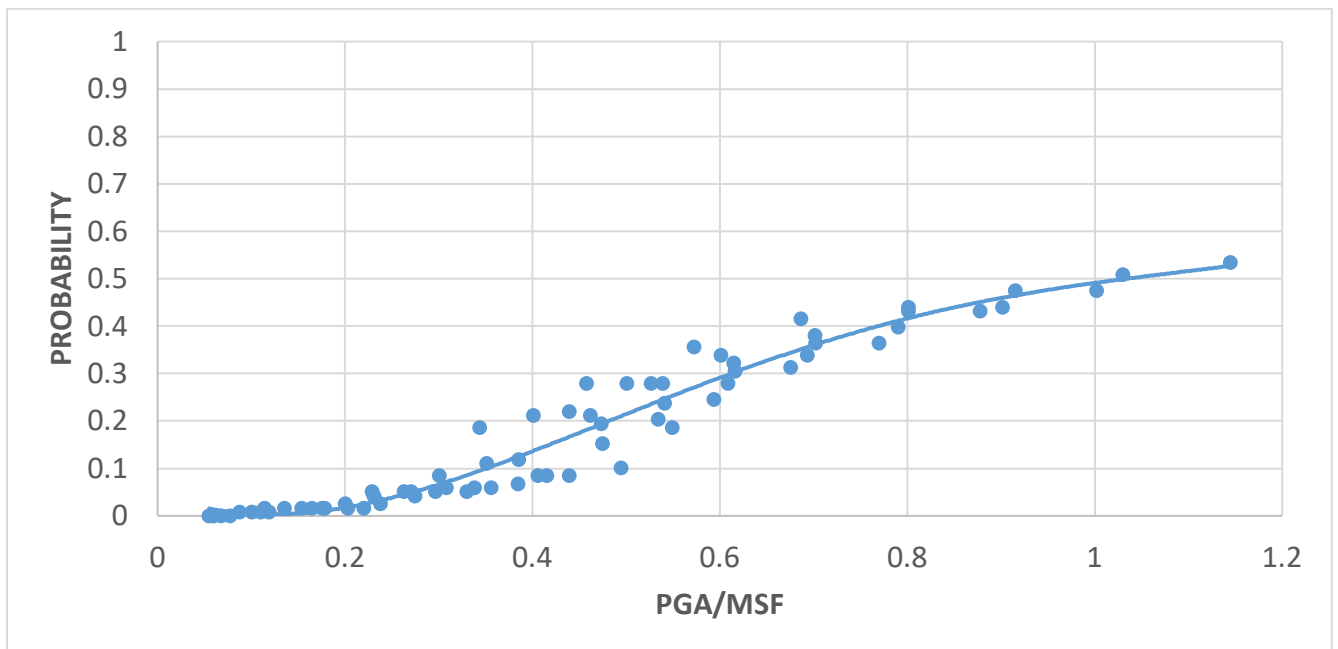
Figure 17: Lowland LPC from SPT data for P[LPI>5].

Figure 18: Lowland LPC from SPT data for P[LPI>15].

We compared the lowland LPCs of Dyer County with the LPCs of Lake County. As shown in Figures 19 and 20, the LPCs of Lake County, which are based on 33 SPT borings, are higher than the LPCs of Dyer County, which are based on 118 SPT borings, for both P[LPI>5] and P[LPI>15]. Also, shown in Figures 19 and 20 are LPCs representing the combined SPT data of both Lake and Dyer County. The LPCs of the combined Dyer and Lake County are closer to the Dyer LPCs because Dyer County LPC is based on 118 SPT boring compared to Lake County LPC that is based on 33 SPT borings.
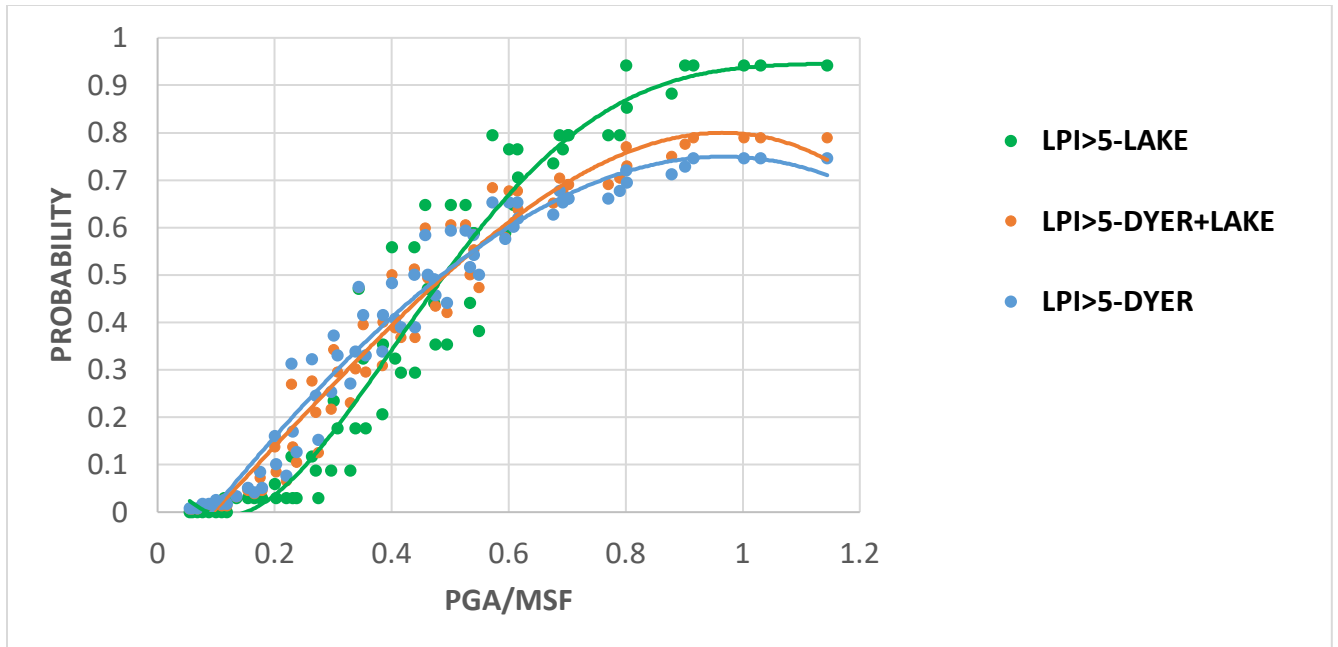
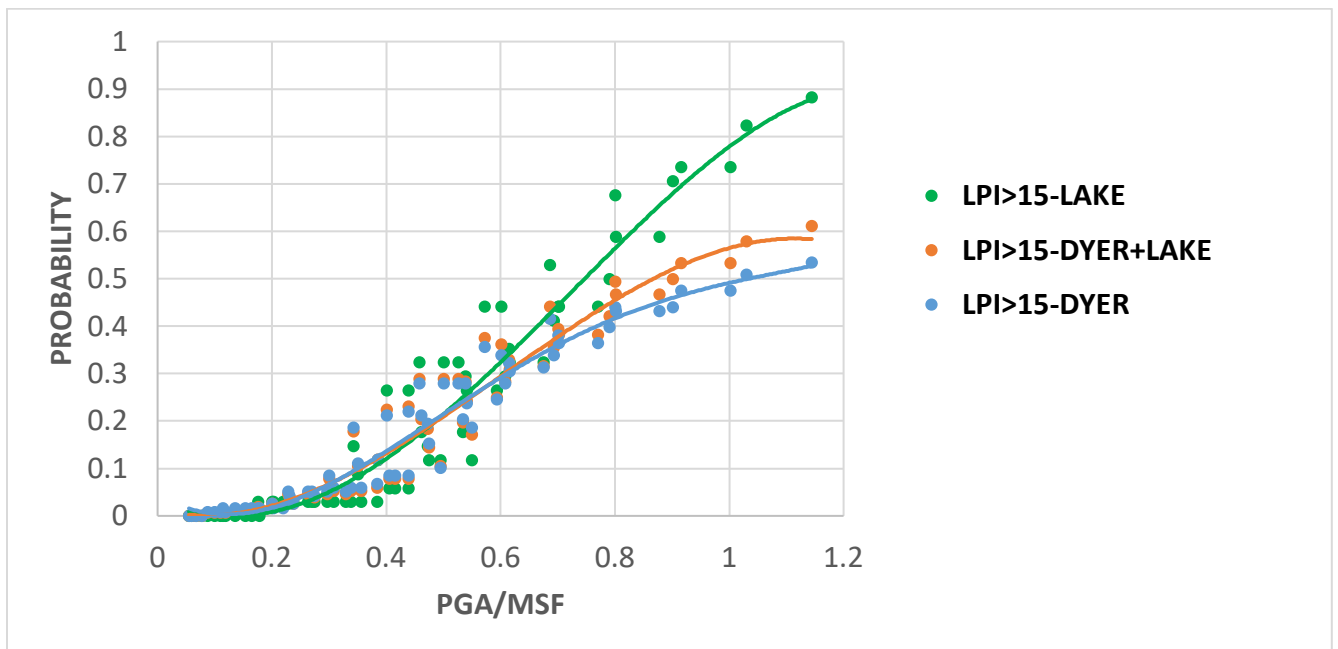Figure 19: Comparison and combination of lowland LPCs of Lake and Dyer Counties for P[LPI>5].

Figure 20: Comparison and combination of lowland LPCs of Lake and Dyer Counties for P[LPI>15].

The non-lowland LPCs of Dyer County were developed based on 22 SPT borings from the intermediate geologic unit and 2 SPT borings from the upland geologic unit. Therefore, the non-lowland LPCs are based on 24 SPT borings. Figures 21 and 22 show the non-lowland LPCs of Dyer County for P[LPI>5] and P[LPI>15], respectively.
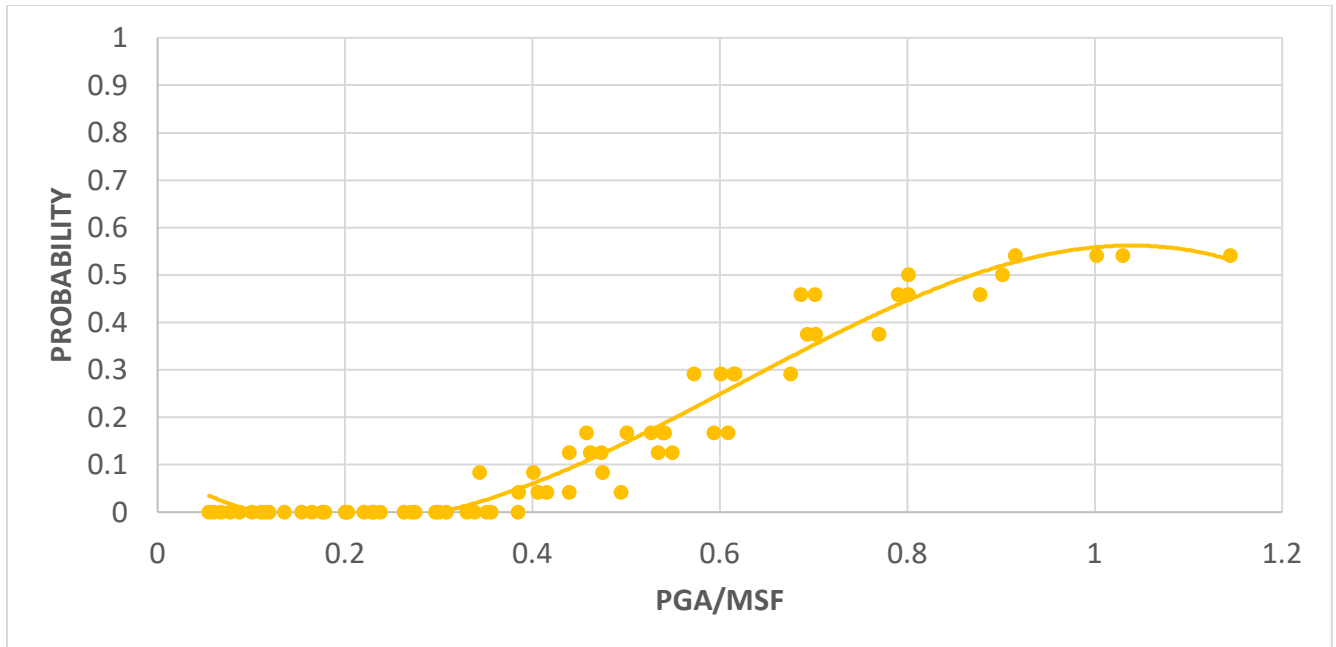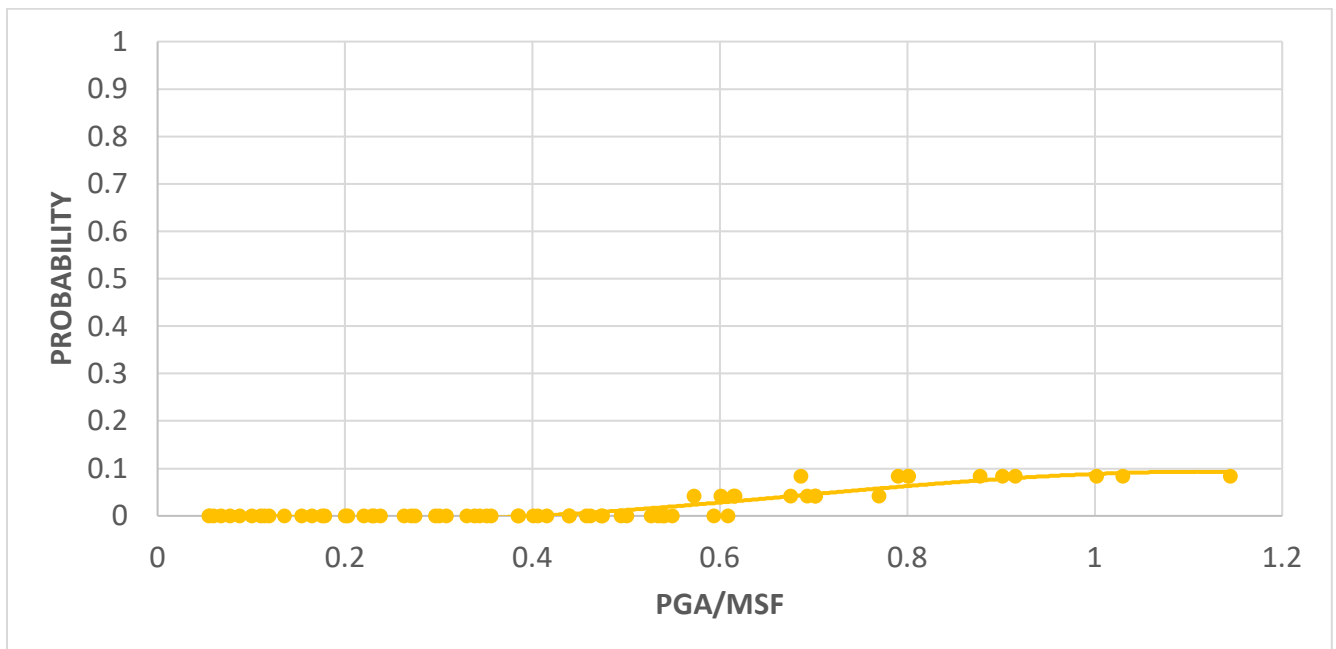
Figure 21: Non-lowland LPC from SPT data for P[LPI>5].

Figure 22: Non-lowland LPC from SPT data for P[LPI>15].

Figure 21 shows an unusually high probability of liquefaction for P[LPI>5] for typical non-lowland subsurface conditions. Based on a further evaluation of the Dyer County non-lowland SPT data, the geometric mean of N_{160cs} is 17 while the liquefaction threshold value of N_{160cs} is less than or equal to 30. N_{160cs} is the equivalent clean sand standard penetration resistance that is used in the evaluation of liquefaction potential based on the simplified method. See Cramer et al. (2015, 2018) for further details about N_{160cs}. Additionally, the geometric mean of soil fines content of the 24 non-lowland borings is 6.6% while the liquefaction threshold value of fines content is less than or equal to 35%. Therefore, since the geometric mean of both N_{160cs} and fines content of the non-

29

lowland soil boring data surpasses the liquefaction threshold values for these parameters, the probability of liquefaction for P[LPI>5] is unusually high for non-lowland areas of Dyer County. Additional soil data from additional soil borings may lower the probability of liquefaction.

LPI$_{ISH}$ based LPCs

Ishihara (1985) evaluated the influence of a non-liquefiable capping soil layer near the ground surface on the surficial manifestation of liquefaction. Based on observations of various earthquakes in Japan, Ishihara noticed that sites having non-liquefiable layers of at least 3 m thick did not show the evidence of the surficial manifestation of liquefaction. Ishihara proposed a generalized LPI relationship that specifically includes the influence of non-liquefiable layers by a correlation between the thickness of the non-liquefiable and the liquefiable stratum based on evaluation of the liquefaction potential index of Ishihara. The Ishihara generalized LPI relationship is referred to as LPI$_{ISH}$ herein and will be presented subsequently.

Maurer et al. (2015) evaluated the performance of LPI$_{ISH}$ method of Ishihara (1985) and the LPI method of Iwasaki et al. (1978, 1982) using data and observations from the Darfield Christchurch, New Zealand earthquakes. Maurer et al. concluded that the performance of the Iwasaki LPI method is inconsistent, and it generally over predicts liquefaction while the LPI$_{ISH}$ method was found to be more in agreement with observations. Thus, Maurer et al. (2015) presented a framework for evaluating liquefaction potential based on the LPI$_{ISH}$ method that considers the influence of a non-liquefiable crust cap on surficial liquefaction manifestation. The final form of Maurer's framework is summarized in equations 1 to 3:

$$LPI_{ISH} = \int_{H1}^{H1+H2} F(FS)\frac{25.56}{z}dz \tag{1}$$

$$F(FS) = \begin{cases} 1 - FS \ if \ FS \leq 1 \cap H1.m(FS) \leq 3 \\ 0 \qquad\qquad\qquad\qquad\qquad otherwise \end{cases} \tag{2}$$

$$m(FS) = \exp\left(\frac{5}{25.56(1-FS)}\right) - 1 \tag{3}$$

Where *H1* and *H2* are the bounds of the liquefiable layer,
m(FS) is an initial slope, unique to each boundary curve that proposed for identification of liquefaction induced damage (after Ishihara 1985),
F(FS) is the factor of safety related function,
z is depth, and *dz* is the differential increment of depth
The key differences between the LPI$_{ISH}$ framework and LPI framework are:
- LPI$_{ISH}$ incorporates the concept of limiting non-liquefiable cap layer thickness.
- Inherently, the LPI parameters assume that each liquefying soil layer equally contributes to the damage potential of the ground surface. The LPI$_{ISH}$ utilizes a power-law depth weighting function instead of the linear depth weighting function that is used in the framework of Iwasaki's LPI (see Figure 23). Therefore, in the LPI$_{ISH}$ framework, shallower liquefiable layers contribute more to the surficial manifestation of liquefaction compared to the LPI framework.
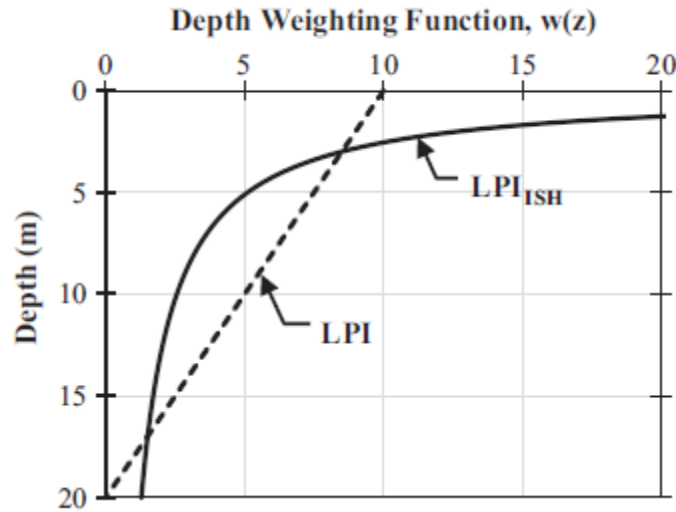
Figure 23: Depth weighting functions of LPI and LPI$_{ISH}$ (from Maurer 2015).

Using Maurer's framework based on LPI$_{ISH}$, we generated new LPCs for both lowland and non-lowland parts of Dyer County. Also, later in this section, we will compare the LPCs obtained based on LPI and LPI$_{ISH}$.

Figures 24 and 25 illustrate the LPCs obtained based on SPT boring data for lowland and non-lowland areas, respectively.
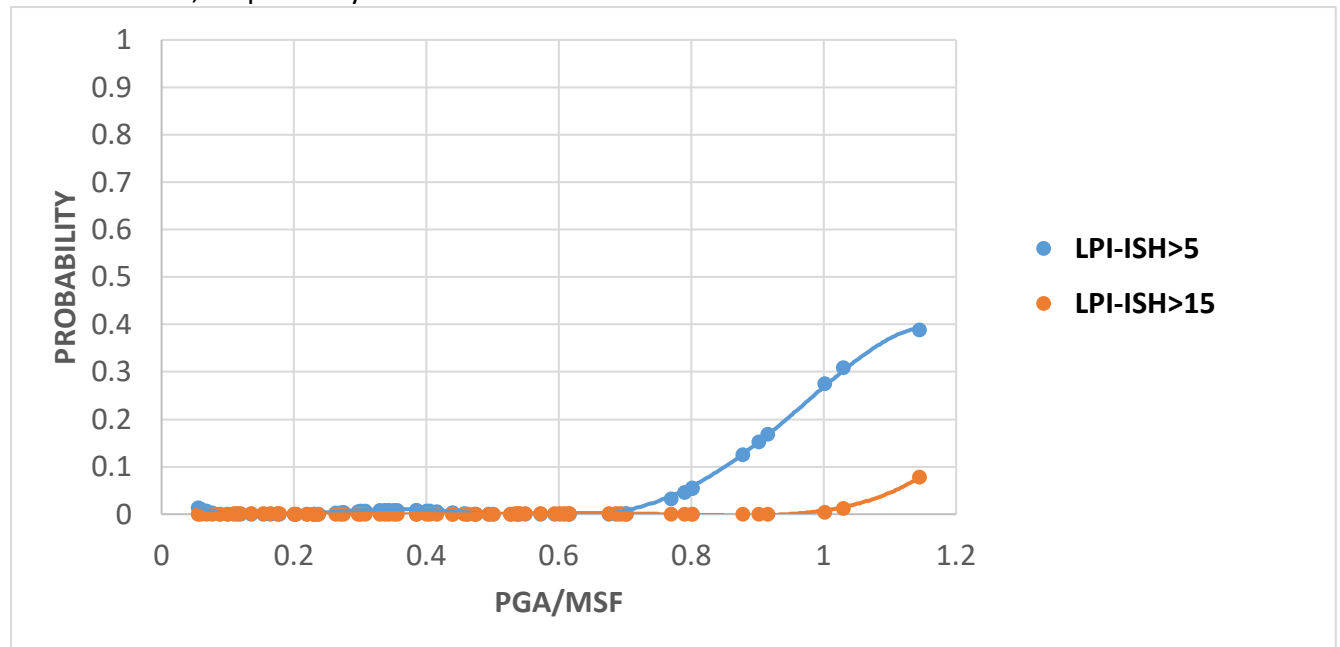

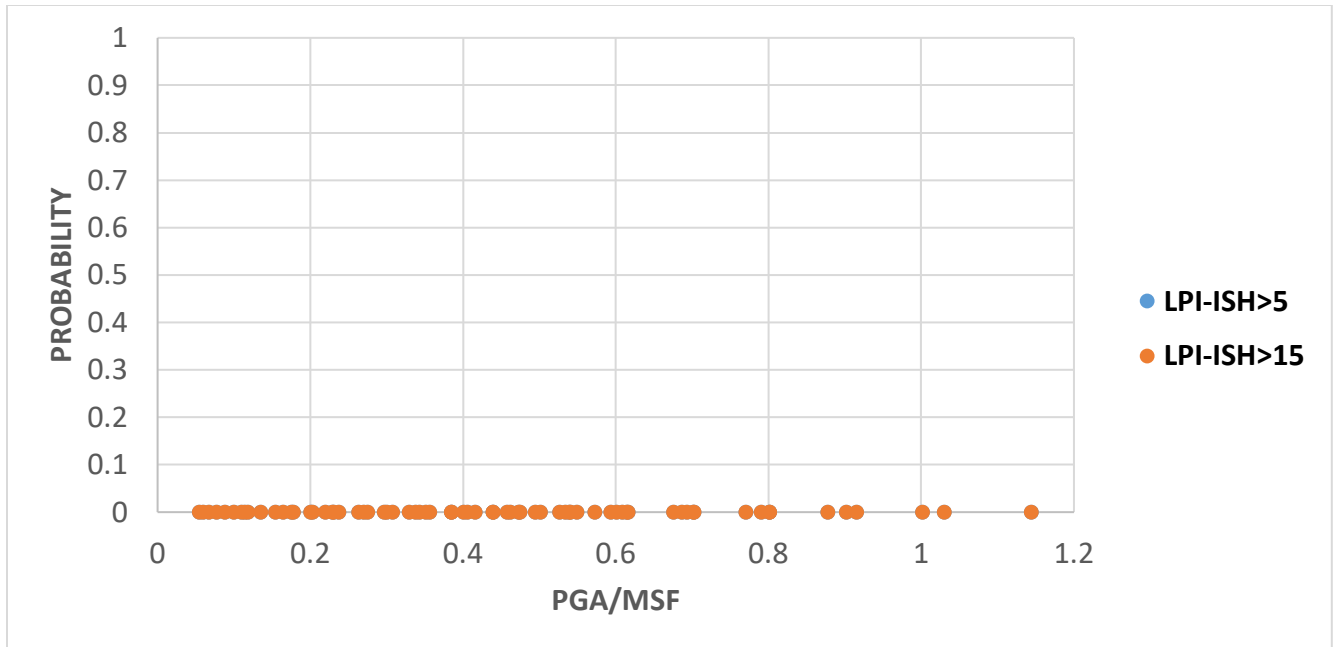Figure 24: LPI$_{ISH}$ based LPCs of lowland geologic unit.

Figure 25: LPI$_{ISH}$ based LPCs of non-Lowland geologic units.

Comparison of LPI- and LPI$_{ISH}$ -based LPCs

Figures 26 and 27 provide a comparison of LPCs for lowland areas of Dyer County for P[LPI>5] and P[LPI>15], respectively. LPI>5 represents the range of moderate to severe liquefaction and LPI>15 represents severe liquefaction. Figures 26 and 27 indicate that the probability of liquefaction provided by the LPCs based on the LPI$_{ISH}$ framework is significantly lower than the probability of liquefaction provided by the LPCs based on the LPI framework especially at higher ratios of PGA/MSF in which the maximum difference is about 45% for P[LPI>5] and 35% for P[LPI>15].
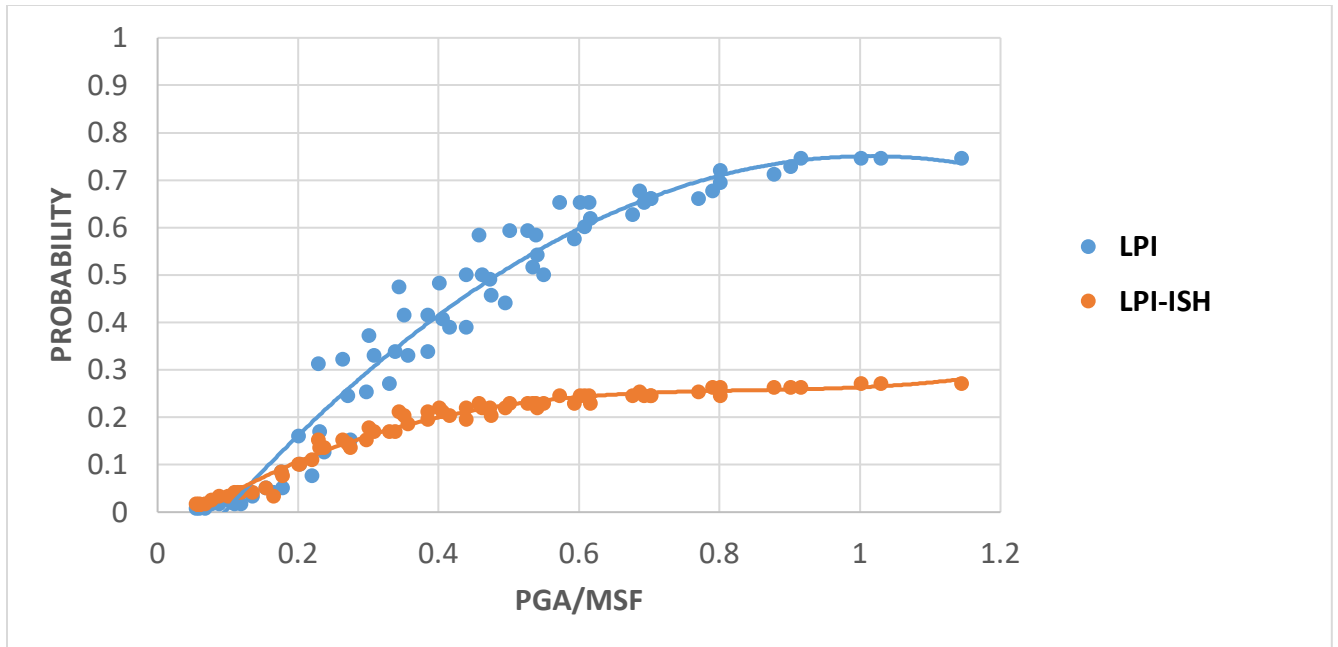
Figure 26: Comparison of LPI- and LPI$_{ISH}$-based lowland LPCs for P[LPI>5].
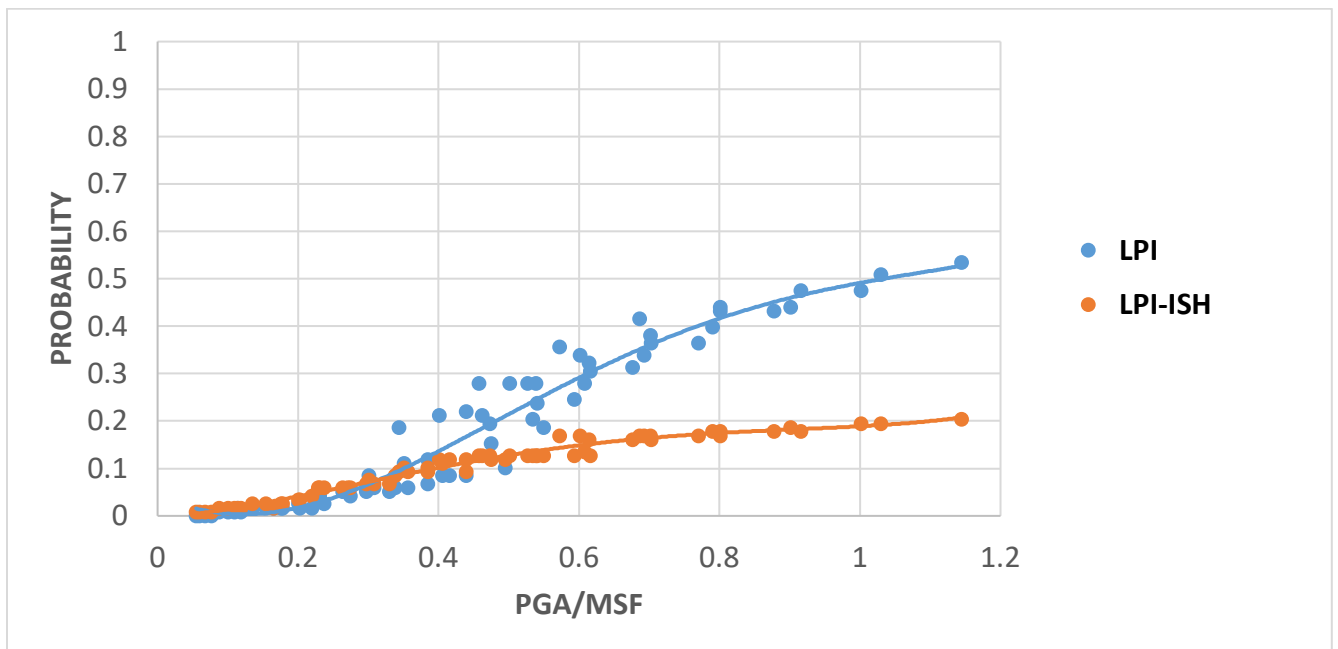

Figure 27: Comparison of LPI- and LPI$_{ISH}$-based lowland LPCs for P[LPI>15].

Figures 28 and 29 provides a comparison of LPCs for the non-lowland areas of Dyer County for P[LPI>5] and P[LPI>15], respectively. Similar to the results of the lowland areas, Figures 28 and 29 indicate that the probability of liquefaction provided by the LPCs based on the LPI$_{ISH}$ framework is lower than the LPCs based on the LPI framework especially at higher ratios of PGA/MSF in which the maximum difference is about 35% for moderate to severe liquefaction (LPI>5) and about 15% for severe liquefaction (LPI>15).

In summary, for both the lowland and the non-lowland areas of Dyer County, the probability of liquefaction provided by the LPCs based on the LPI$_{ISH}$ framework are lower than the LPCs based on the LPI framework especially at higher ratios of PGA/MSF.
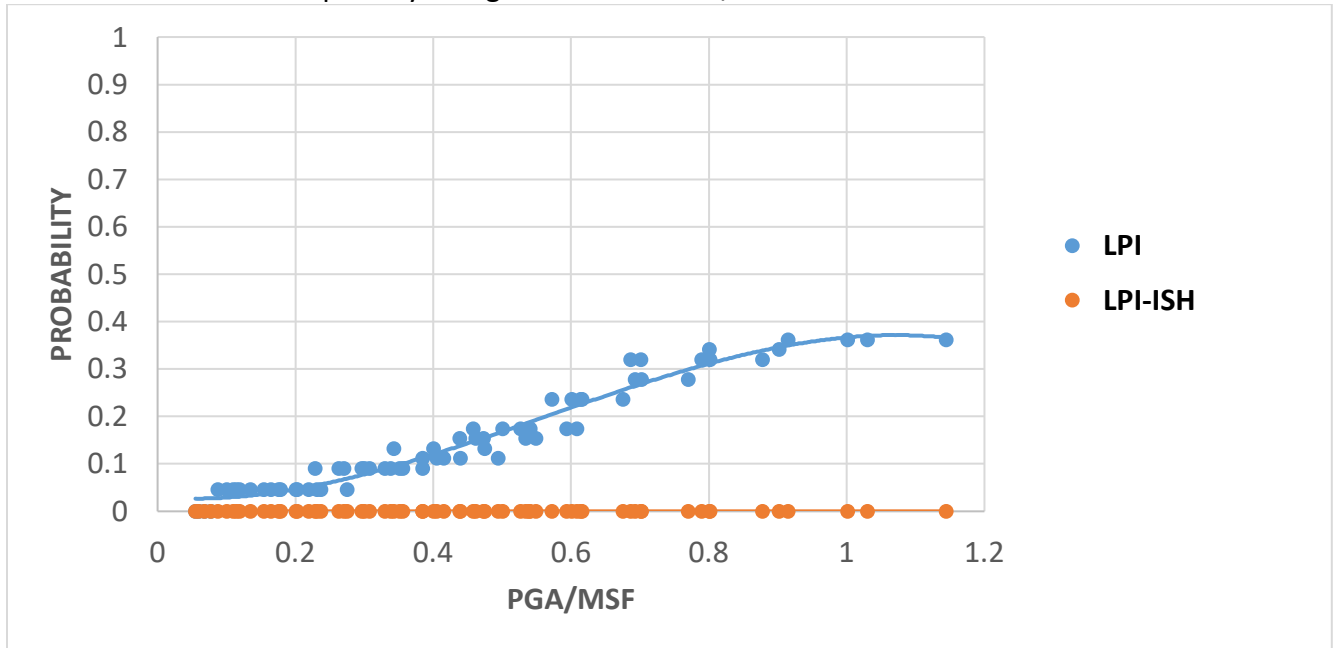

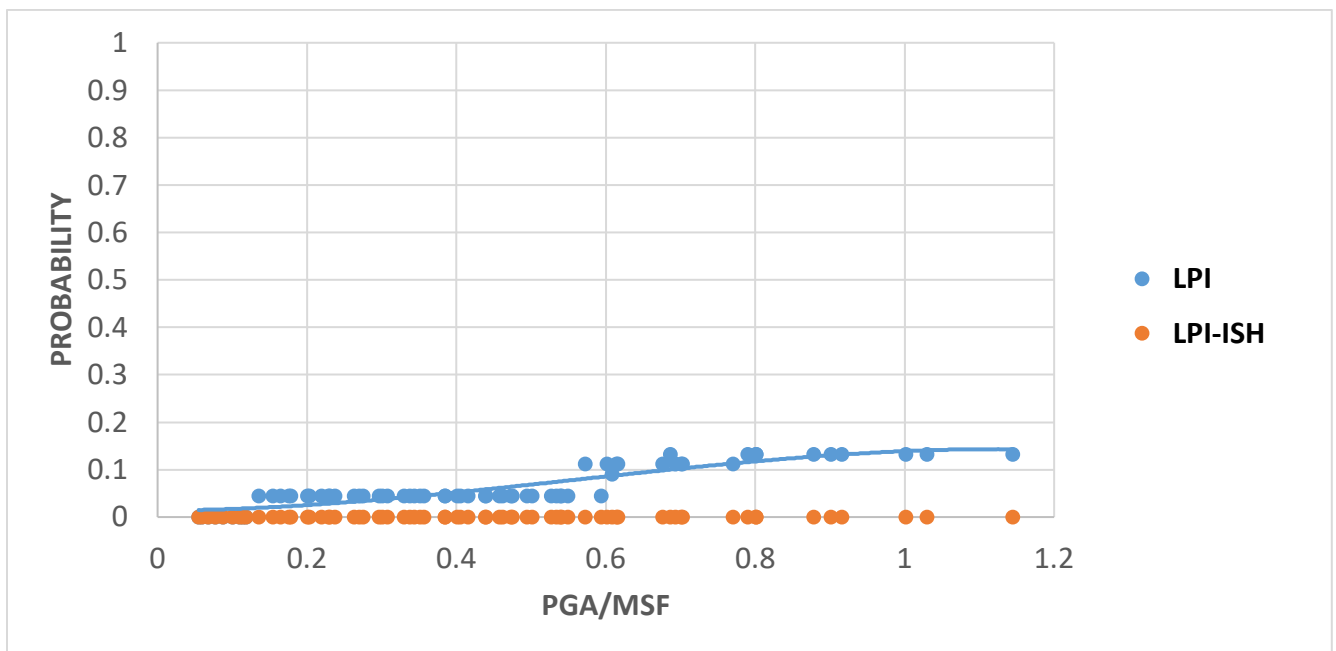Figure 28: Comparison of LPI- and LPI$_{ISH}$-based non-lowland LPCs for P[LPI>5].

Figure 29: Comparison of LPI- and LPI$_{ISH}$-based non-lowland LPCs for P[LPI>15].

<u>Liquefaction Probability Curves Based on the Shear Wave Velocity (*Vs*)</u>

The second method used to develop the LPCs of Dyer County was based on *Vs* profile data. A total of 11 *Vs* profiles with a minimum depth requirement of 20 m (66 ft) were obtained within

Dyer County. Figure 13 shows the locations of the *Vs* profiles in relation to the distribution of the geologic units of Dyer County and Table 4 provides the number of *Vs* profiles within each geologic unit type. All 11 *Vs* profiles were located within the non-lowland portions of Dyer County. No *Vs* profiles were available within the lowland areas. Therefore, LPCs based on *Vs* data could be developed only for non-lowland areas.

We utilized the same procedure we used to develop the LPCs based on *Vs* data for Lake County (Cramer et al., 2019). The Cyclic Resistance Ratio (CRR), Cyclic Stress Ratio (CSR), and FS were estimated based on the *Vs* profiles for every 2 ft (0.6 m) depth interval up to a depth of 66ft (20 m) for each *Vs* profile location. The *Vs* based LPCs were developed for the same range of PGA and M_w as the ranges incorporated in developing LPCs based on SPT data as described in the Liquefaction Probability Curves Based on the Standard Penetration Test (SPT) section of this report. Figures 30 and 31 show the *Vs* based LPCs of non-lowland part of Dyer County for P[LPI>5] and P[LPI>15], respectively.
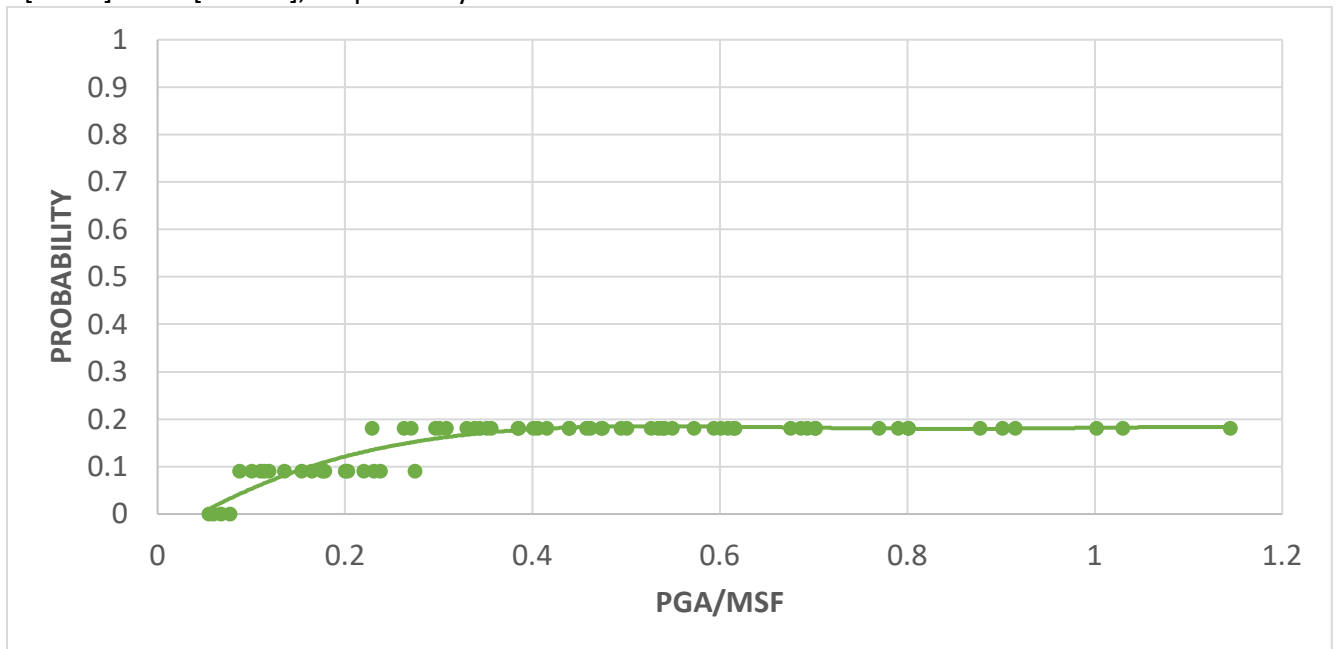

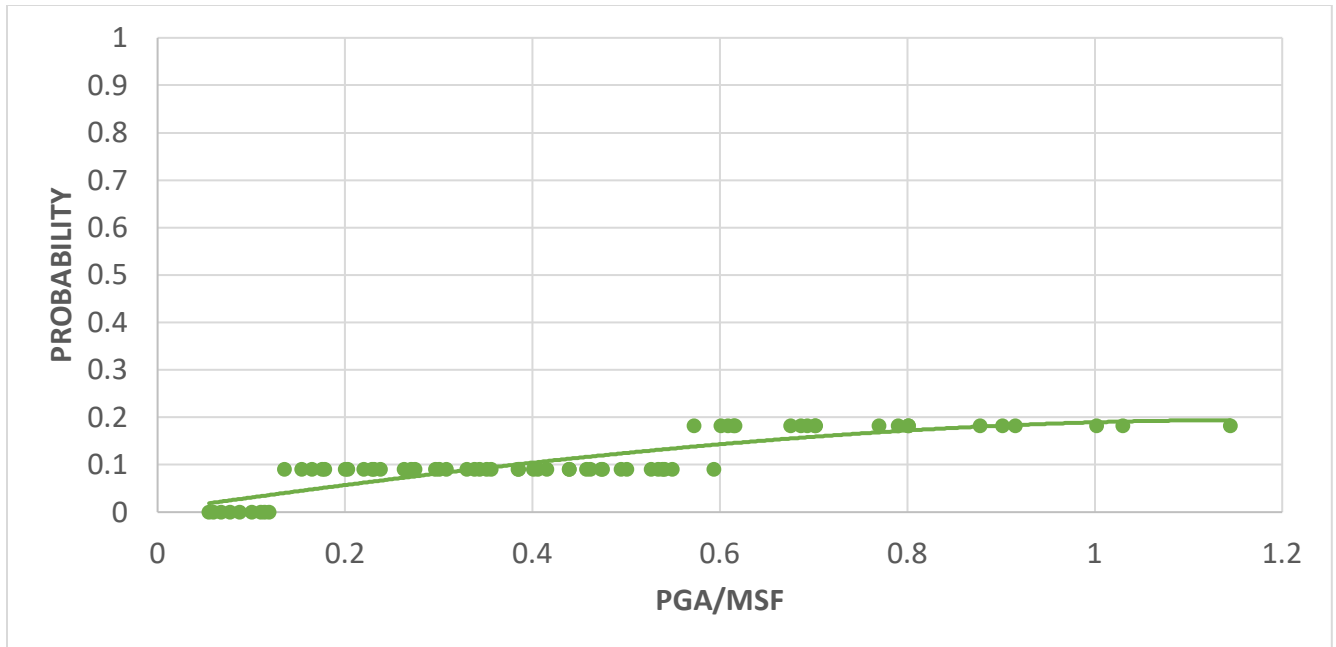Figure 30: Non-lowland *Vs* based LPCs for P[LPI>5].

Figure 31: Non-lowland *Vs* based LPCs for P[LPI>15].

The probability of LPI>5 is typically greater than the probability of LPI>15 as was obtained in Figures 21 and 22 for the LPCs based on SPT data. However, for the LPCs based on *Vs* data shown in Figures 30 and 31, at P[LPI>5] the LPC indicates the same probability value of ~20% at PGA/MSF of 0.2 and higher. At P[LPI>15] the LPC reaches a maximum probability of ~20% at PGA/MSF of 0.6 and higher. Therefore, the LPC of LPI>5 is higher than LPC of LPI>15 at PGA/MSF between 0.2 to 0.6.

The main uncertainty of analysis based on *Vs* profile data is the limited number of profiles available, only 11. Additionally, as noted in the Lake County report (Cramer et al., 2019) the other uncertainty of *Vs* based analysis of liquefaction potential is the unavailability of USCS classifications of the soil layers, so the fines content had to be conservatively estimated using the procedure described in the Lake County report.

Comparison of Liquefaction Probability Curves Based on SPT and *Vs* Methods

A comparison of the LPCs based on SPT N-values and *Vs* profiles is presented in this section. Figures 32 and 33 provides a comparison of non-lowland LPCs obtained by SPT and *Vs* data for P[LPI>5] and P[LPI>15]. A comparison of LPCs can only be made for the non-lowland parts of Dyer County because no *Vs* profile data was available within lowland parts of Dyer County. For P[LPI>5] there is no agreement between SPT- and *Vs*-based LPCs for almost the entire range of PGA/MSF. For PGA/MSF of 0 to 0.5, the *Vs* based LPC shows higher probabilities and for PGA/MSF of 0.5 to 1.2, the SPT based LPC provides higher probability values by about 40% at PGA/MSF of 0.9. For P[LPI>15], the *Vs* based LPC yields higher probabilities for all PGA/MSF ratios evaluated by about 10%.
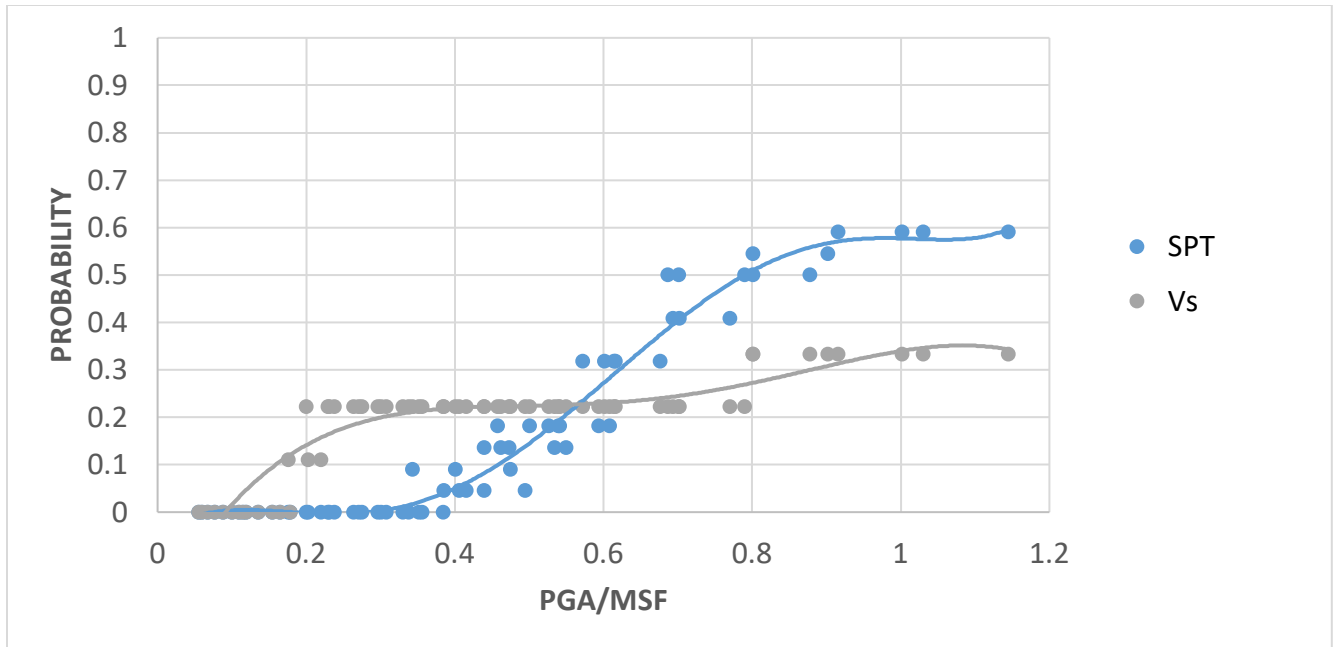
Figure 32: Comparison of LPCs based on SPT data and shear wave velocity profiles for P[LPI>5] for non-lowland parts of Dyer County.

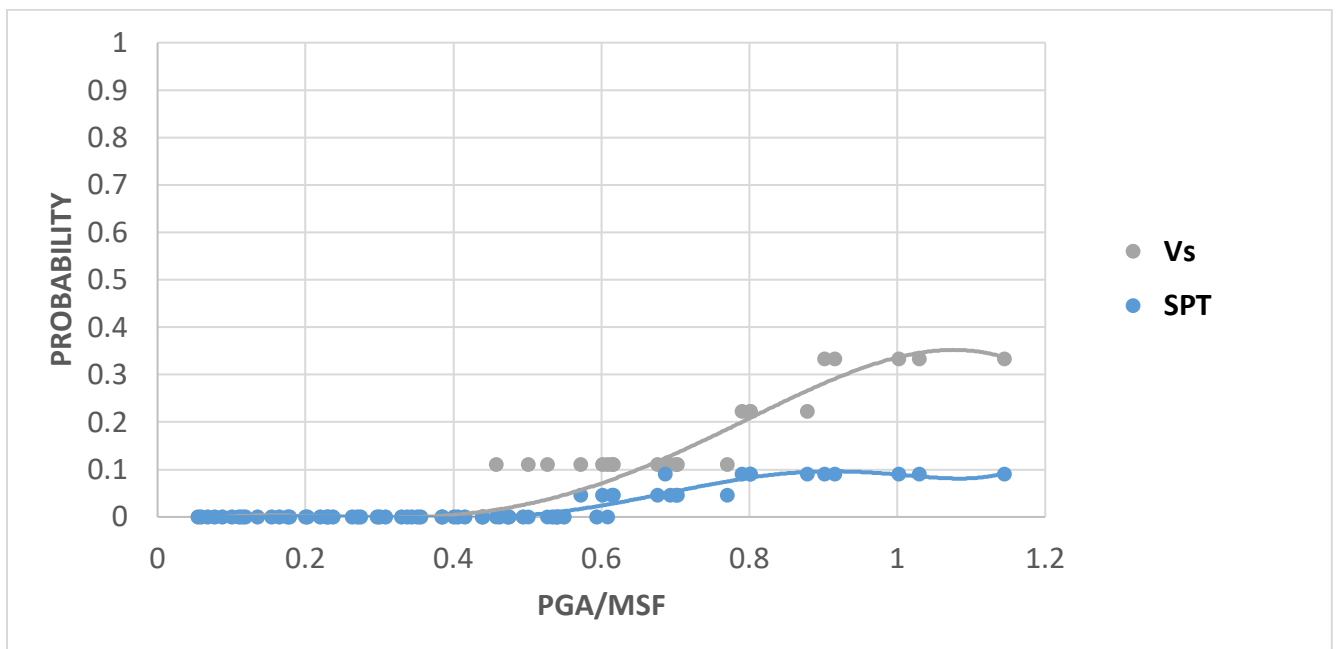Figure 33: Comparison of LPCs based on SPT data and shear wave velocity profiles for P[LPI>15] for non-lowland parts of Dyer County.

LPCs for liquefaction hazard maps of Dyer County

The liquefaction hazard maps are developed based on the LPCs for each geology type. In this section, we discuss the recommended LPCs for lowland and non-lowland parts of Dyer County that are used to develop liquefaction hazard maps of Dyer County.

Lowland LPCs Recommendation

For lowland part of Dyer County because there was not any *Vs* profile available within lowland, therefore it was suggested that the liquefaction hazard maps of lowland part of Dyer County be based on LPCs developed from SPT data of 118 soil borings. SPT based LPCs of lowland part of Dyer County for LPI>5, and LPI>15 is presented in Figures 34 and 35, respectively. As described in SPT method section, because the geology of Lake County was lowland, we combined the SPT data of Lake County and lowland part of Dyer County and developed LPCs based on the combined data (See Figures 19 and 20) that we can possibly use to develop liquefaction hazard maps for all five counties of the study after data is evaluated from all five counties.
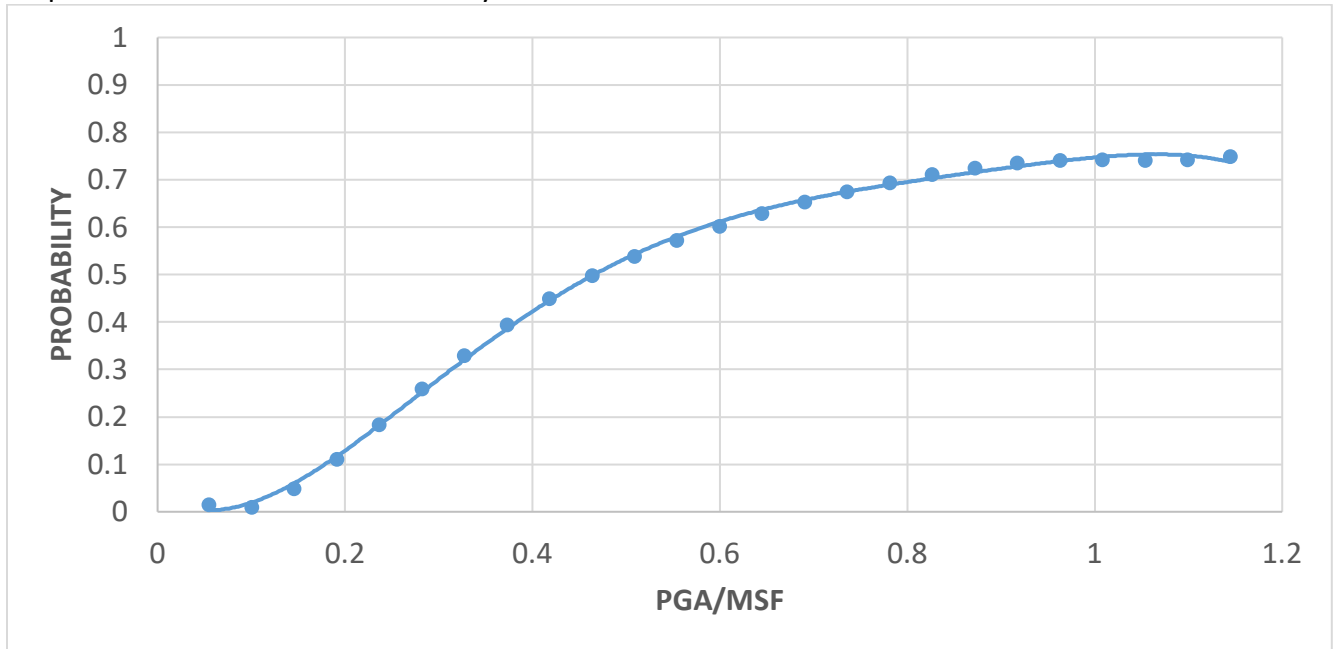

Figure 34: SPT-based LPC for P[LPI>5] of the lowland part of Dyer County.

Figure 35: SPT-based LPC for P[LPI>15] of the lowland part of Dyer County.

Non-lowland LPCs Recommendation

As noted in the Liquefaction Probability Curves Based on the Standard Penetration Test section of this report, Figure 21 shows an unusually high probability of liquefaction for P[LPI>5] for typical non-lowland subsurface conditions. Therefore, for the non-lowland parts of Dyer County, LPCs were developed based on combining the SPT and *Vs* LPCs. Figures 36 and 37 show the non-lowland LPCs for P[LPI>5], and P[LPI>15] obtained from the combined SPT and *Vs* data that was used in the developing the liquefaction hazard maps.

Figure 36: LPC for P[LPI>5] of non-lowland part of Dyer County.

Figure 37: LPC for P[LPI>15] of non-lowland part of Dyer County

Geotechnical summary

We used the same general procedures to develop LPCs based on SPT-N and *Vs* profile data that we used to develop the Lake County LPCs (Cramer et al., 2019). However, unlike Lake County that consisted predominantly of only one type of surficial geology, the surficial geology of Dyer County consists of lowland, intermediate, and upland geologic units. Based on the methodology

used to develop liquefaction hazard maps of Shelby County, TN (Cramer et al., 2015; Cramer et al., 2018), LPCs are developed to represent each geological unit. However, most SPT-N boring data available is from the lowland and insufficient boring data to develop LPCs is available from the intermediate and upland units. Therefore, we combined the boring data of these two geologic units (intermediate and uplands) to represent the non-lowland parts of Dyer County. Thus, LPCs were developed for only lowland and non-lowland parts of Dyer County. Figures 17 and 18 provide the lowland LPCs P[LPI>5] and P[LPI>15], respectively. Figures 21 and 22 show the non-lowland LPCs for P[LPI>5] and P[LPI>15], respectively.

We also developed LPCs that included the influence of a non-liquefiable capping soil layer near the ground surface on the surficial manifestation of liquefaction based on the Maurer et al. (2015) methodology that is based on the method of Ishihara (1985) and is referred herein as the LPI$_{ISH}$ method. Figures 24 and 25 illustrate the LPCs obtained using the LPI$_{ISH}$ method and based on SPT boring data for lowland and non-lowland areas, respectively. For both the lowland and the non-lowland areas of Dyer County, the probability of liquefaction provided by the LPCs based on the LPI$_{ISH}$ framework are lower than the LPCs based on the LPI framework especially at higher ratios of PGA/MSF.

LPCs were also developed based on *Vs* profile data. All 11 *Vs* profiles within Dyer County were located within the non-lowland portions of Dyer County. No *Vs* profiles were available within the lowland areas. Therefore, LPCs based on *Vs* data could be developed only for non-lowland areas. We utilized the same procedure we used to develop the LPCs based on *Vs* data for Lake County (Cramer et al., 2019). Figures 30 and 31 show the *Vs* based LPCs of non-lowland part of the Dyer County for P[LPI>5] and P[LPI>15], respectively. Based on a comparison of SPT and *Vs* LPCs of the non-lowland parts of Dyer County, there is no agreement between SPT- and *Vs*-based LPCs for almost the entire range of PGA/MSF.

For lowland parts of Dyer County, it was suggested that the liquefaction hazard maps of the lowland parts of Dyer County be based on LPCs developed from SPT data of 118 soil borings because no *Vs* data is available within the lowlands. SPT based LPCs of lowland part of Dyer County for LPI>5, and LPI>15 is presented in Figures 34 and 35, respectively. For the non-lowland parts of Dyer County, it was recommended that the liquefaction hazard maps be based on LPCs developed based on combining the SPT and *Vs* LPCs as shown in Figures 36 and 37. Combined LPCs from both SPT and *Vs* is recommended because the LPCs based on only SPT data provided by Figure 21 shows an unusually high probability of liquefaction for P[LPI>5] for typical non-lowland subsurface conditions.

It is also recommended that liquefaction hazard maps be developed based on LPCs that consider the influence of a non-liquefiable capping soil layer near the ground surface on the surficial manifestation of liquefaction as shown by Figures 24 and 25.

Seismic Measurements

Introduction

Multichannel Analysis of Surface Waves (MASW) is a geophysical exploration technique that measures shear-wave velocity of underground layers using the dispersion of surface waves along an array of geophones. The MASW seismic survey obtains velocity structure of the layers using surface waves.

The seismic refraction method is sensitive to low velocity layers. If low velocity layers are not detected, the results of seismic refraction may be compromised, while seismic reflection can detect geological features not seen in refraction tests. Geophysical exploration at shallow depths (less than 50 meters) can be a challenge. Invasive procedures such as downhole and crosshole seismic surveys can be expensive. Non-invasive procedures such as MASW can be advantageous and economical and can be a viable alternative.

In the MASW method, an array of geophones captures the surface waves that are generated by an energy source such as a sledgehammer or a heavier source (Figure 38). The changes in amplitude and arrival times are measured using a post-processing software at different frequencies (e.g., SurfSeis, developed by Kansas Geological Survey, KGS). These "changes" are associated with the dispersion of surface waves. Complicated propagation of surface waves has unique characteristics that can relate the amplitude of surface waves with shear-wave velocity, depth, and frequency. In a few words, amplitude (and consequently, velocity) of certain frequency of surface waves (phase velocity) is affected by the shear-velocity structure of the ground down to certain depths. This combination provides us with valuable information called dispersion curves, which is a plot of phase velocity versus frequency. Figure 39 shows the amplitude variation of surface waves with respect to wavelength, which is the normalized depth on the vertical axis and normalized motion (amplitude at depth z over amplitude at surface) on the abscissa. As shown in Figure 40, longer wavelength (or lower frequencies) can sample larger depths.
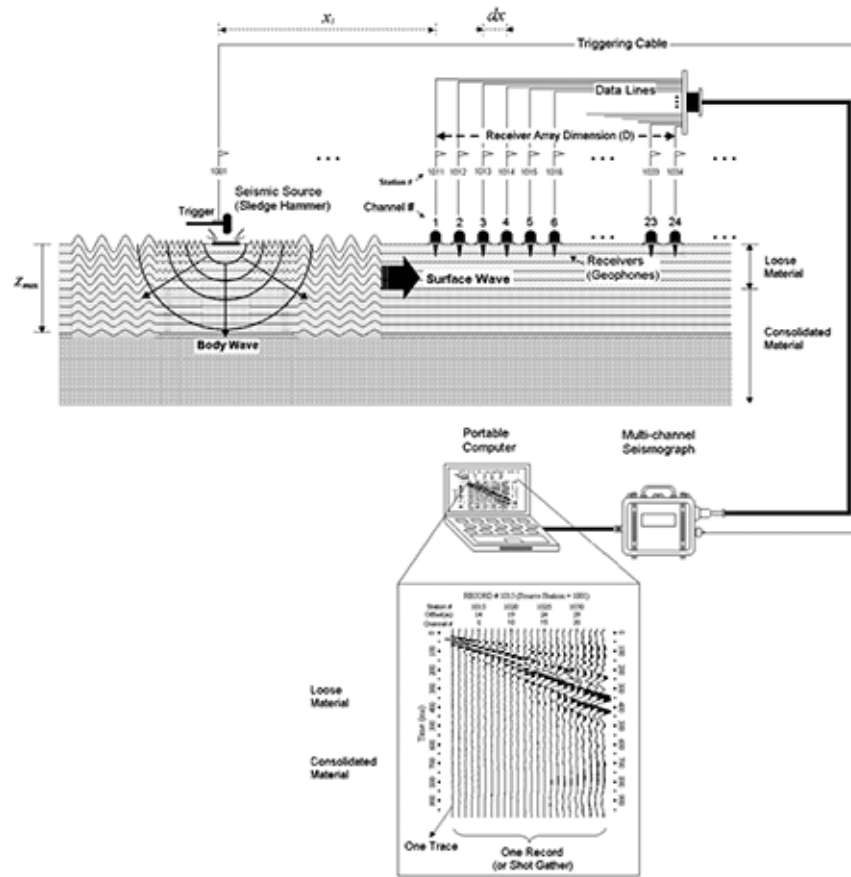
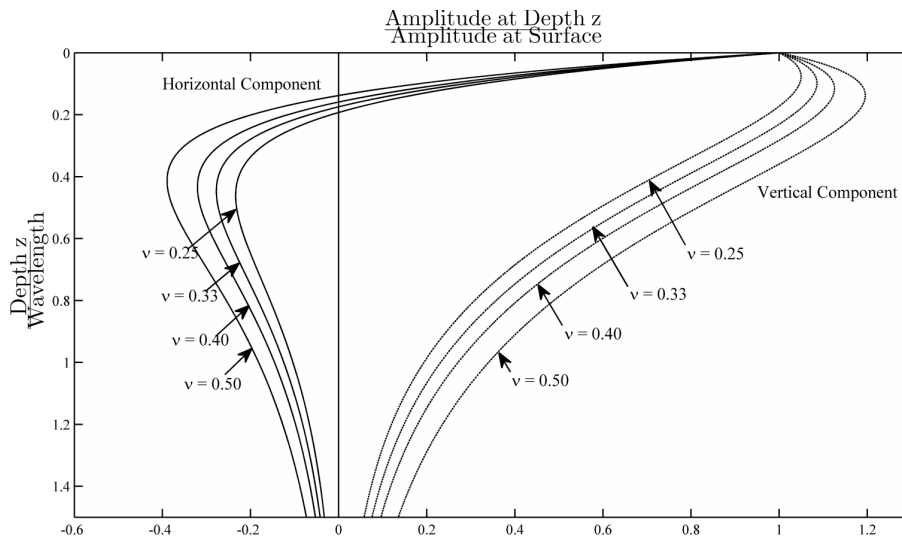Figure 38: Active MASW test setup. (from KGS.ku.edu).

Figure 39: Variation of horizontal and vertical normalized components of displacements induced by Rayleigh waves with normalized depth in a homogeneous isotropic, elastic half-space.
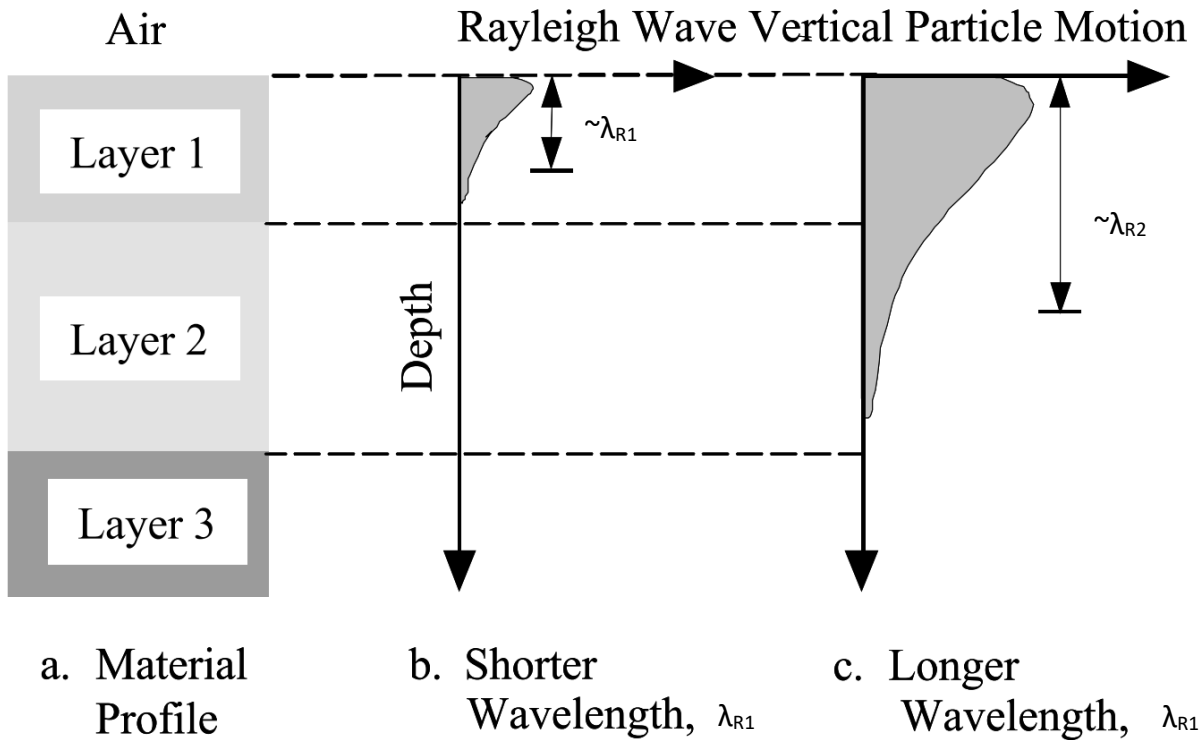
Figure 40: Depth sampled by Rayleigh waves with different wavelengths (Stokoe II and Santamarina, 2000).

Finally, through and iterative inversion process using the SurfSeis software, the best matching velocity profile is obtained. It is important to mention that the inversion process may produce several shear-wave velocity profiles with similar dispersion curves matching the experimental dispersion curve which is referred to as the non-uniqueness of the inversion process. There are some provisions embedded in the software that can remove irrelevant velocity profiles. Also, geological studies and prior expert knowledge can help mitigating the non-uniqueness issue.

MASW Equipment and Testing procedure

In all the 12 sites that we performed MASW survey in the Dyer County, we used a 144 m linear array of 72 4.5 Hz geophones with 2 meters of spacing between geophones. Our active energy source was a Propelled Energy Generator (PEG – Figure 41). This device has a 40 kg mass that is driven down using an elastic band, which is stretched using the motor mounted on the device. The energy produced by quick drop of the weight was experimentally considered enough for the entire length of the array plus a 16m offset from the first geophone.

We started shooting at a 16 m offset from the first geophone and advanced every 4 meters through the middle of the spread. Each location was shot three times. Several shots per location can help reduce the effects of noise by stacking the records. Stacking will average out the noise and enhance the main signal, to reach a higher signal to noise ratio.

To obtain deeper velocity structures (e.g., lower frequency range) we recorded ambient noise using the Refraction Microtremor (ReMi) seismic survey. An array of 24 geophones with 10 ft spacing was placed at the same location and several 32s second records of data was acquired multiple times. The dispersion curve obtained using the MASW seismic survey was augmented with the dispersion curve points obtained by the ReMi procedure to better estimate the shear-wave velocity of deeper layers of the soil structure. We used the SeisOpt ReMi software to process data collected using the ReMi seismic survey.

Figure 41: Propelled Energy Generator used as an Active Source.

Data Processing

Data processing is performed using the SurfSeis software. The recordings were analyzed to obtain the "Overtone Images" (Figure 42). In Figure 42 and 43, the vertical axis is the phase velocity in m/sec and the horizontal axis is the frequency. The dispersion curves were automatically picked, and visually checked. Furthermore, the dispersion curve obtained using the ReMi procedure were combined with the MASW dispersion curve as shown in Figure 43. In some cases, dispersion curves from MASW is augmented with ReMi at low frequencies to obtain information at greater depths. Then, the dispersion curves were inverted to obtain the shear-wave velocity profile associated with the site. In Figure 43, the orange curve is the high energy (the middle of the overtone image from ReMi analysis) and the gray curve is the lower energy curve (the lower margin of the overtone image). Lower limit of the apparent phase velocities can be recognized as the true phase velocities (Louie, 2001).
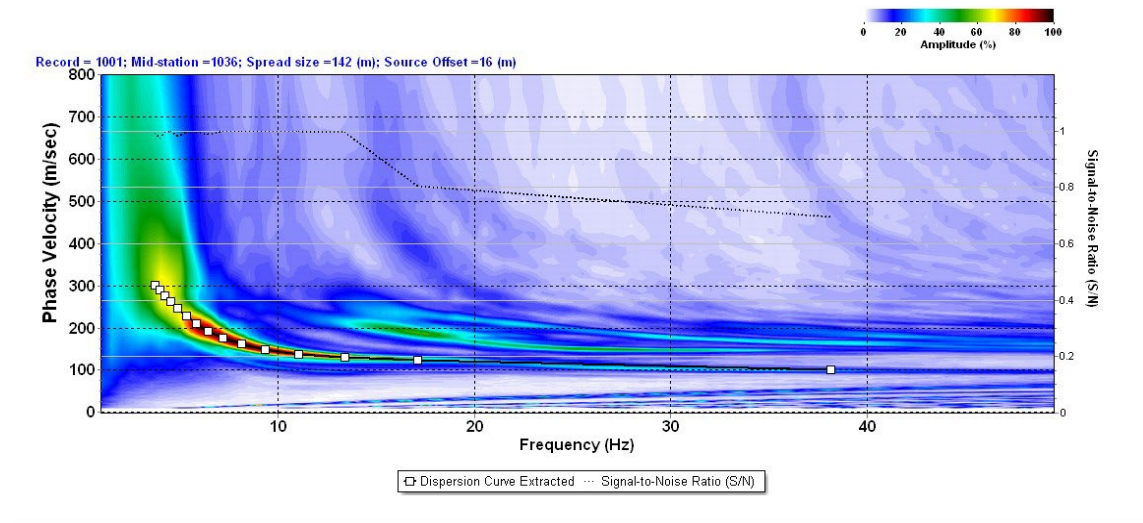
Figure 42: A sample of the dispersion curve obtained by the Surfseis Software.
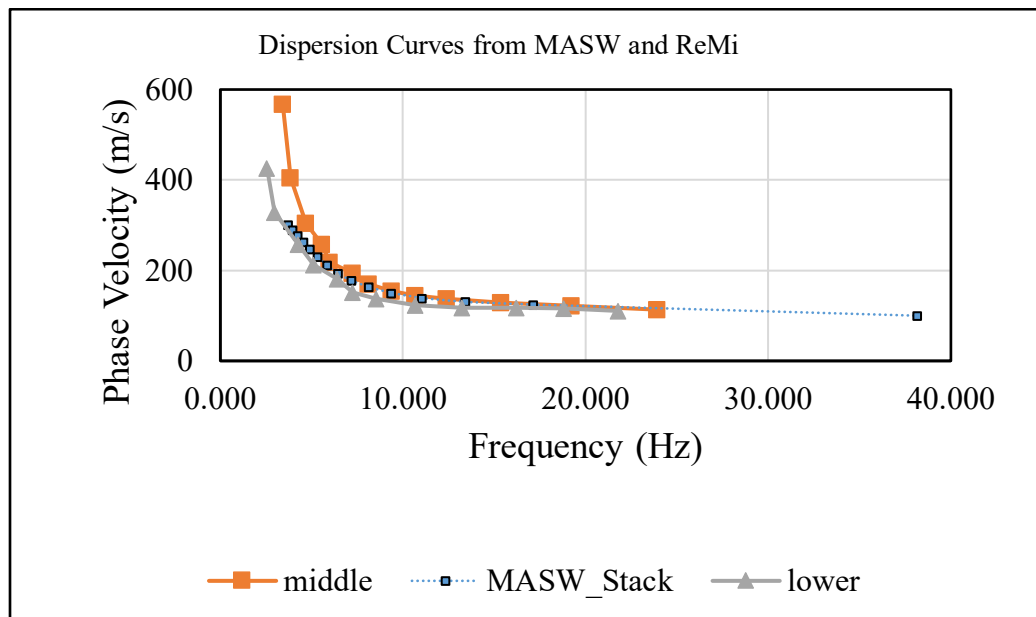

Figure 43: Comparison of dispersion curves obtained with MASW and ReMi.

Depth of investigation is proportional to the largest wavelength captured by the instruments (Schuler, 2008).

$$Depth\ of\ Investigation\ =\ 0.4 \times Wavelength\ =\ 0.4 \times Velocity\ /\ frequency$$

Depth of investigation depends on a few parameters.
- Corner frequency of the geophones, which was 4.5Hz in our case that is a widely and

  practically used device for surface exploration methods.

- Energy source. The energy source should be strong and capable of generating enough low frequencies.

- Velocity of subsurface soil. The faster the velocities, the greater depth we can measure.

- Noise in the area. A noisy location can obscure wave motion at long distances, where the wave has attenuated.

Results

The final results of 12 MASW and ReMi seismic surveys (Figure 44) in Dyer County are summarized in this section (Figure 45). We were able to obtain shear-wave velocity profiles to depths of about 30m to 70m. We developed a representative non-lowlands velocity profile with depth from the 12 MASW profiles. Our study confirms that the MASW procedure can estimate down to 50m depth with acceptable accuracy. Data quantity does not support the reliability and accuracy at depths higher than 50m. In general, uncertainty increases with depth.
In some cases, we included higher modes into our inversion process to enhance the resolution of the velocity profiles. Although, the estimated depth of the velocity profile is only dependent on the wavelength (frequency) of the modes, meaning that including higher modes does not increase the depth of conversion. Yet, the benefit of recognizing higher modes is to increase the resolution of the profile and decreasing the uncertainty of the inversion process.

Figure 46 presents the mean and standard deviation of the velocity profiles with depth at 20 MASW non-lowlands measurement sites in Dyer and Lauderdale Counties (see Cramer et al., 2020 for details concerning the Lauderdale County MASW measurements). The 20 measurements were broken down into 8 intermediate, 7 terrace, and 5 uplands sites and average velocity profiles determined separately for each group of MASW profiles. In Figure 46 it is clear that these three non-lowlands group average profiles cluster close together and seem distinct from the Lake County representative lowlands profile. The representative Dyer County non-lowlands profile is also shown following the intermediate, terrace, and uplands average velocity profiles. Thus, only a lowlands and non-lowlands representative profile, with their uncertainties, are needed for seismic hazard calculations in Dyer County.

We compare in Figure 47 the two Dyer County representative velocity profiles with the uplands average profile of Romero and Rix (2001) and a representative uplands site velocity profile for Shelby County. At shallower depths less than 20 m, the uplands profiles agree quite well. In Dyer County the top of the faster velocity Eocene sediments can be as shallow as 20 m or less, which can start biasing the MASW profiles to faster velocities especially below 30 m. In Dyer County in the non-lowland areas, the top of the Eocene is typically 30 m and less, although some locations reach a depth of 70 m to the top of the Eocene. A check of the estimated depth to the top of the Eocene at MASW sites from the geology model with the depth at which the Vs exceeds 500 m/s (estimated Eocene Vs) in the MASW profiles shows a fairly good correlation both in Dyer and Lake Counties.
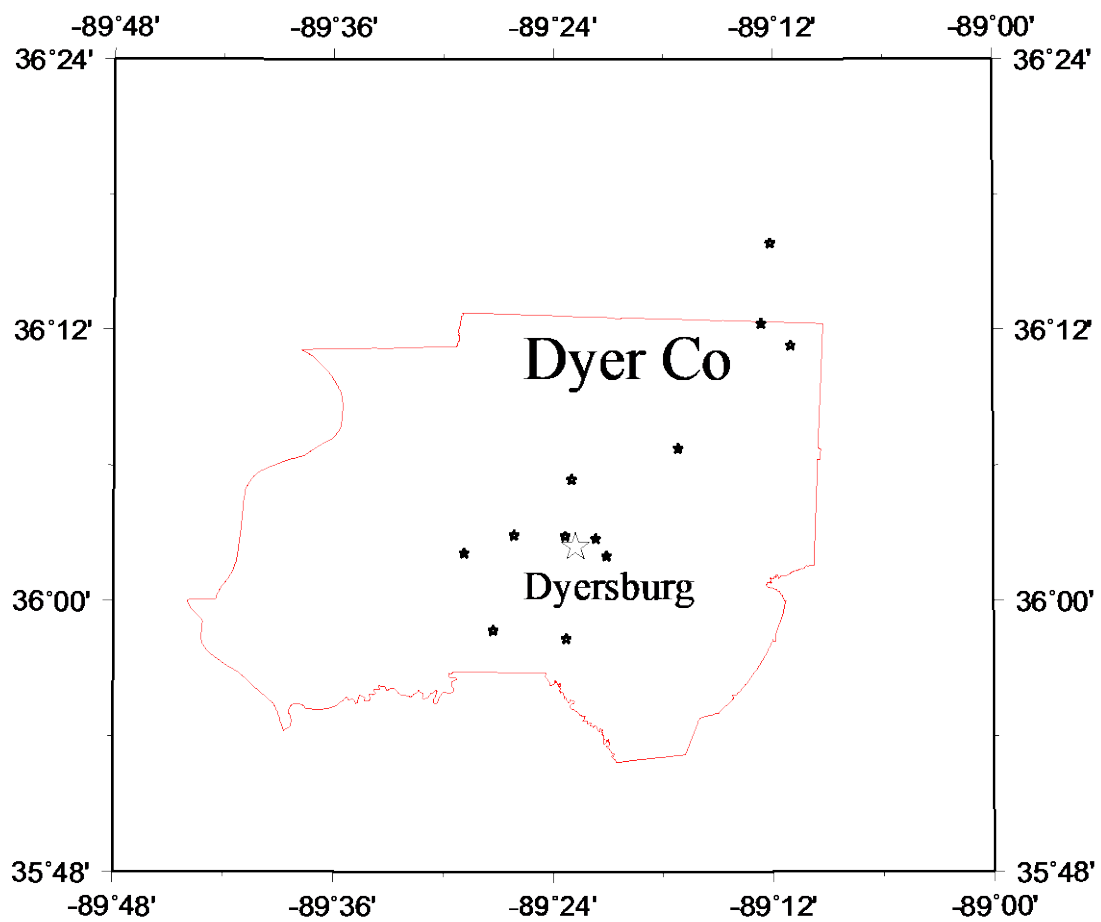
Dyer Co MASW Sites

Figure 44: Location of MASW measurements (filled stars) in and near Dyer County (red outline).
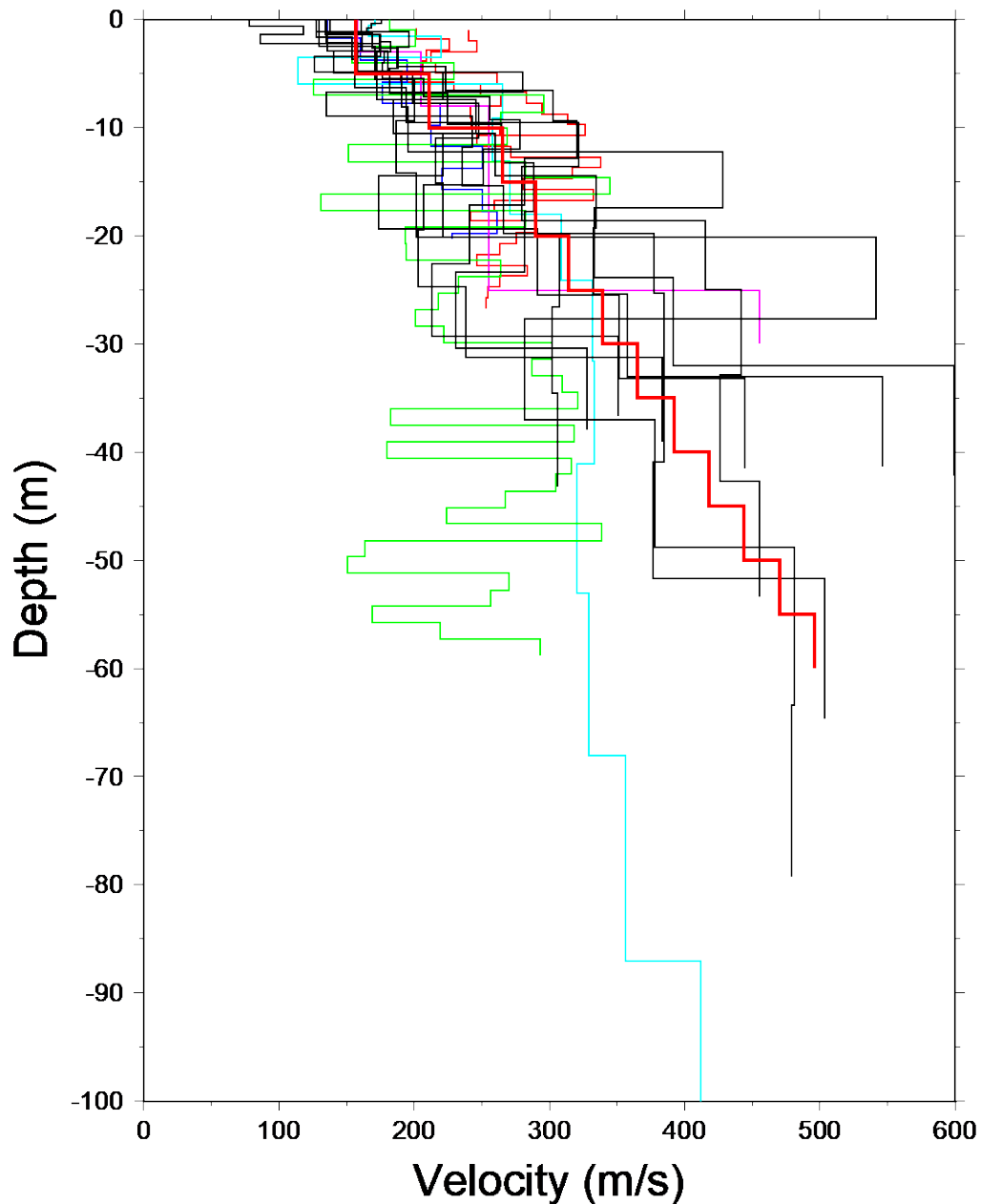
Figure 45: Comparing the velocity profiles obtained via testing at 12 sites (black lines) and 3 published profiles (colored lines) in and near Dyer County. The thick red line is the non-lowlands profile developed from the Dyer County non-lowlands MASW profiles as representative of the velocity gradient in the Quaternary soils.
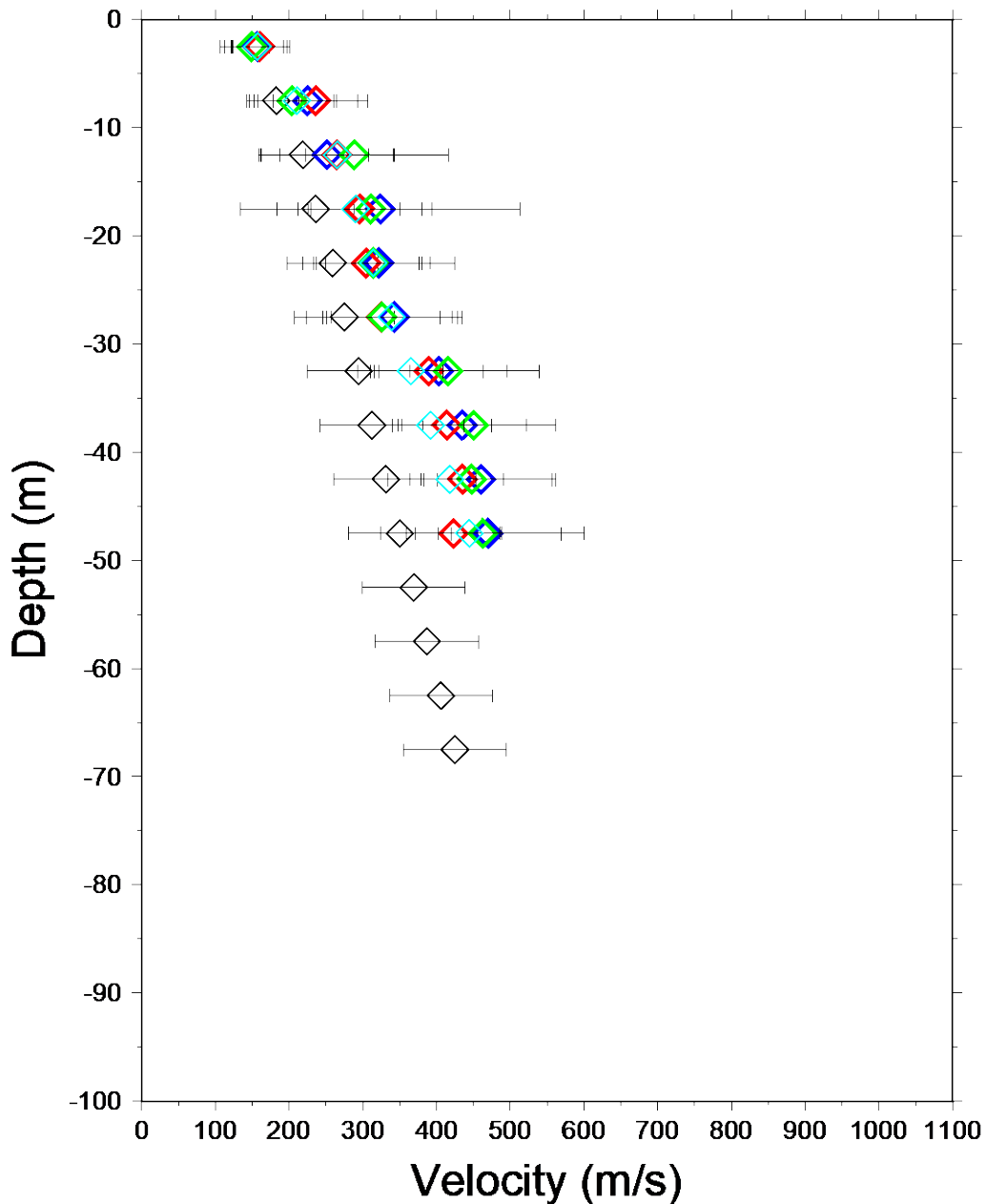
Figure 46: Mean and standard deviation of 8 intermediate (blue), 7 terrace (red), and 5 uplands (green) velocity profiles in Dyer and Lauderdale Counties. Also shown are the adopted velocity profiles (with uncertainties) for non-lowlands in Dyer County (cyan) and lowlands in Dyer and Lake Counties (black).
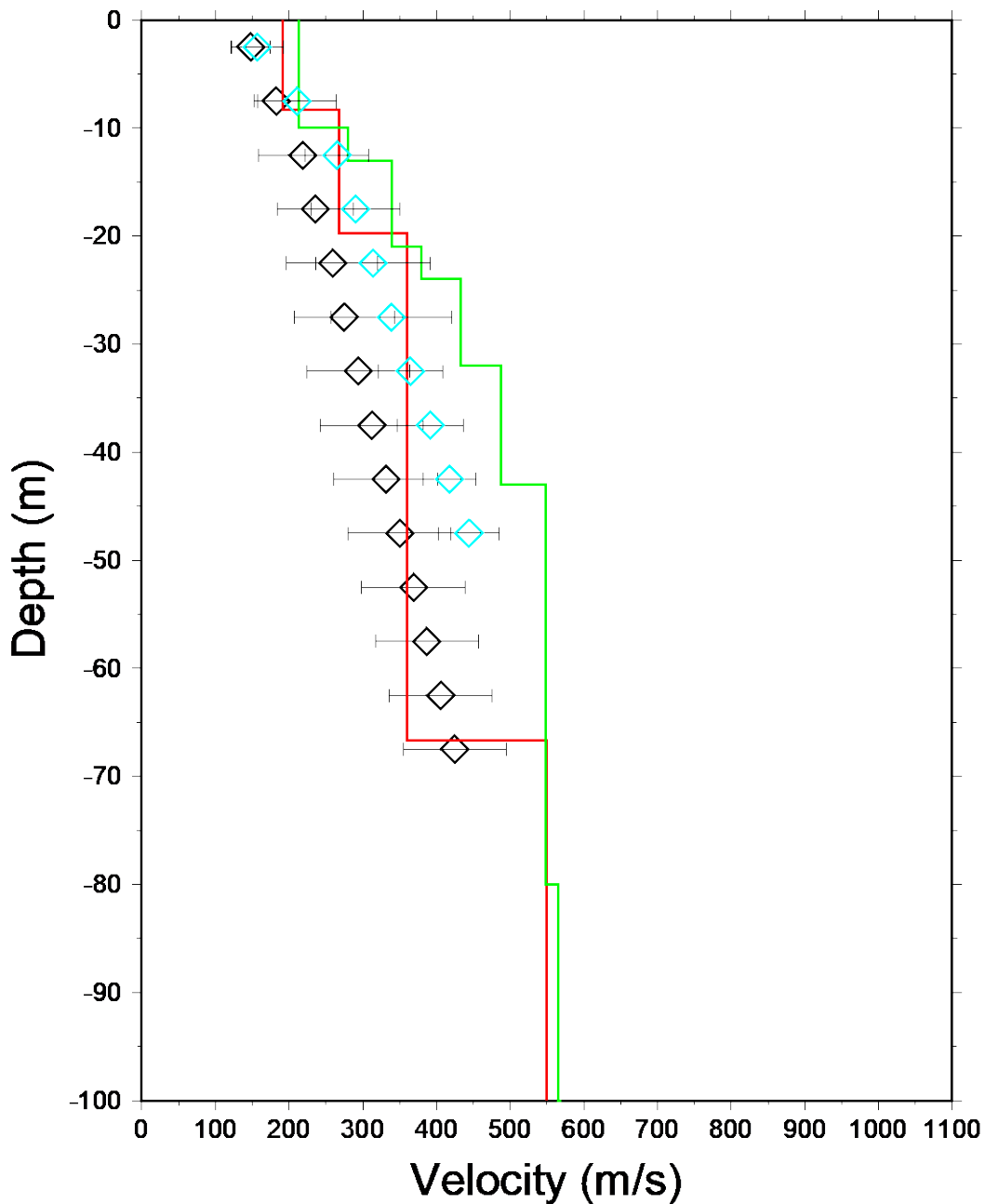
DyLa Co Vs Profiles

Figure 47: Comparison of adopted lowlands (black) and non-lowlands (cyan) velocity profiles for Dyer County with the Romero and Rix (2001) uplands average profile (green line) and typical velocity profile (red line) in Shelby County.

Hazard Maps Development

Methodology

A standard methodology for including the effects of local geology in seismic and liquefaction hazard estimates was used in this study. We followed the approach of Cramer et al. (2006, 2008, 2014, 2017, and 2018a) of developing site amplification distributions on a grid, applying those distributions to modify hard rock hazard curves to geology-specific hazard curves and develop seismic hazard maps, and then applying geology-specific liquefaction probability curves to develop liquefaction hazard maps. The site amplification distributions are based on the 3D geological, geotechnical, and seismological models developed above for Dyer County. The 2014 U.S. Geological Survey (USGS) National Seismic Hazard Project's seismic hazard model (seismic sources and ground motion attenuation model of Petersen et al., 2014) for hard rock was modified using our Dyer County site amplification distributions. Probabilistic seismic hazard maps were generated from the USGS probabilistic model and scenario (deterministic) seismic hazard maps were generated using selected scenario fault ruptures (earthquakes) and the USGS ground motion attenuation model. The resulting peak ground acceleration (PGA) seismic hazard maps were then modified using appropriate Dyer County liquefaction probability curves (discussed above) to generate liquefaction hazard maps (both probabilistic and scenario).

Dyer County Shear-wave Velocity Model

Seismic hazard maps with the effects of local geology depend on developing site amplification distributions on a grid for the 3D geology of the study area. The 3D geology is converted to geologic (sediment) profiles on a uniform grid. The geology layers are converted to shear-wave velocity (Vs) profiles at each grid point and input to a geotechnical soil response program (SHAKE91), along with appropriate geotechnical properties, to develop site response distributions at each grid point using the University of Memphis High Performance Computing (HPC) facility. The site amplification distributions model frequency and amplitude dependent amplification/deamplification at the surface of hard rock ground motions input at the bottom of the sediment profile.

The Dyer County representative velocity models used were developed from published and measured Vs profiles in and near the county as described above. Three separate models were developed for Dyer County, two for the Quaternary sediments above the top of the Eocene deposits and one for the geologic layers from the Eocene to the Paleozoic. The two Quaternary representative velocity models were divided between lowlands and non-lowlands as shown in Figures 46 and 47 above.

The Quaternary Vs models are a step-wise gradient model developed from the shallow Vs observations with different gradients for lowlands and non-lowlands models. The depth to the top of the Eocene layer varies for each profile between less than 30 m and 70 m depth so the gradient trend was projected downward from the all Quaternary sediment trend above 30 m to 50 -70 m in 5 m depth steps. The Eocene Vs jumps to 515 m/s at the top of that layer. Appro-

priate uncertainties based on the statistics (standard deviation) of the profile averaging at each depth interval were developed and applied in the sediment profile randomization process employed in the development of the site amplification distributions at each grid point.

The Eocene to Paleozoic Vs model is the same as developed for Lake County (Cramer et al., 2019). It was developed from the CUSSO deep hole site in Kentucky (Woolery et al., 2016) and published deeper embayment measurements in and near Lake County plus Vs models from Shelby County (Cramer et al., 2006). The borehole geological information mainly constrained the depths to the top of the Eocene, Cretaceous, and Paleozoic (bedrock) layers. In Lake County, very limited observations were available for other intermediate geological layers such as the top of the Memphis Sand, Flour Island clay, Fort Pillow sand, and Old Breastworks clay. The depth to the top of these four geological layers are needed to define the geology and Vs profiles beneath Dyer County. Using the limited observations in Lake County for these four layers and the better constrained isopachs for the top of the Eocene and Cretaceous, we developed a scheme to estimate the depth to the tops of the four intermediate layers between the Eocene and Cretaceous layers. Taking the depth difference between the tops of the Eocene and Cretaceous layers as unity, statistical estimates (average and standard deviation) were determined from the few available measurements for the depth difference between the top of the Eocene and the tops of each intermediate layer. The results in Table 6 are in fraction of the distance between the tops of the Eocene and Cretaceous. We then used these averages and standard deviations to estimate the depth with uncertainty to the top of the intermediate layers at each grid point. Vs values and uncertainties assigned to each intermediate layer was determined from the CUSSO Vs profile and checked and adjusted with available deeper Vs profile observations in Lake County and from the Shelby Co model. Figure 48 and Table 7 show the resulting deeper Vs model and uncertainties used in the site amplification distribution calculations at each grid point.

As a further check on the intermediate Vs profile model developed for Lake County, we compared our model and available observations with the Vs profile from ambient noise (surface-waves) based Vs profile by Chunyu Liu (Figure 49). Liu's results are from the Non-Volcanic Tremor (NVT) L-shaped array of 19 broadband stations with a 60m spacing (600 m on a side). The NVT array was located near Mooring in Lake County. Clearly in Figure 49 below 150 m depths the Liu profile agrees with our model and other observations within the uncertainty. Above 150 m the Liu profile estimates of Vs are lower, but still within uncertainty, although with a loss of resolution in Liu's profile above 50 m. Liu did find an Vs anisotropy between 100 and 140 m depths.

Grids

There is one grid size used in our Dyer County study. The 3D geology for the depth to the top of the Eocene, Cretaceous and Paleocene layers where provided on a 0.005-degree grid (~500 m). These geology inputs were combined using the Quaternary and deeper Vs models discussed above for site amplification distribution and seismic hazard calculations. The final seismic and liquefaction hazard maps use this 0.005-degree grid spacing.
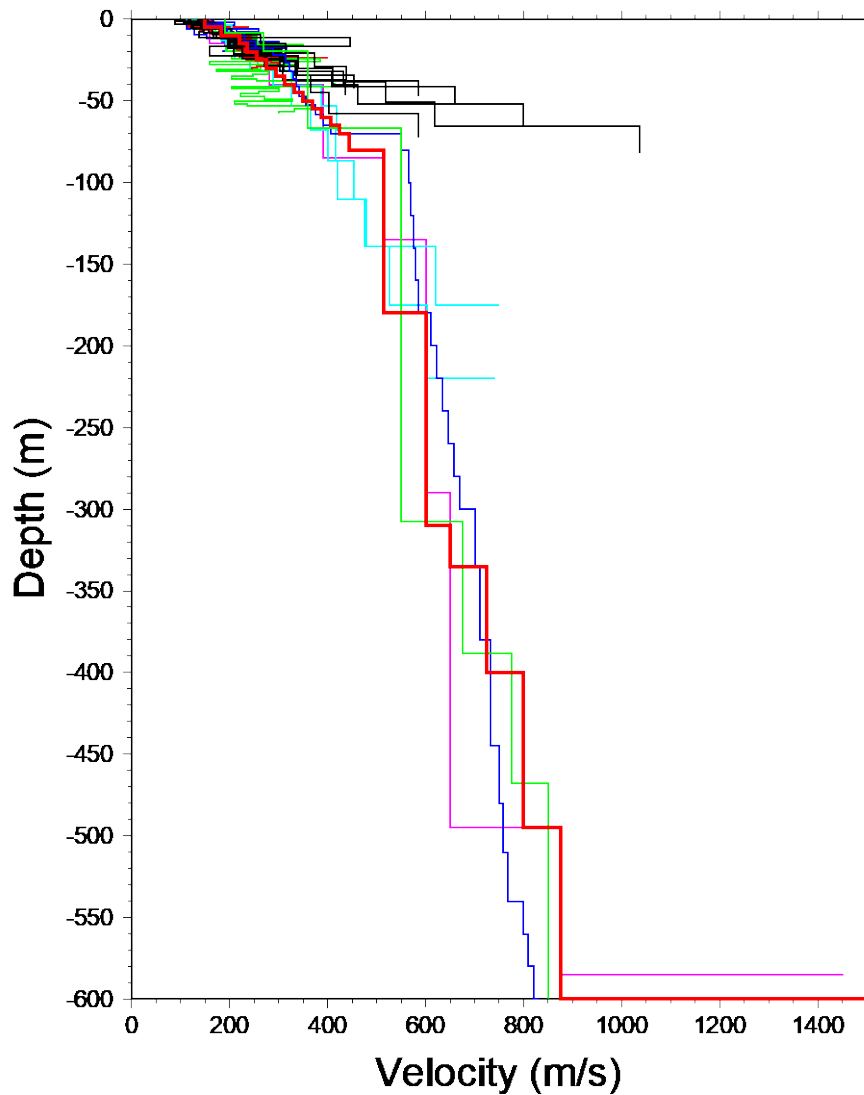
Figure 48: Vs profiles down to 600 m depth with Lake County Quaternary Vs model shown in heavy red line. Thin colored lines are published Vs profiles. Thin black lines are MASW profiles measured as a part of this study. The magneta profile is the CUSSO (Kentucky) deephole profile. The deeper green profile is the Shelby County reference profile. The blue profile is the Romero and Rix (2001) profile.

Table 6: Intermediate layer statistics in fraction of Cretaceous-Eocene depth difference.

Top of Formation	Fractional Distance	Fractional Std. Deviation	# of Observations
Memphis Sand	0.234	±0.029	6
Flour Island (clay)	0.546	±0.034	6
Fort Pillow (sand)	0.611	±0.048	5
Old Breastworks (clay)	0.771	±0.035	5

Table 7: Geotechnical profile used in 3D geology hazard model. Uncertainties are one std. deviation.

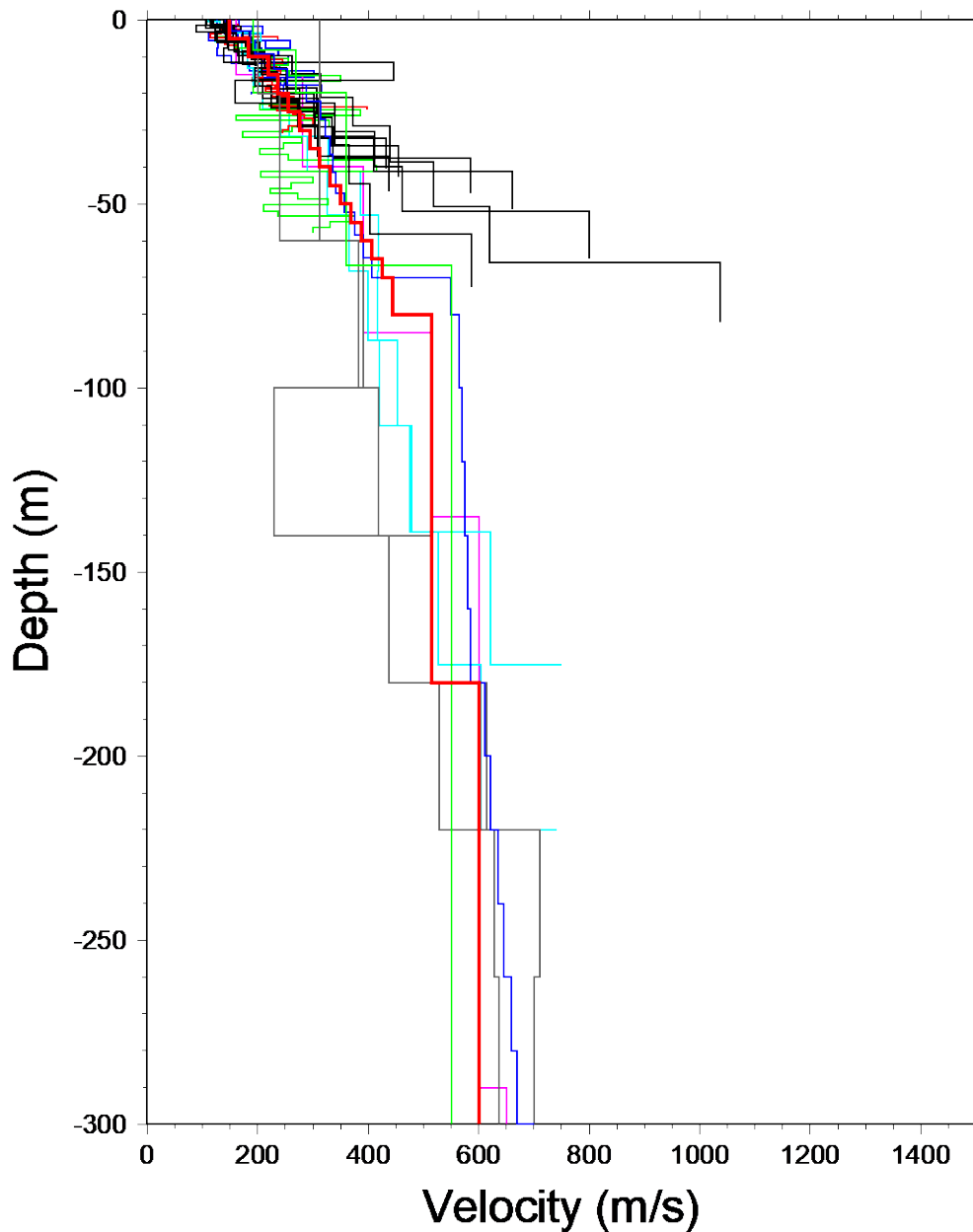| Formation	DepthToTop(m)	Damping	Density(g/cc)	Velocity(m/s)
Alluvium	0.	0.05	2.00	148±13
	5.±0.75	0.05	2.00	183±15
	10.±0.75	0.03	2.00	219±30
	15.±0.75	0.03	2.00	236±26
	20.±0.75	0.03	2.00	259±31
	25.±0.75	0.03	2.00	275±34
	30.±0.75	0.02	2.00	294±35
	35.±0.75	0.02	2.00	312±35
	40.±0.75	0.02	2.00	331±35
	45.±0.75	0.02	2.00	350±35
	50.±0.75	0.02	2.00	369±35
	55.±0.75	0.02	2.00	387±35
	60.±0.75	0.02	2.00	406±35
	65.±0.75	0.02	2.00	425±35
	70.±0.75	0.02	2.00	444±35
Eocene	80.±1.00	0.02	2.00	515±127
Memphis Sand	180±12	0.02	2.00	600±50
Flour Island	310±7.5	0.02	2.00	650±25
Fort Pillow	335±15	0.01	2.00	725±15
Old Breastworks	400±13	0.01	2.00	800±25
Cretaceous	495±13	0.01	2.50	875±63
Paleozoic	600±13	0.001	2.80	2800

Lake Co Vs Profiles

Figure 49: Vs profiles down to 300 m depth with Lake County Quaternary Vs model shown in heavy red line. The grey lines are Chunyu Liu's NVT profiles. The other profiles are colored as indicated in Figure 48.

Time History Database

The site amplification distribution calculations use a suite of input time histories (seismograms) at the bedrock/sediment interface to estimate sediment response. Time histories are required by soil response computer programs to estimate site response. The time histories used are listed in Table 8 and have been used by Cramer et al. (2006, 2017, and 2018) in similar seismic hazard analyses. At each grid point, the time history used is randomly selected for each iteration in the soil profile randomization to properly include uncertainty in the site amplification distribution calculations.

Table 8: Strong motion time series on rock used in the analysis (Cramer, 2006).

Earthquake	Station	Components
1989 **M** 6.9 Loma Prieta, California	G01	E, N
1992 **M** 7.1 Cape Mendocino, California	CPM	E, N
1992 **M** 7.3 Landers, California	JOS	E, N
1995 **M** 6.9 Kobe, Japan	KJM	E, N
1999 **M** 7.4 Kocaeli, Turkey	GBZ	W
	IZT	S
1999 **M** 7.6 Chi-Chi, Taiwan	TCU	N, W
1999 **M** 7.1 Duzce, Turkey	1060	E, N
Atkinson and Beresnev (2002)	**M** 7.5 and **M** 8.0 at Memphis, Tennessee	

Hazard Maps

Seismic and liquefaction hazard maps have been developed for both probabilistic and scenario cases. Probabilistic hazard maps have been generated for 10%, 5%, and 2% probability of exceedance in 50 years. The 2%-in-50-year maps correspond to current building code standards and represent up to the 80 percentile New Madrid seismic ground motions. 5%-in-50-year maps are similar to median scenario ground motion maps for the **M**7 earthquakes in the New Madrid seismic zone and represent up to 60 percentile ground motions. The 10%-in-50-year maps correspond to an older design standard and only represent up to 35 percentile ground motions from the New Madrid seismic zone (NMSZ) sources. The 10%-in-50-year maps do not adequately represent expected median ground motions from New Madrid 1811-1812 earthquakes, are no longer recommended for design purposes by regulatory agencies, and are not presented here.

Median ground motion scenario (deterministic) hazard maps have been generated for seven scenario earthquakes (Table 9 and Figure 50A,B) and represent median expected ground motions from those earthquakes. The scenarios are for the largest earthquakes from the 1811-1812 New Madrid sequence, a **M**6 earthquakes in 1843, and for a hypothetical **M**5.8 earthquake in Dyer County. Because of its distance from Dyer County and low expected ground motions, the historical **M**6 in 1895 earthquake is not included in our collection of scenarios for

Dyer County. The **M**5.8 scenario represents the effects of recent **M**5.5-6.0 Central and Eastern North American earthquakes if a similar size earthquake were to occur in Dyer County.

The ground motion periods represented in the Dyer County seismic hazard maps are peak ground acceleration (PGA), 0.2 s, and 1.0 s. 0.3 s maps have also been generated for compatibility with HAZUS, a risk and loss assessment package commonly used in loss analysis. The 0.2 and 0.3 s hazard maps are similar so the 0.3 s hazard maps are not shown in this report.

Table 9: Scenario earthquakes used in Dyer County study.
M 7.7 on the Reelfoot Thrust (central segment)
M 7.5 on the Cottonwood Grove Fault (SW segment)
M 7.3 on the New Madrid North Fault (NE segment)
M 6.9 "Dawn" Aftershock (2 alternatives)
M 6.2 near Marked Tree, Arkansas (1843 earthquake)
Hypothetical M 5.8 earthquake near Dyersburg (recent CEUS earthquakes)

Figure 50A: Potential scenario ruptures for Dyer County. 1811–1812 **M**7 ruptures indicted by **M**7.5, **M**7.3, and **M**7.7. 1811 **M**6.9s indicate two alternative "Dawn" aftershock ruptures. 1843 and 1895 **M**6.2s indicate historic end of seismic zone ruptures.
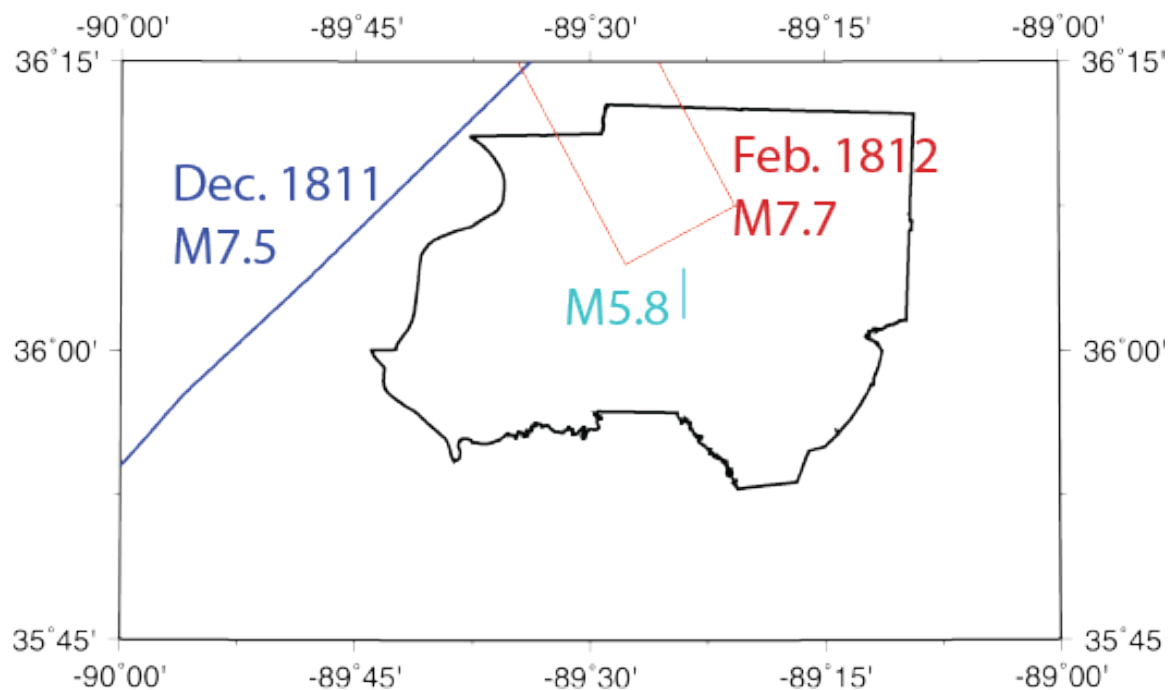
Figure 50B: Scenario ruptures close to Dyer County. The Dec. 1811 is strike-slip mainshock rupture extending out of the map view. The Feb. 1812 is trust mainshock rupture mostly out of map view. The **M**5.8 is a hypothetical earthquake in Dyer County.

Seismic Hazard Maps

Figures 51 - 53 show the 5%-in-50-year probabilistic seismic hazard maps for Dyer County for PGA, 0.2 s, and 1.0 s. The background maps are the equivalent USGS national seismic hazard maps for B/C boundary conditions (Vs30 = 760 m/s). At short periods (PGA and 0.2 s) the Dyer County range of values is 0.4 – 1.1 g (g is the acceleration of gravity at the earth's surface – 9.80665 m/s). At long periods (1.0 s) the range is 0.4 – 0.8 g. Short period seismic hazard is for 1-2 story buildings, while long period hazard is for ~10 story buildings.

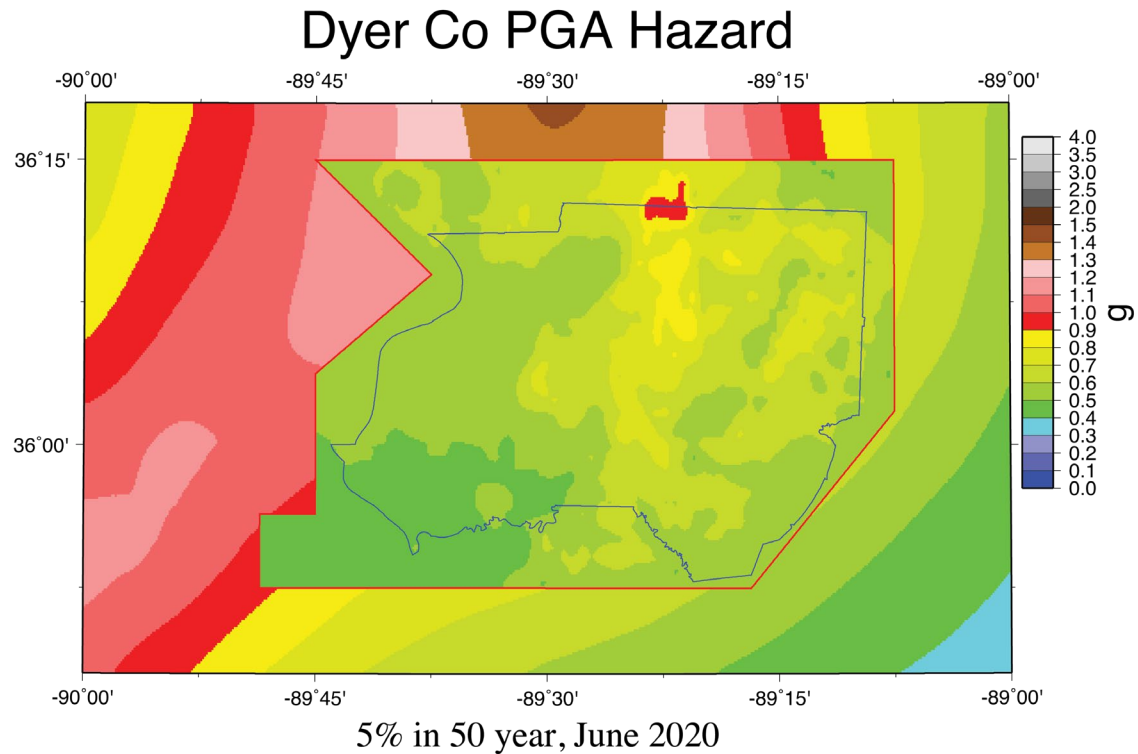# Dyer Co PGA Hazard

5% in 50 year, June 2020

Figure 51: 5%-in-50-year PGA hazard map for Dyer County with the effects of local geology inset on the U.S. Geological Survey's national seismic hazard map for BC boundary conditions.
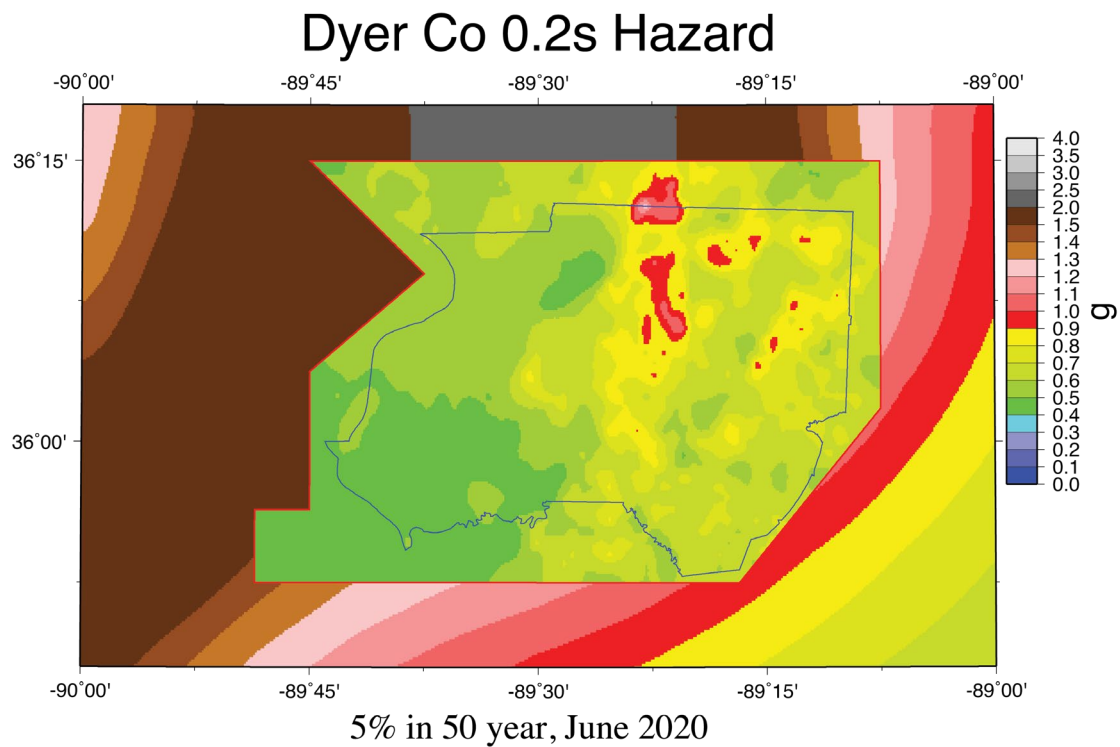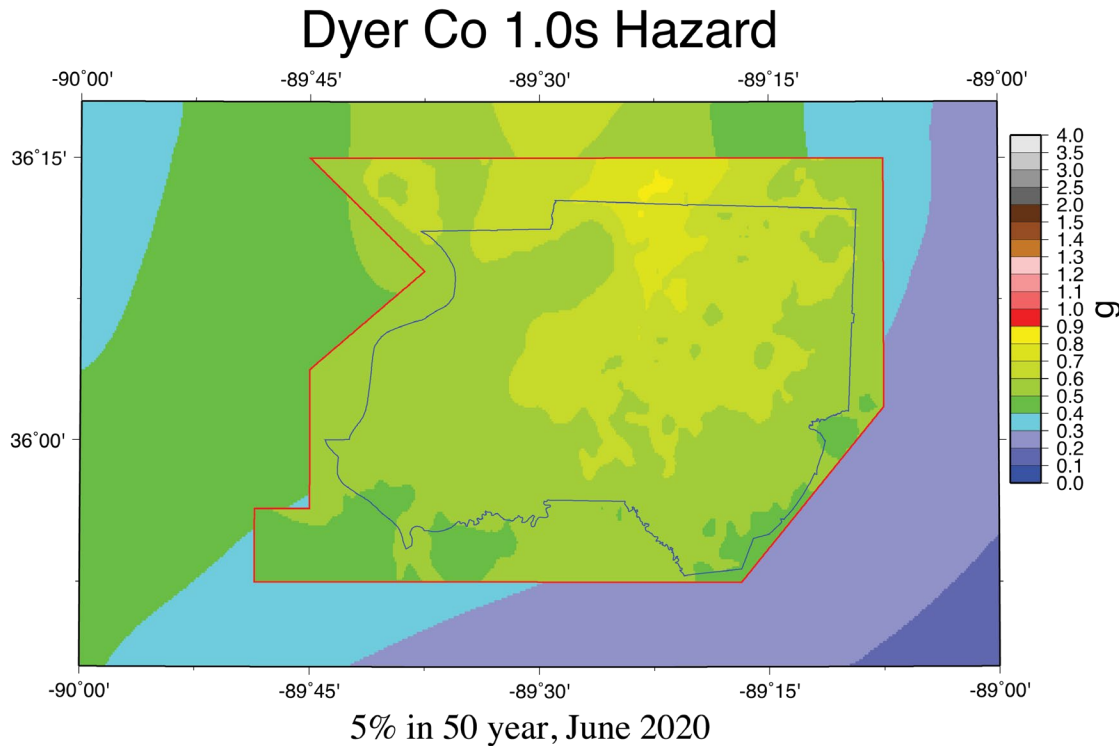
Dyer Co 0.2s Hazard

5% in 50 year, June 2020

Figure 52: 5%-in-50-year 0.2 s hazard map for Dyer County with the effects of local geology inset on the U.S. Geological Survey's national seismic hazard map for BC boundary conditions.

Dyer Co 1.0s Hazard

5% in 50 year, June 2020

Figure 53: 5%-in-50-year 1.0 s hazard map for Dyer County with the effects of local geology inset on the U.S. Geological Survey's national seismic hazard map for BC boundary conditions.

Figures 54 - 56 show the 2%-in-50-year probabilistic seismic hazard maps for Dyer County. The hazard range is high than the 5%-in-50-year maps: 0.6 – 1.4 g for PGA, 0.6 – 1.5 g for 0.2 s, and 0.6 – 1.3 g for 1.0 s.

The probabilistic seismic hazard maps with the effect of local geology show a short period reduction of 30% to 70% and a long period amplification of 10% to 100% relative to the USGS national seismic hazard maps at the same periods. The short period reduction is due to estimated ground motion nonlinear soil effects strongly reducing the high ground motions expected near the earthquake sources. The long period amplification is due to the reduced nonlinear effects and increase dominance of soil column resonant effects amplifying ground motions. As we progress further from the earthquake sources the ground motion level decreases, the nonlinear effects decrease, and the dominance of resonance effects increases. In Shelby County, about 50 km from the New Madrid earthquake sources, Cramer et al. (2018a) show Shelby County seismic hazard maps with 40 – 60% decreases at short period and 50 – 100 % increases at long period over the USGS national seismic hazard maps. Another feature of the probabilistic seismic hazard maps is the very high ground motion estimates exceeding 0.9 g in the north central portion of the county. These high estimates are due to Quaternary sediment cover thinning to less than 10 m in thickness. This deceases the nonlinear effects, particularly at short periods, and increases ground motions and hazard. This north central Dyer county region is also close to the earthquake sources in the model.
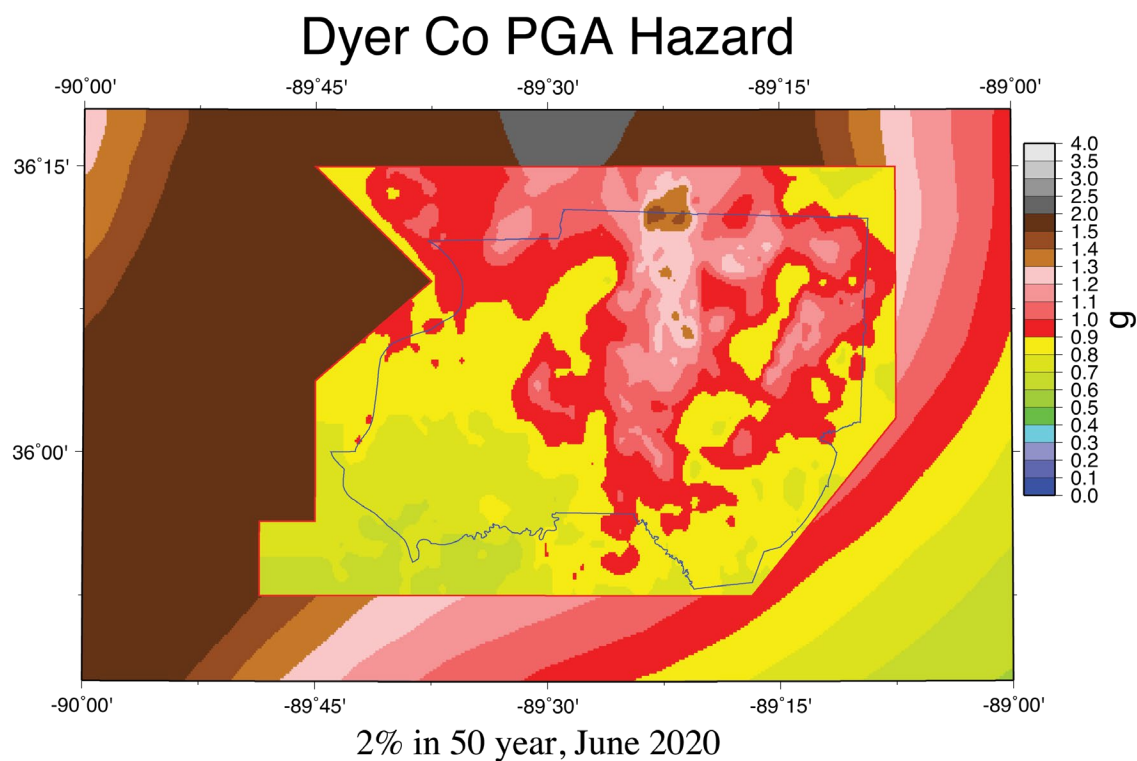
61

Dyer Co PGA Hazard

2% in 50 year, June 2020

Figure 54: 2%-in-50-year PGA hazard map for Dyer County with the effects of local geology inset on the U.S. Geological Survey's national seismic hazard map for BC boundary conditions.
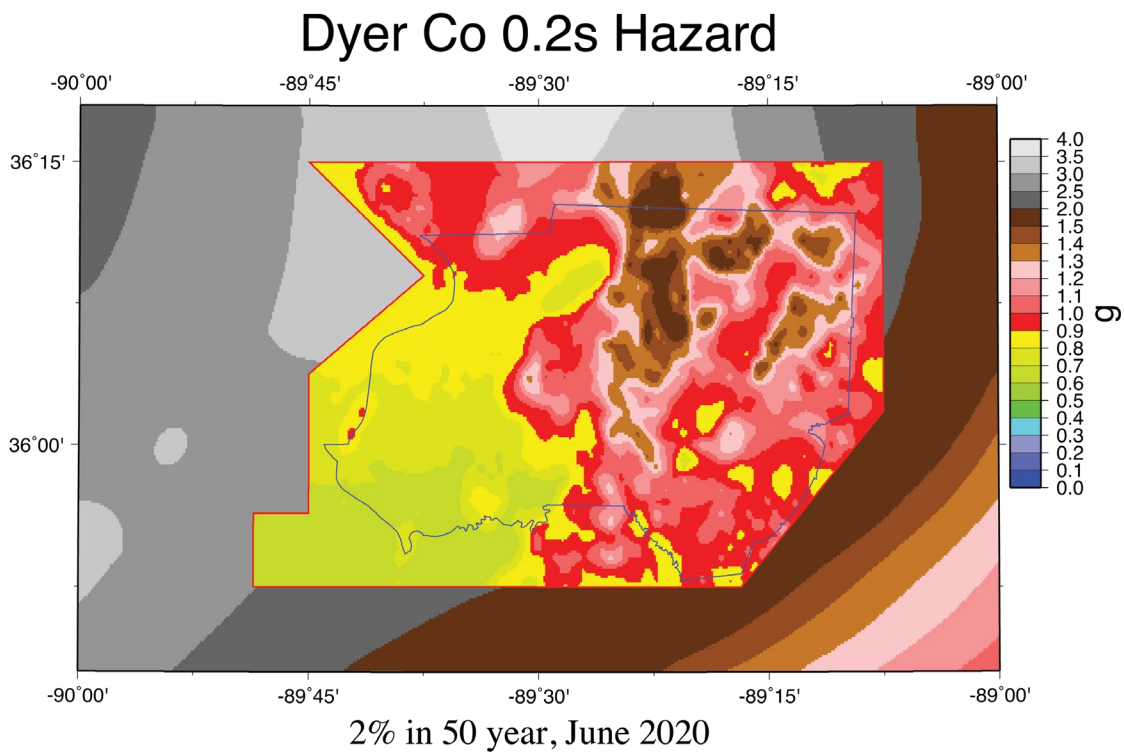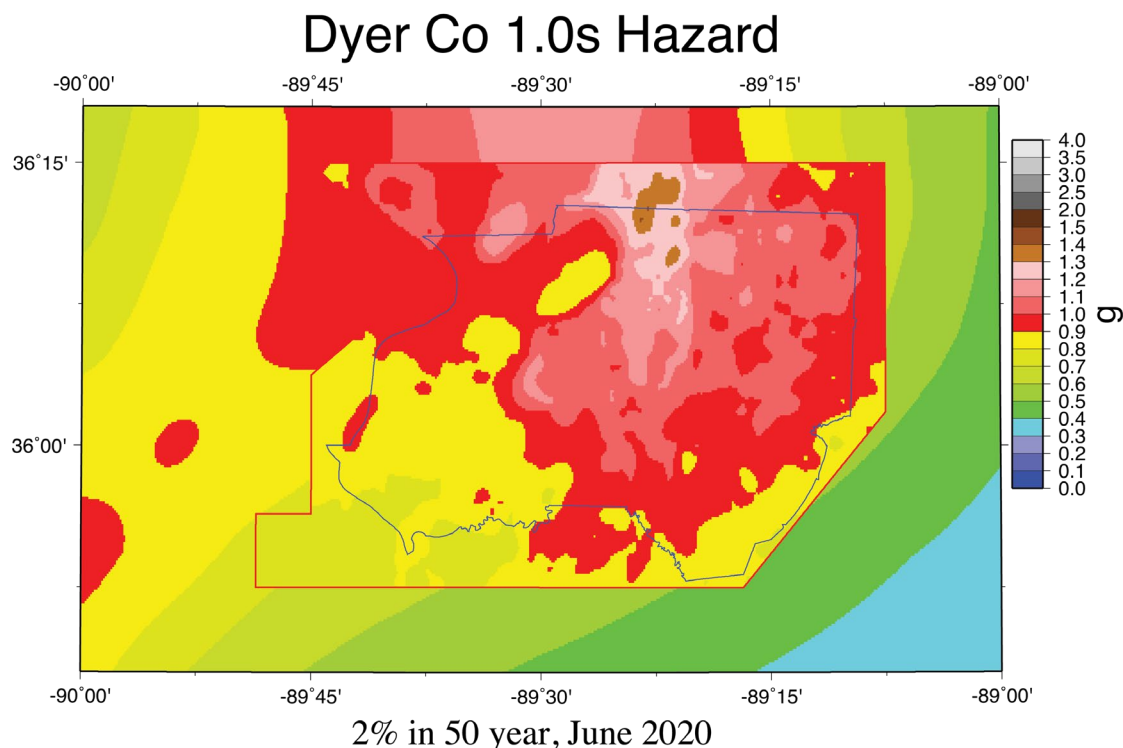
Dyer Co 0.2s Hazard

2% in 50 year, June 2020

Figure 55: 2%-in-50-year 0.2 s hazard map for Dyer County with the effects of local geology inset on the U.S. Geological Survey's national seismic hazard map for BC boundary conditions.

Dyer Co 1.0s Hazard

2% in 50 year, June 2020

Figure 56: 2%-in-50-year 1.0 s hazard map for Dyer County with the effects of local geology inset on the U.S. Geological Survey's national seismic hazard map for BC boundary conditions.

Figures 57 - 63 present the PGA, 0.2 s, and 1.0 s seismic hazard maps for the seven scenarios of Table 9. There are no equivalent comparisons to the USGS probabilistic maps for these scenarios. At all periods shown, the M7 New Madrid scenario hazard maps range from 0.3 to 1.2 g for a repeat of the M7.7 February 1812 earthquake, from 0.3 to 0.6 g for the repeat of the M7.5 December 1811 earthquake, and 0.1 to 0.4 g for the repeat of the M7.3 January 1812 earthquake. The M6.9 largest aftershock hazard map alternatives range from 0.1 to 0.6 g if on the northern end of the SW arm and 0.2 to 0.9 g if on the east end of the Reelfoot thrust. The M6.2 1843 scenario ground motions are 0.1 to 0.2 g, and the M5.8 hypothetical Dyer County earthquake ground motions ranges from 0.1 – 0.6 g. Thus, both the scenario and probabilistic seismic hazard maps show similar ground motion levels at short and long periods due to the close proximity of ruptures and the effect of soils of the Mississippi embayment. These scenarios continue to show the higher hazard in the north central portion of the county seen in the probabilistic hazard maps, due to the thin Quaternary sediment in that region along with the proximity to seismic sources in several cases.
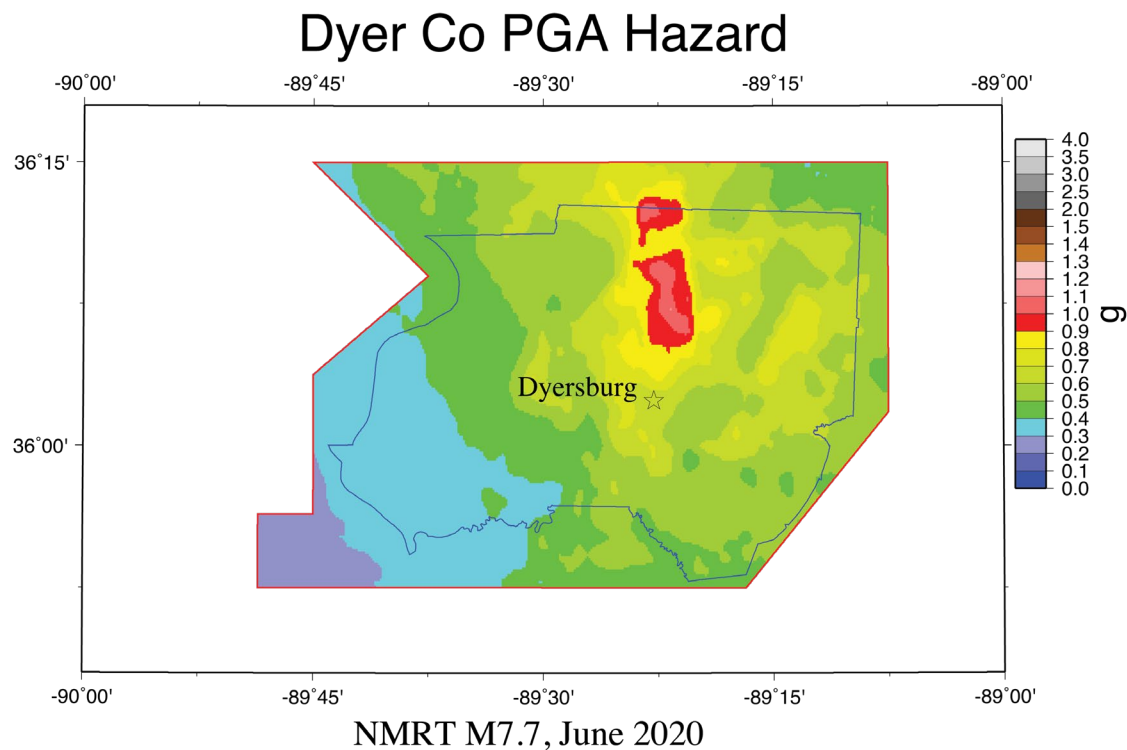
Dyer Co PGA Hazard

NMRT M7.7, June 2020

Figure 57A: Scenario PGA hazard map for a M7.7 earthquake on the Reelfoot Thrust (central segment of NMSZ) for Dyer County with the effects of local geology.
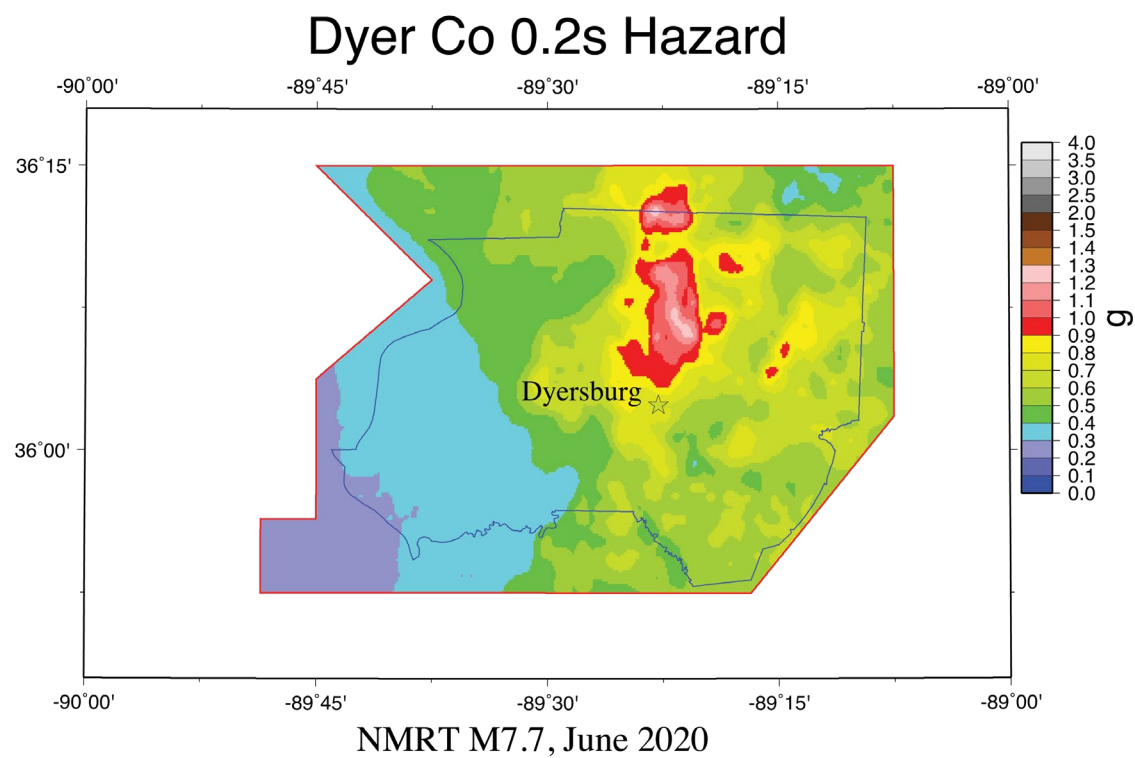
Dyer Co 0.2s Hazard

NMRT M7.7, June 2020

Figure 57B: Scenario 0.2 s hazard map for a M7.7 earthquake on the Reelfoot Thrust (central segment of NMSZ) for Dyer County with the effects of local geology.
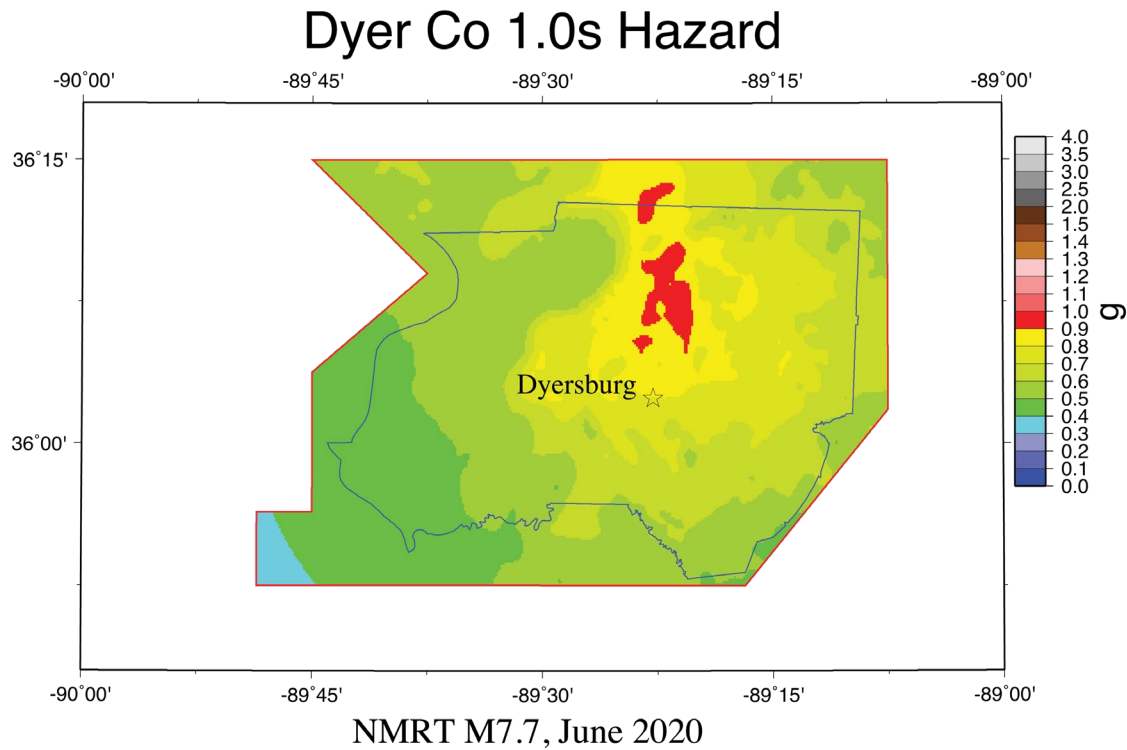
Dyer Co 1.0s Hazard

NMRT M7.7, June 2020

Figure 57C: Scenario 1.0 s hazard map for a M7.7 earthquake on the Reelfoot Thrust (central segment of NMSZ) for Dyer County with the effects of local geology.
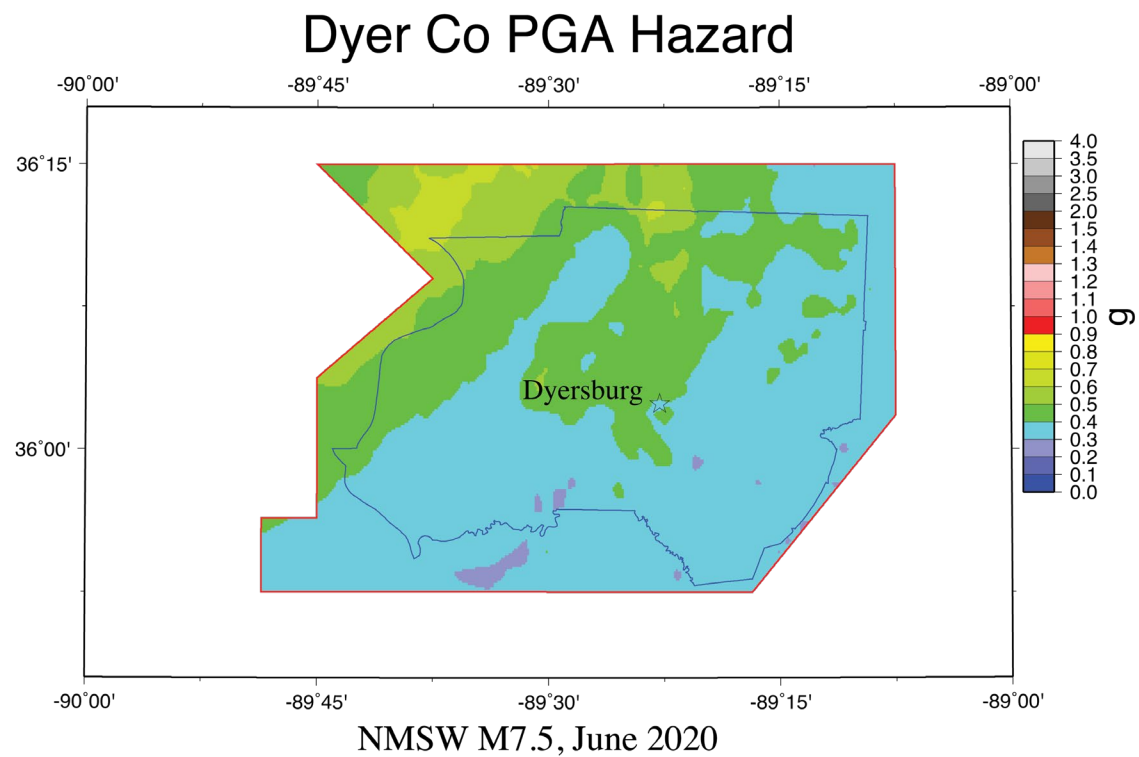
Dyer Co PGA Hazard

NMSW M7.5, June 2020

Figure 58A: Scenario PGA hazard map for a M7.5 earthquake on the Cottonwood Grove Fault (SW segment of NMSZ) for Dyer County with the effects of local geology.
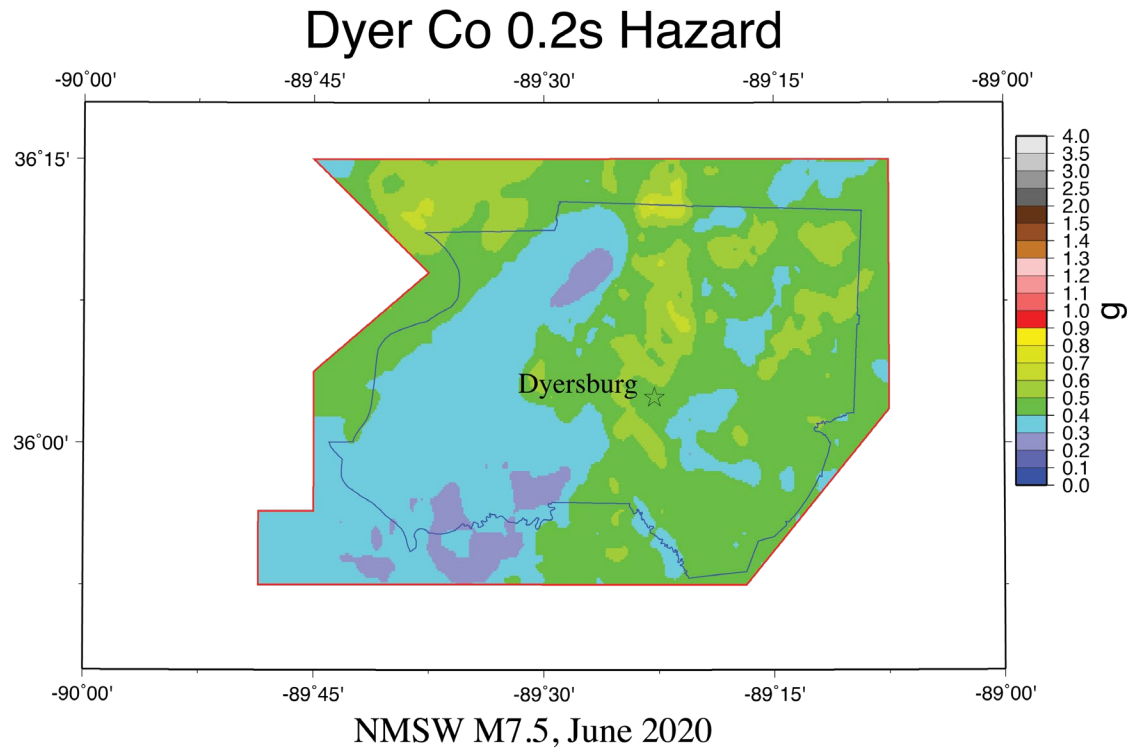
Dyer Co 0.2s Hazard

NMSW M7.5, June 2020

Figure 58B: Scenario 0.2 s hazard map for a M7.5 earthquake on the Cottonwood Grove Fault (SW segment of NMSZ) for Dyer County with the effects of local geology.
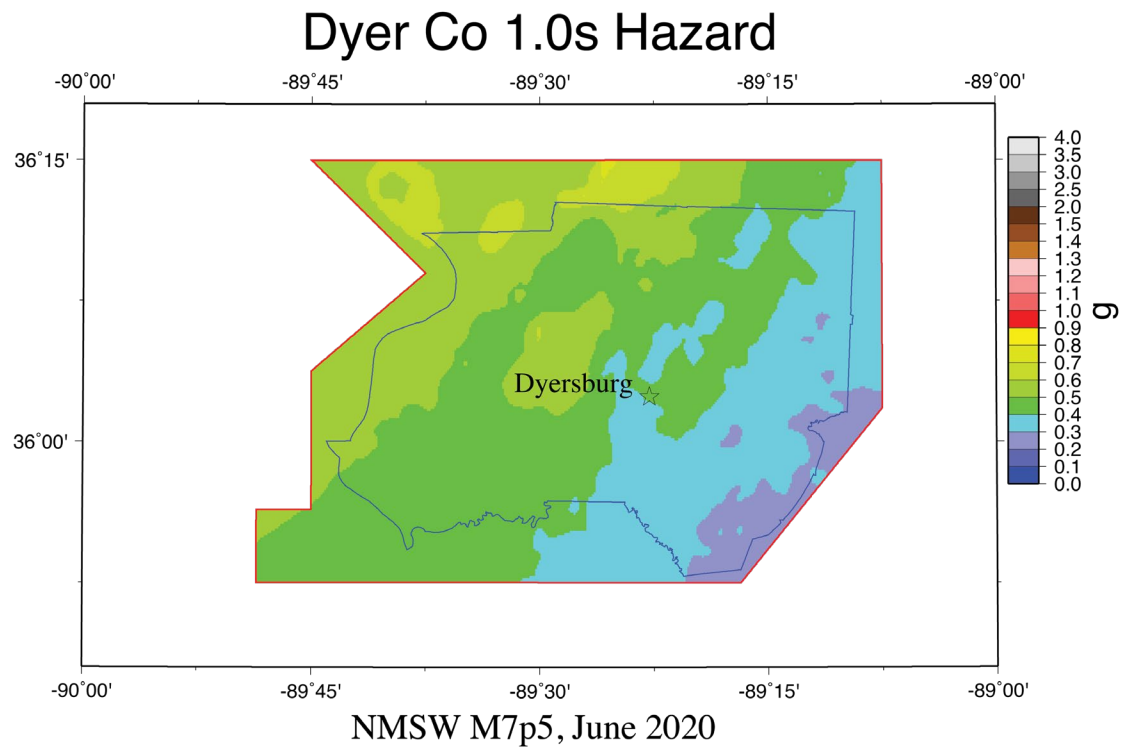
Dyer Co 1.0s Hazard

NMSW M7p5, June 2020

Figure 58C: Scenario 1.0 s hazard map for a M7.5 earthquake on the Cottonwood Grove Fault (SW segment of NMSZ) for Dyer County with the effects of local geology.
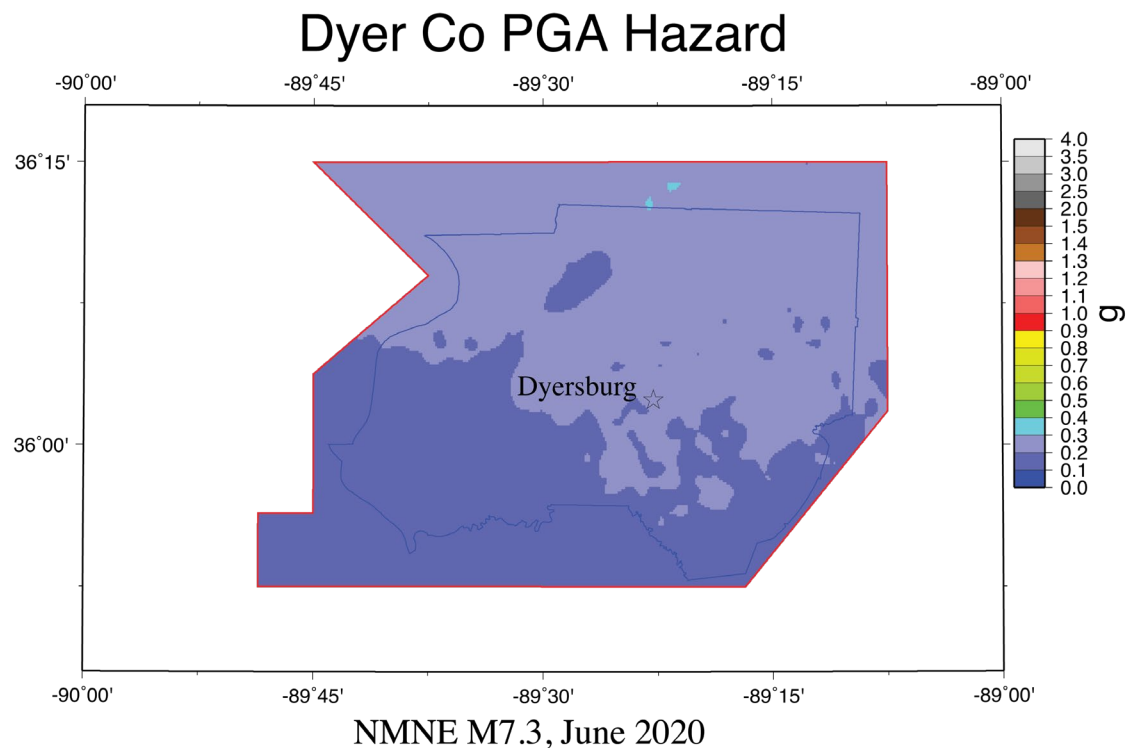
Figure 59A: Scenario PGA hazard map for a M7.3 earthquake on the New Madrid North Fault (NE segment of NMSZ) for Dyer County with the effects of local geology.
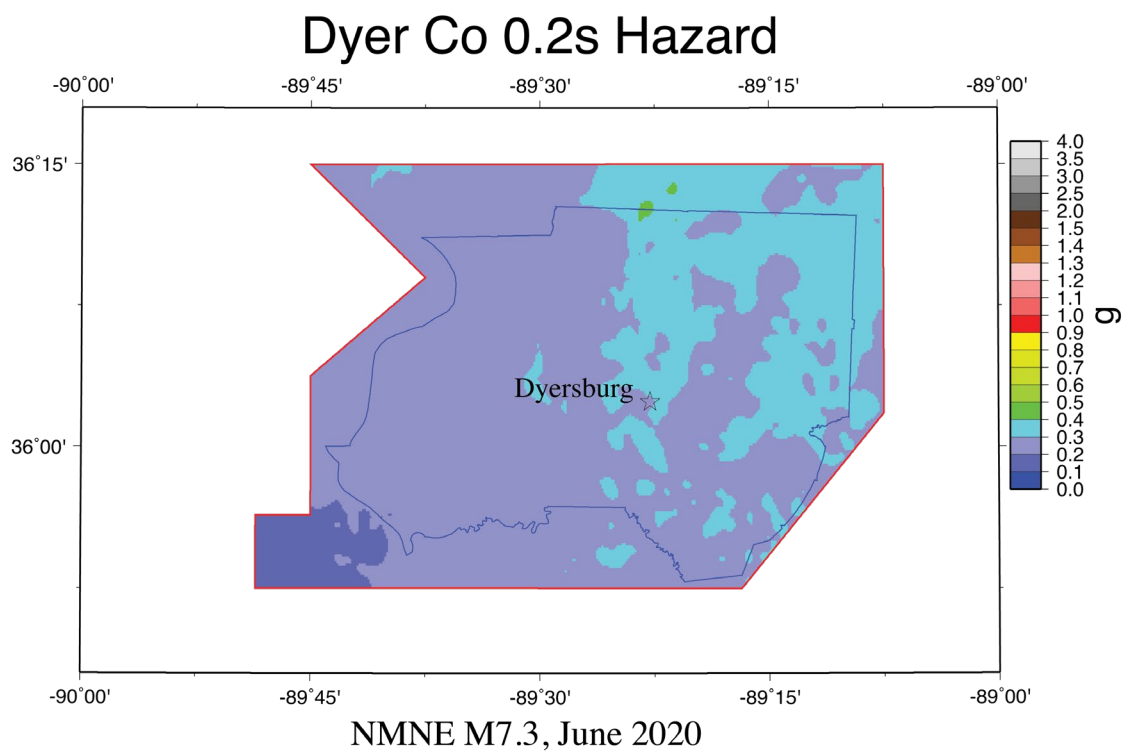

Figure 59B: Scenario 0.2 s hazard map for a M7.3 earthquake on the New Madrid North Fault (NE segment of NMSZ) for Dyer County with the effects of local geology.
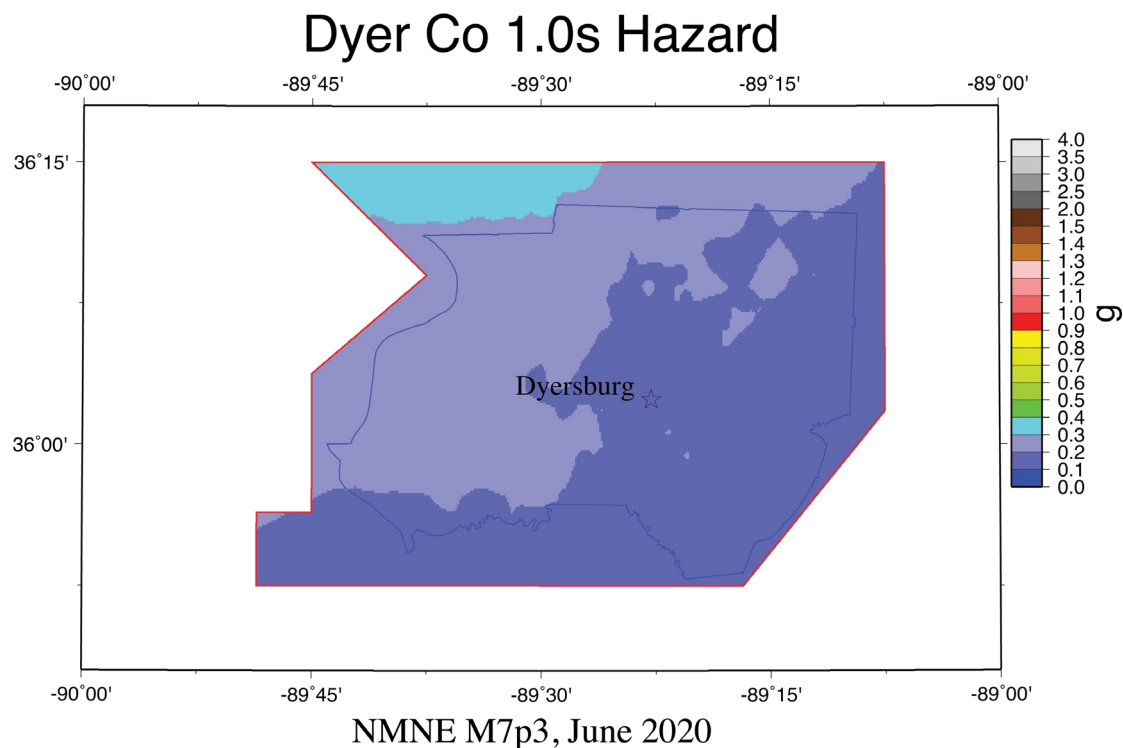
Dyer Co 1.0s Hazard

NMNE M7p3, June 2020

Figure 59C: Scenario 1.0 s hazard map for a M7.3 earthquake on the New Madrid North Fault (NE segment of NMSZ) for Dyer County with the effects of local geology.
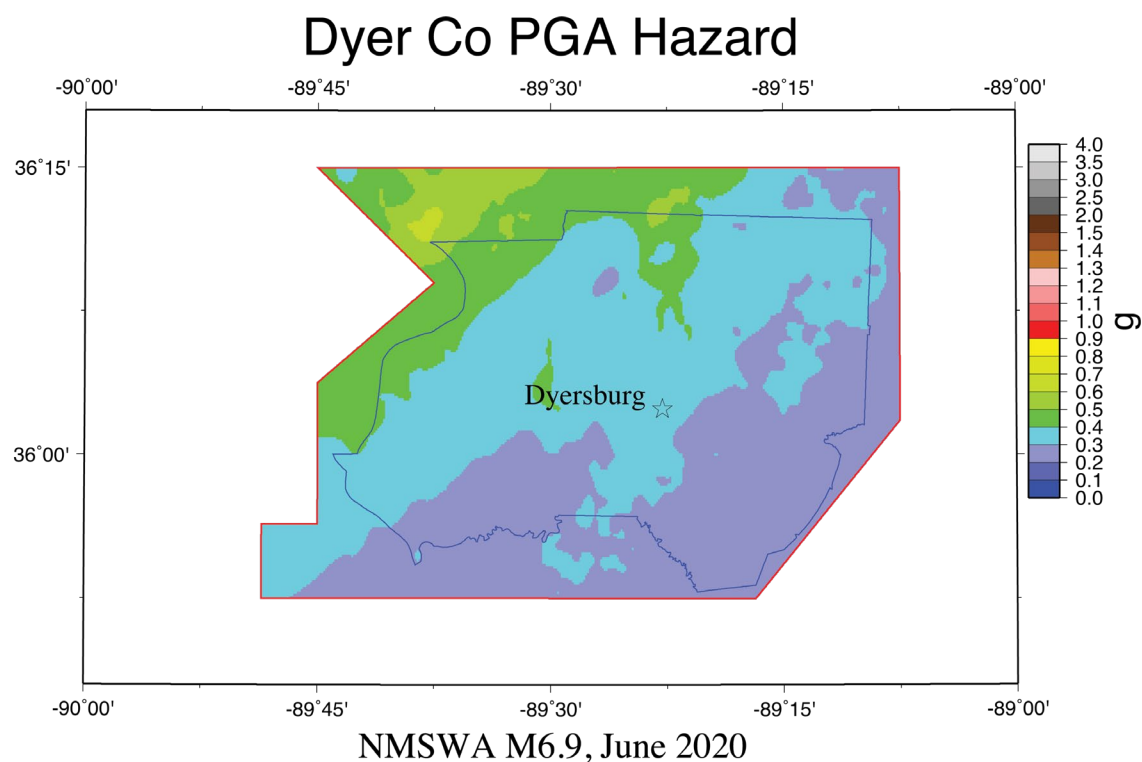
Dyer Co PGA Hazard

NMSWA M6.9, June 2020

Figure 60A: Scenario PGA hazard map for a M6.9 "Dawn" aftershock (alt. 1) on the Cottonwood Grove Fault (SW segment of NMSZ) for Dyer County with the effects of local geology.
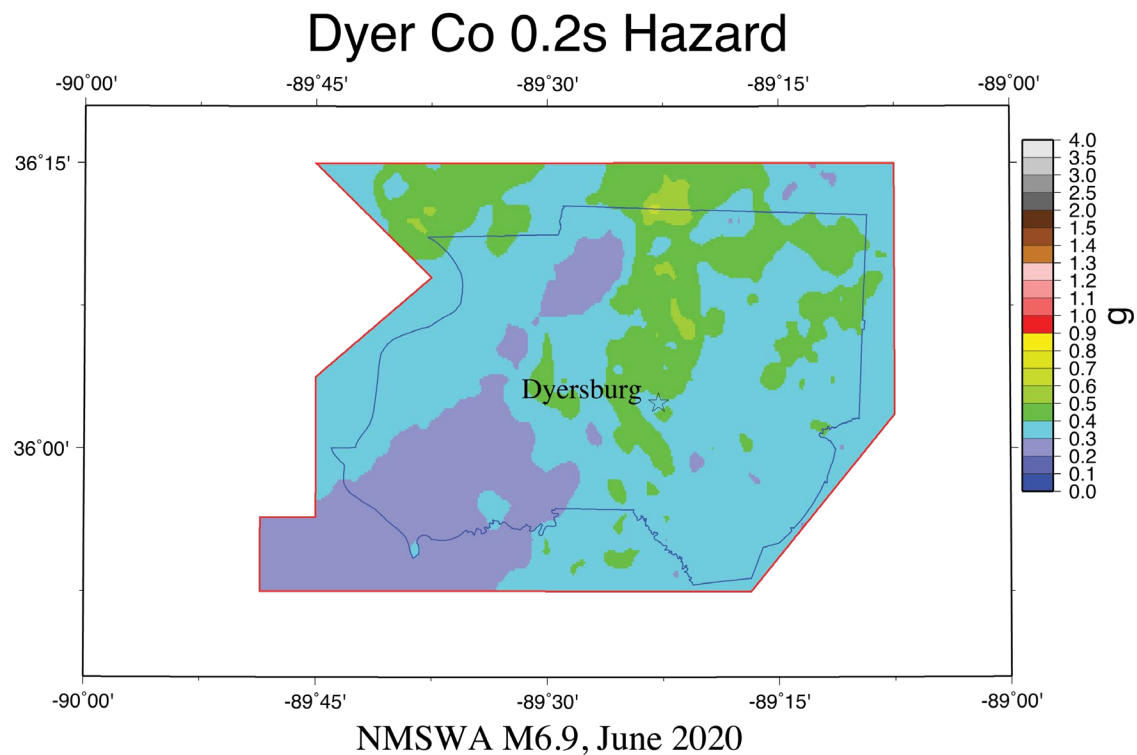
Dyer Co 0.2s Hazard

NMSWA M6.9, June 2020

Figure 60B: Scenario 0.2 s hazard map for a M6.9 "Dawn" aftershock (alt. 1) on the Cottonwood Grove Fault (SW segment of NMSZ) for Dyer County with the effects of local geology.

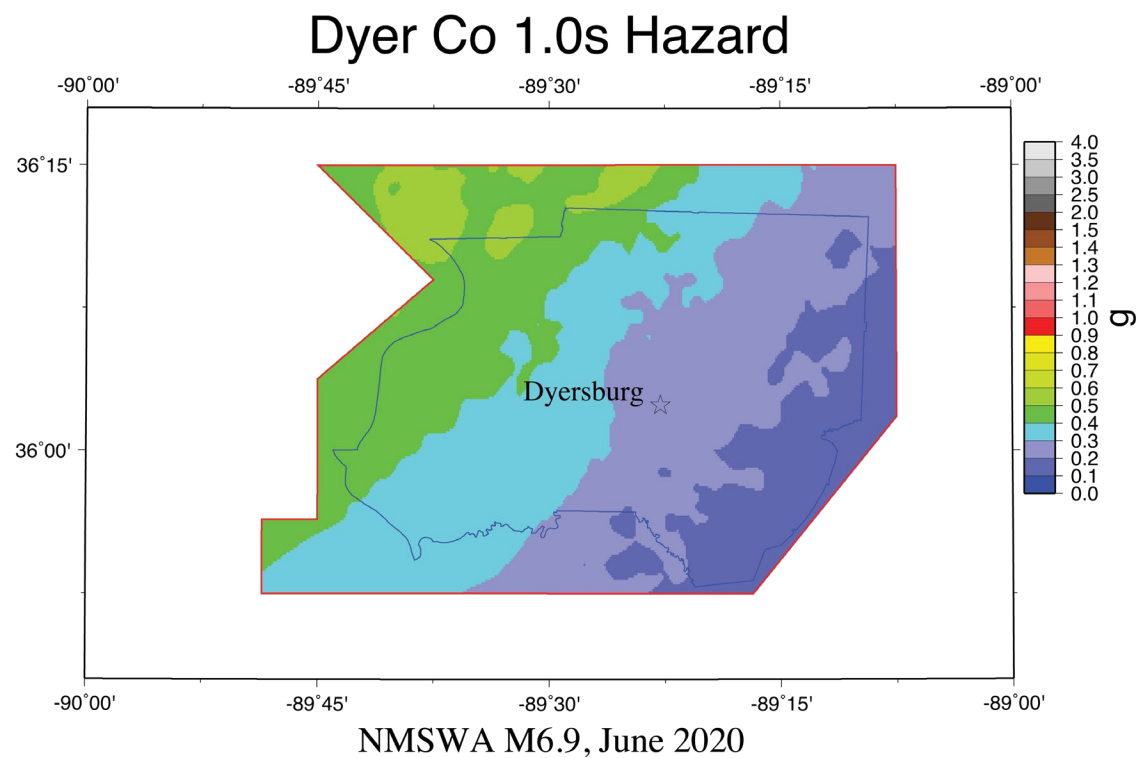## Dyer Co 1.0s Hazard

NMSWA M6.9, June 2020

Figure 60C: Scenario 1.0 s hazard map for a M6.9 "Dawn" aftershock (alt. 1) on the Cottonwood Grove Fault (SW segment of NMSZ) for Dyer County with the effects of local geology.
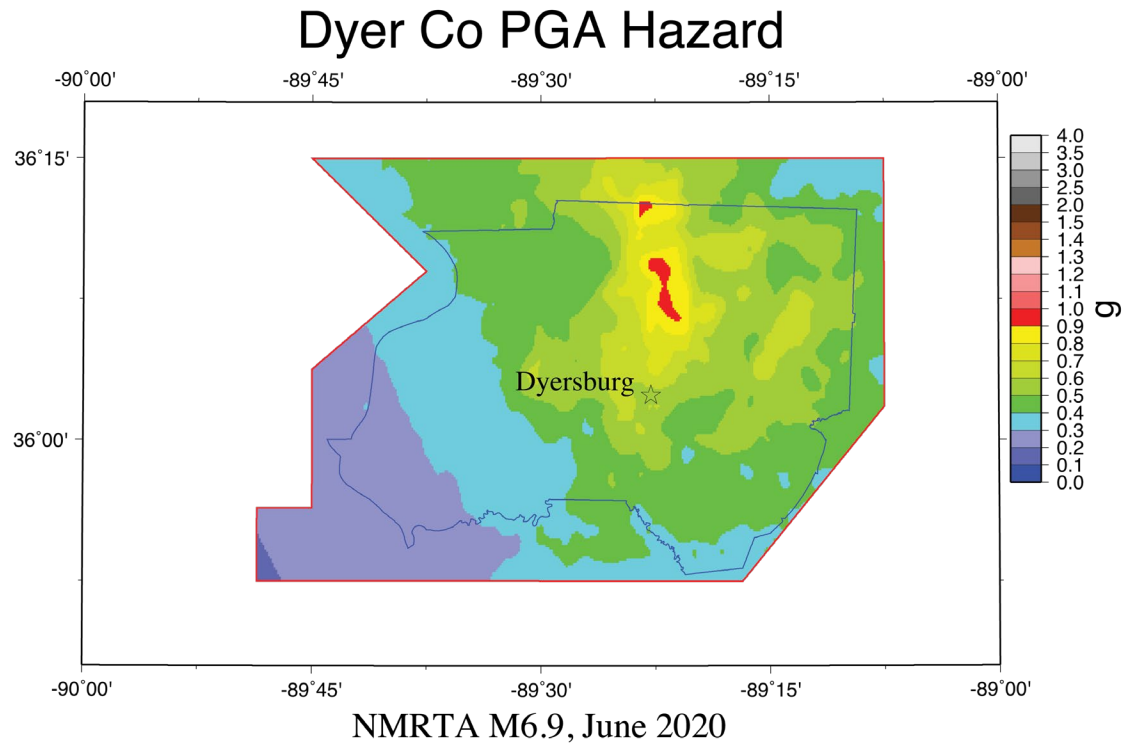
Dyer Co PGA Hazard

NMRTA M6.9, June 2020

Figure 61A: Scenario PGA hazard map for a M6.9 "Dawn" aftershock (alt. 2) on the Reelfoot Thrust (central segment of NMSZ) for Dyer County with the effects of local geology.

Dyer Co 0.2s Hazard

NMRTA M6.9, June 2020

Figure 61B: Scenario 0.2 s hazard map for a M6.9 "Dawn" aftershock (alt. 2) on the Reelfoot Thrust (central segment of NMSZ) for Dyer County with the effects of local geology.

Dyer Co 1.0s Hazard

NMSWA M6.9, June 2020

Figure 60C: Scenario 1.0 s hazard map for a M6.9 "Dawn" aftershock (alt. 2) on the Reelfoot Thrust (central segment of NMSZ) for Dyer County with the effects of local geology.
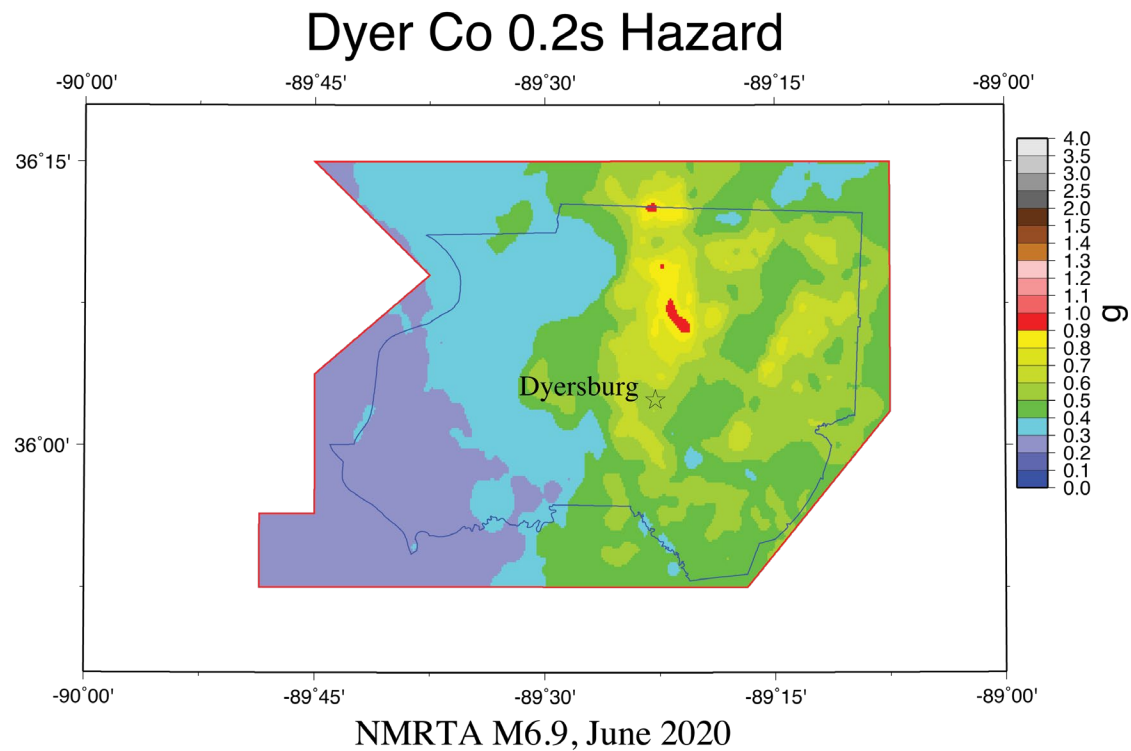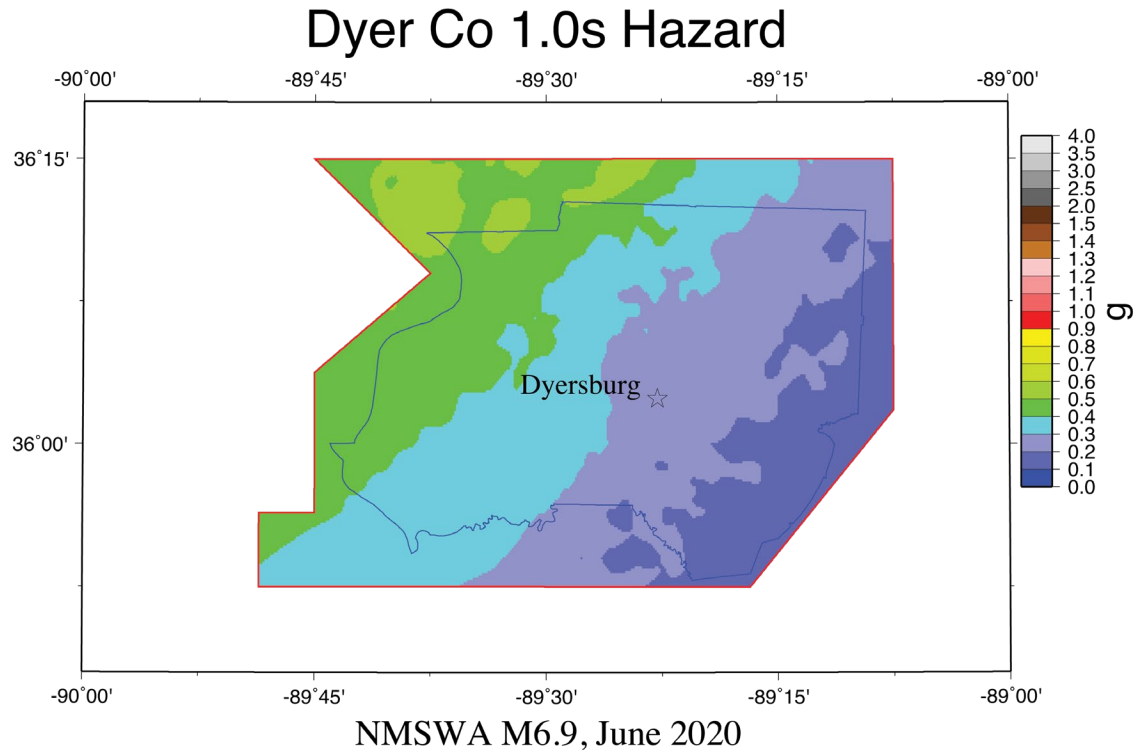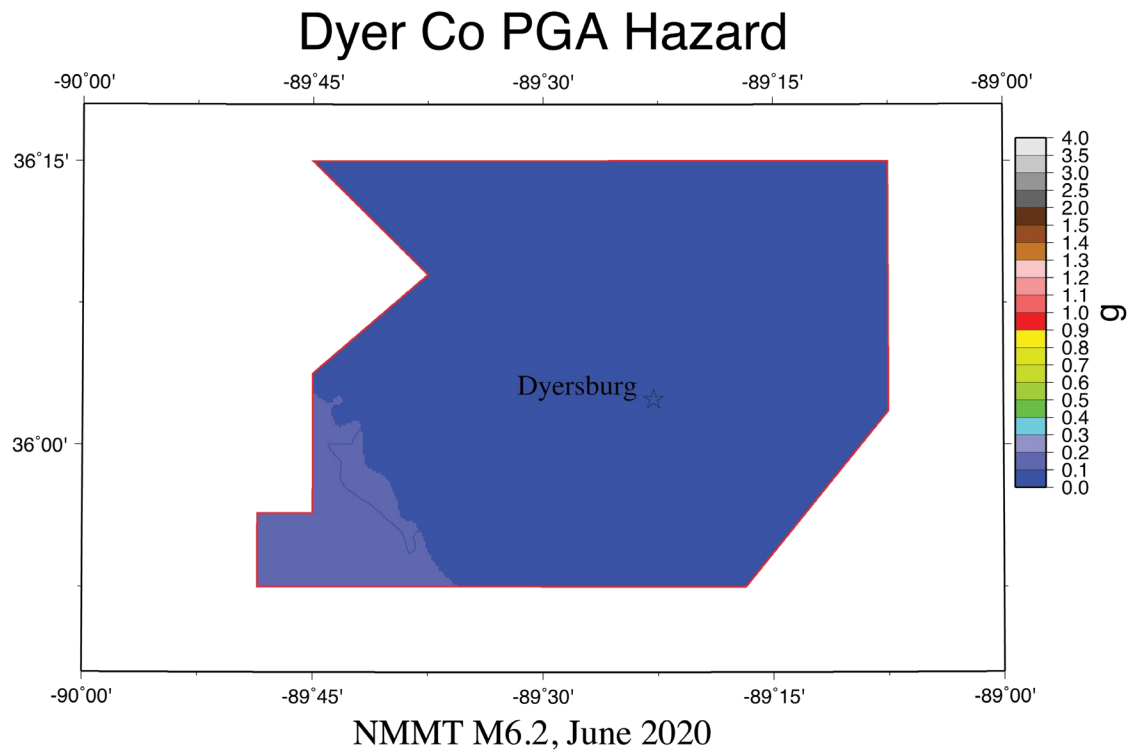
Dyer Co PGA Hazard

NMMT M6.2, June 2020

Figure 62A: Scenario PGA hazard map for a M6.2 on the Cottonwood Grove Fault (1843 Marked Tree – SW segment of NMSZ) for Dye County with the effects of local geology.

Dyer Co 0.2s Hazard

NMMT M6.2, June 2020

Figure 62B: Scenario 0.2 s hazard map for a M6.2 on the Cottonwood Grove Fault (1843 Marked Tree – SW segment of NMSZ) for Dyer County with the effects of local geology.

Dyer Co 1.0s Hazard

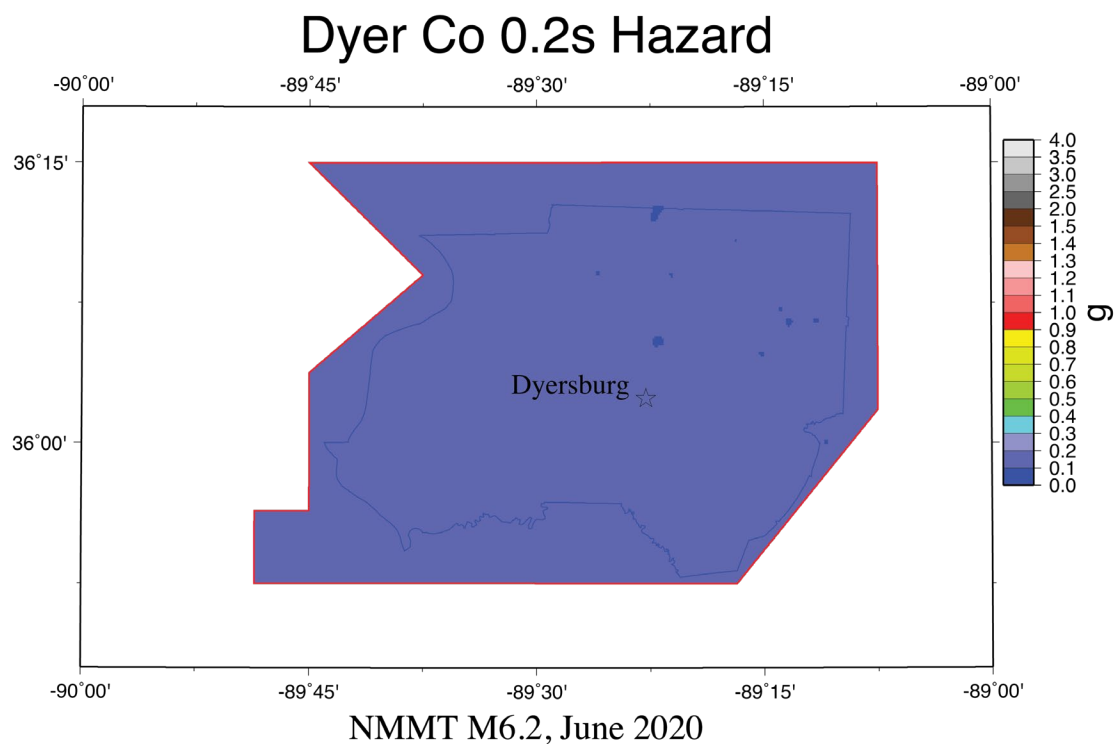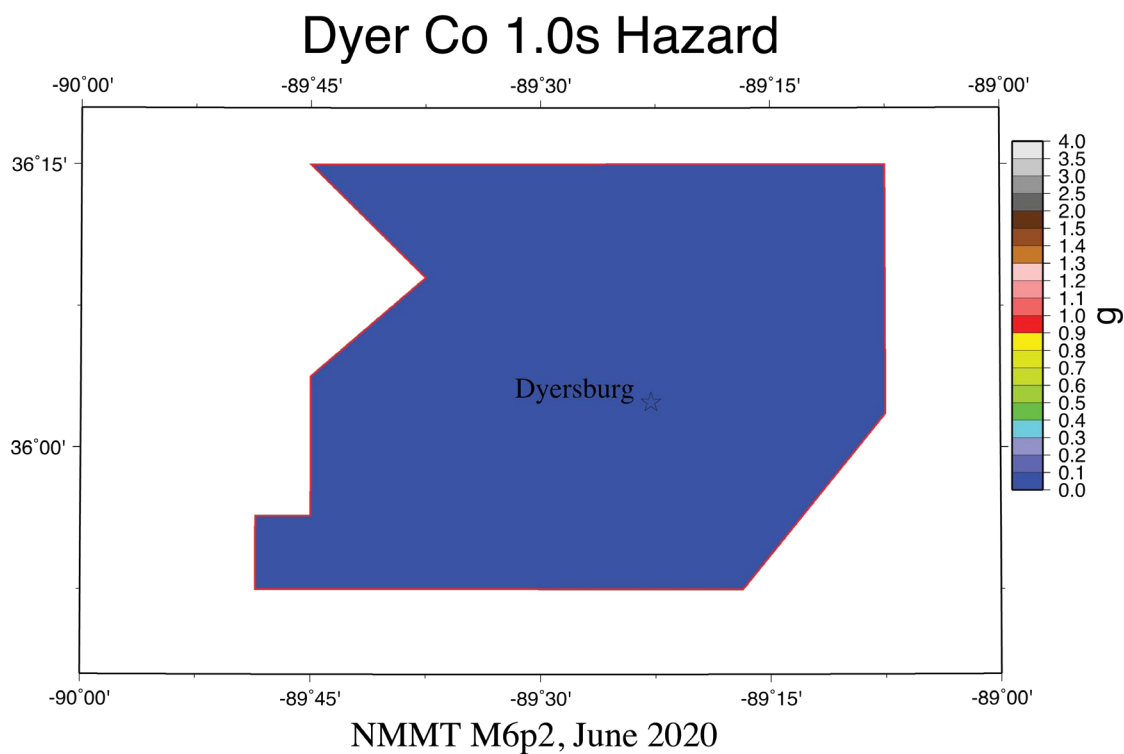NMMT M6p2, June 2020

Figure 62C: Scenario 1.0 s hazard map for a M6.2 on the Cottonwood Grove Fault (1843 Marked Tree – SW segment of NMSZ) for Dyer County with the effects of local geology.

Dyer Co PGA Hazard

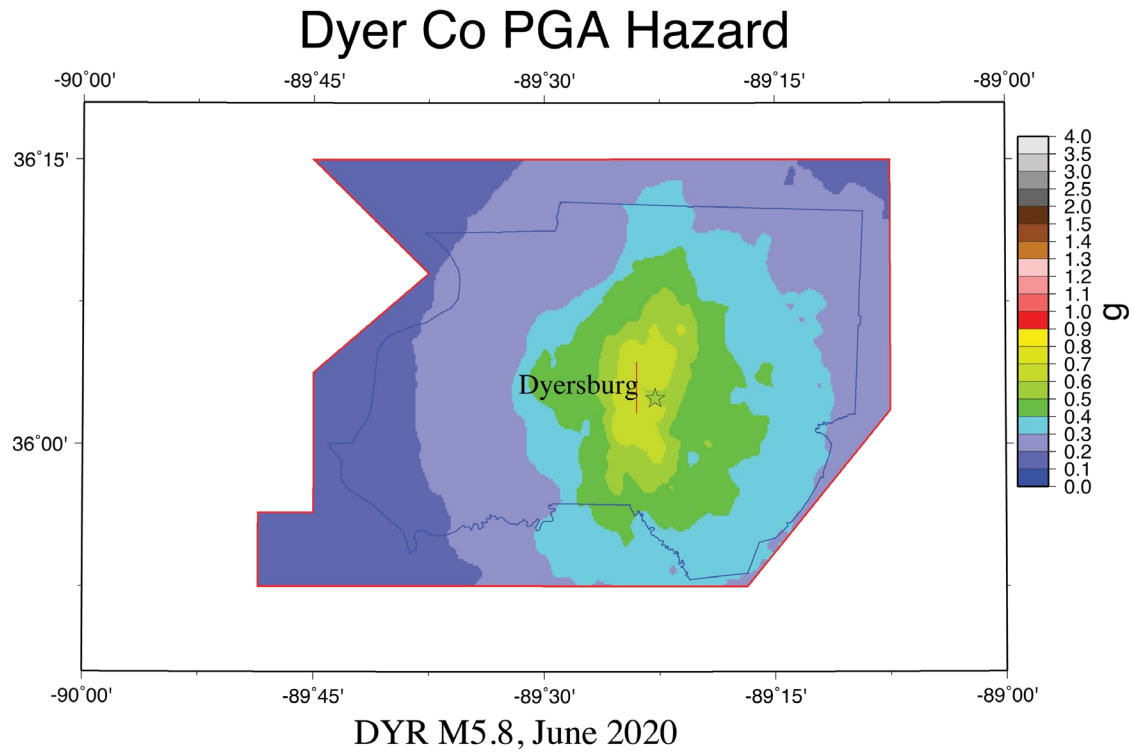DYR M5.8, June 2020

Figure 63A: Scenario PGA hazard map for a M5.8 hypothetical earthquake for Dyer County with the effects of local geology. Red line indicates location of source fault.

Dyer Co 0.2s Hazard

DYR M5.8, June 2020

Figure 63B: Scenario 0.2 s hazard map for a M5.8 hypothetical earthquake for Dyer County with the effects of local geology. Red line indicates location of source fault.
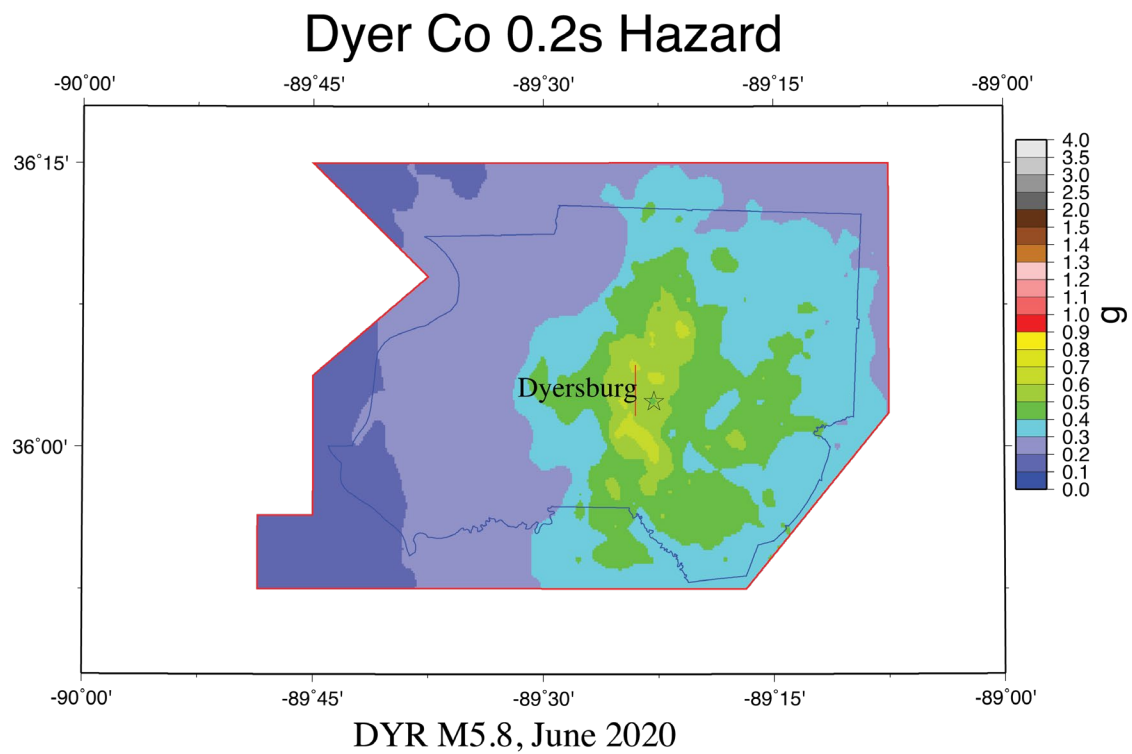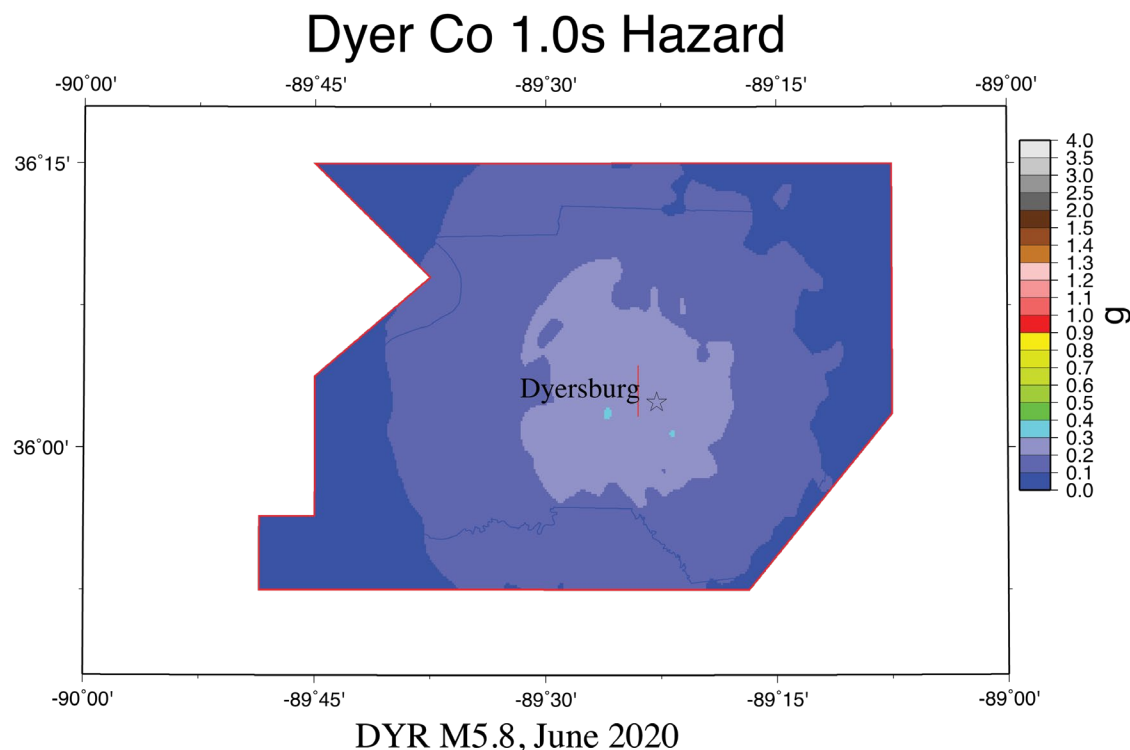
Dyer Co 1.0s Hazard

DYR M5.8, June 2020

Figure 63C: Scenario 1.0 s hazard map for a M5.8 hypothetical earthquake for Dyer County with the effects of local geology. Red line indicates location of source fault.

Liquefaction Hazard Maps

To generate the liquefaction hazard maps for Dyer County, we used the SPT-based liquefaction probability curves (LPCs) recommended above in Figures 34 and 36 for lowlands and non-lowlands, respectively. The LPCs are for Liquefaction Probability Index (LPI) exceeding 5, which is for the manifestation of liquefaction at the surface (moderate to severe liquefaction). These LPC were used to maintain compatibility with the liquefaction maps we generated for Lake County (Cramer et al., 2019). Thus, our liquefaction hazard maps are for the probability of moderate to severe liquefaction. If the LPIish moderate to severe liquefaction LPCs for the effects of non-liquefiable crust of Figures 24 and 25 are used, the liquefaction hazard would be reduced.

Figures 64 - 71 show the two probabilistic and six scenario liquefaction hazard maps derived from the equivalent PGA seismic hazard maps shown above. The probabilistic liquefaction hazard maps show 40 – 70% probability of liquefaction in the lowlands and about 10% in the non-lowlands for 5%-in-50-years, and about 70 – 80% in the lowlands and about 40% in the non-lowlands for 2%-in-50-years probability of liquefaction in Dyer County. The M7.7 scenario on the Reelfoot Thrust liquefaction hazard map shows 20 – 70% probability of liquefaction in the lowlands and 10 – 20% in the non-lowlands. For the M7.5 scenario on the SW arm, the liquefaction hazard map shows 20 – 50% in the lowlands and about 10% in the non-lowlands. The M7.3 scenario on the NE arm shows about 10% or less probability of liquefaction. The

largest aftershock alternatives show 20 – 70% probability of liquefaction in the lowlands and 10 – 20% in the non-lowlands. And the M5.8 hypothetical Dyer County earthquake shows 0 – 40% probability of liquefaction (low). The 1843 and 1895 M6.2 scenarios do not produce any significant liquefaction hazard and are not shown. The liquefaction hazard is high for the near M7 and greater earthquake scenarios.

Figure 64: 5%-in-50-year liquefaction hazard map for moderate to severe liquefaction at the surface (LPI > 5) for Dyer County including the effects of local geology.
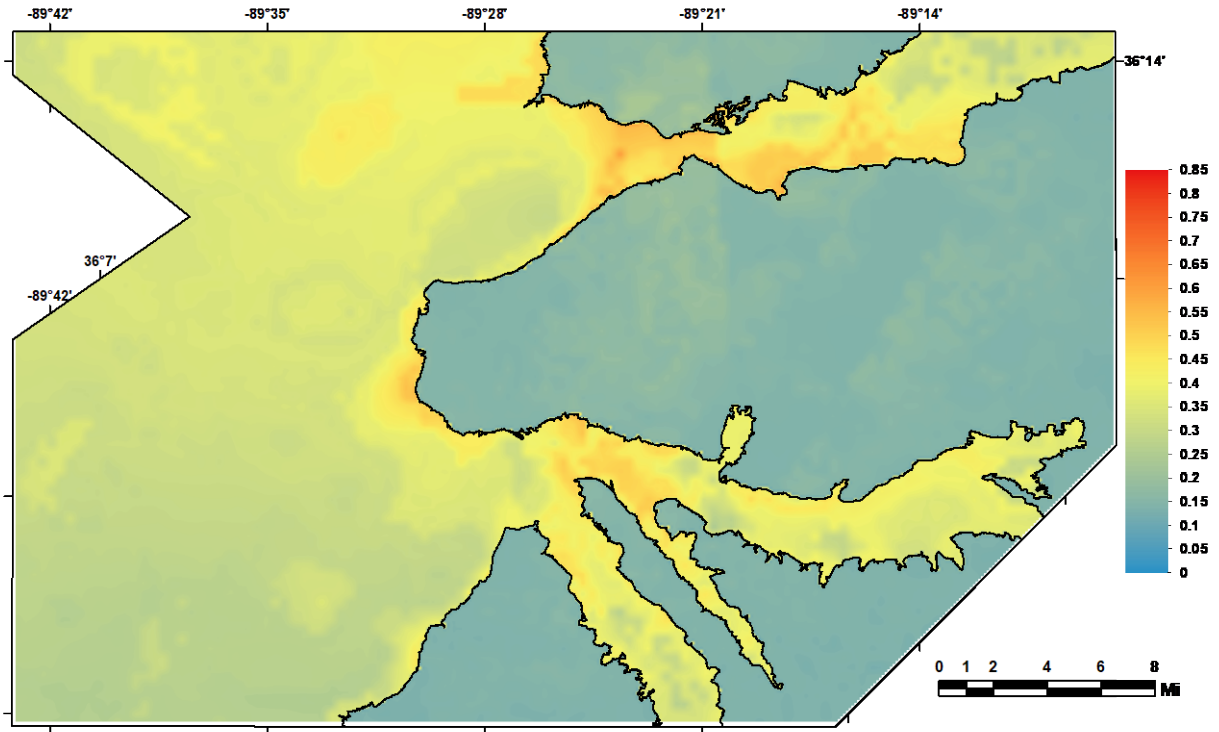
Figure 65: 2%-in-50-year liquefaction hazard map for moderate to severe liquefaction at the surface (LPI > 5) for Dyer County including the effects of local geology.

Figure 66: Scenario liquefaction hazard map for moderate to severe liquefaction at the surface (LPI > 5) for a M7.7 earthquake on the Reelfoot Thrust (central segment of NMSZ).

Figure 67: Scenario liquefaction hazard map for moderate to severe liquefaction at the surface (LPI > 5) for a M7.5 earthquake on the Cottonwood Grove Fault (SW segment of NMSZ).

Figure 68: Scenario liquefaction hazard map for moderate to severe liquefaction at the surface (LPI > 5) for a M7.3 earthquake on the New Madrid North Fault (NE segment of NMSZ).

Figure 69: Scenario liquefaction hazard map for moderate to severe liquefaction (LPI > 5) for a M6.9 "Dawn" aftershock (alt. 1) on the Cottonwood Grove Fault (SW segment of NMSZ).

Figure 70: Scenario liquefaction hazard map for moderate to severe liquefaction (LPI > 5) for a M6.9 "Dawn" aftershock (alt. 2) on the Reelfoot Thrust (central segment of NMSZ).
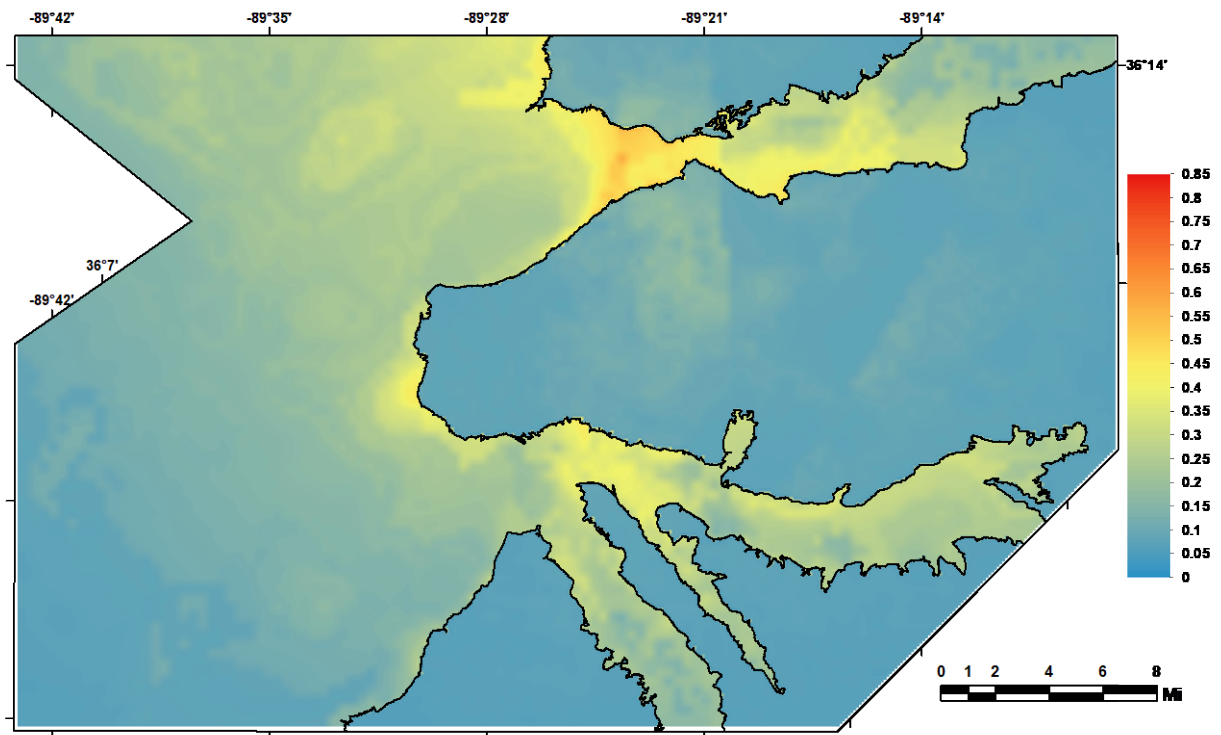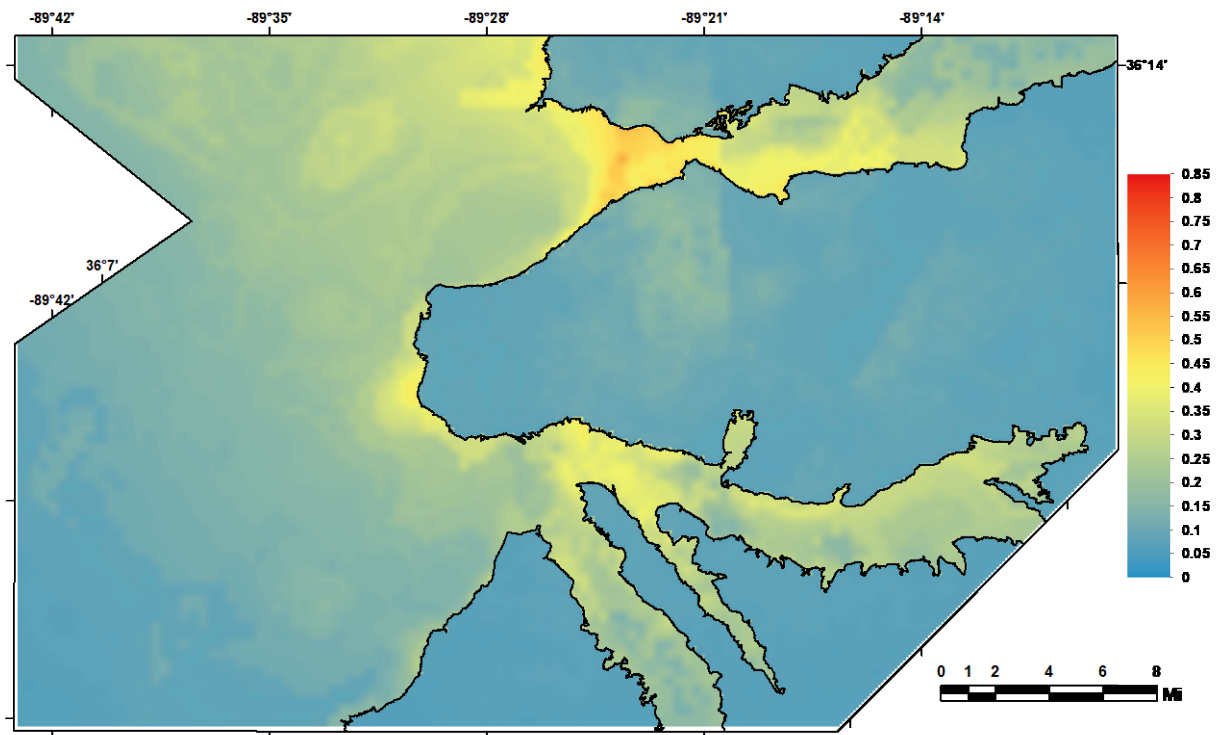
Figure 71: Scenario liquefaction hazard map for moderate to severe liquefaction (LPI > 5) for a M5.8 hypothetical Dyer County earthquake (near Dyersburg).

Conclusions

We have produced seismic and liquefaction hazard maps that include the effects of local geology for Dyer County. The products from this effort include a 3D geology database and model, a geotechnical database and liquefaction probability curves (LPCs), shear-wave velocity (Vs) measurements and models, and probabilistic and scenario hazard maps for Dyer County. The geology model is detailed for the Quaternary sediments down to depths of 300 ft (100 m) and more generalized for the Eocene to Paleozoic formations. Paleozoic limestones form the bedrock of the model. The geotechnical database includes information on water table depths, standard penetration tests (SPT), seismic cone penetration tests (CPT), and shallow Vs information. It was used to generate LPCs based on SPT and Vs measurements to add to the published LPCs based on Mississippi embayment CPT measurements. The liquefaction hazard maps for Dyer County were based on our developed LPCs for lowlands and non-lowlands. Shallow Vs measurements were made at 12 Dyer County sites and added to 3 published Vs profiles from the region. The Vs measurements were used to generate a typical Quaternary Vs profile for non-lowlands areas. Deeper published information from the region developed for

Lake County were used to constrain the Eocene to Paleozoic Vs reference profile used in this study. Seismic and liquefaction hazard maps were generated that include the new geological, geotechnical, and seismological information gathered. The hazard maps are both probabilistic (5% and 2% probability of being exceeded in 50 years) and for seven earthquake scenarios. Seismic hazard maps show a 30-70% decrease in hazard at short periods and a 10-100% increase at long periods compared with USGS NSHMP maps, which are for a uniform standard geology not found in western Tennessee. Liquefaction hazard maps show high hazard in Dyer County for four of the five M7 New Madrid scenarios, and low hazard for the M7.3 NE arm and M5.8 hypothetical Dyer County earthquakes. The 1843 and 1895 M6.2 scenarios do not produce any significant liquefaction hazard due to more distant epicenters and a shorter duration of strong shaking.

References

Chiu, J. M., Johnston, A. C., and Yang, Y. T., 1992. Imaging the active faults of the central New Madrid seismic zone using PANDA array data. *Seismological Research Letters* **63**, p. 375-93

Cox, R.T., Van Arsdale, R.B., Harris, J.B., and Larsen, D., 2001, Neotectonics of the southeastern Reelfoot Rift zone margin, central United States, and implications for regional strain accommodation. *Geology* **29**, p. 419-422.

Cox, R.T., J. Cherryhomes, J. B. Harris, D. Larsen, R. B. Van Arsdale, S. L. Forman, 2006. Paleoseismology of the southeastern Reelfoot rift in western Tennessee and implications for intraplate fault zone evolution. *Tectonics* **25**, p. 1-17.

Cox, R.T., Lumsden, D.N., and Van Arsdale, R.B., 2014. Possible relict meanders of the Pliocene Mississippi River and their implications. *Journal of Geology* **122**, p. 609-622.

Cramer, C.H., J.S. Gomberg, E.S. Schweig, B.A. Waldron, and K. Tucker, 2006. First USGS urban seismic hazard maps predict the effects of soils, *Seism. Res. Lett.* **77**, 23-29.

Cramer, C.H., 2006. Quantifying the uncertainty in site amplification modeling and its effects on site-specific seismic-hazard estimation in the Mississippi embayment and adjacent areas, *Bull. Seism. Soc. Am.* **96**, 2008-2020.

Cramer, C.H., G. Rix, and K. Tucker, 2008. Probabilistic liquefaction hazard maps for Memphis, Tennessee, *Seis. Res. Lett.* **79**, 416-423.

Cramer, C.H., and O.S. Boyd, 2014, Why the New Madrid earthquakes are M7–8 and the Charleston earthquake is ~M7, *Bull. Seism. Soc. Am.* **104**, 2884-2903.

Cramer, C.H., R.B. Van Arsdale, M.S. Dhar, D. Pryne, and J. Paul, 2014. Updating of urban seismic-hazard maps for Memphis and Shelby County, Tennessee: geology and Vs observations, *Seis. Res. Lett.* **85**, 986-996.

Cramer, C.H., G. Patterson, and David Arellano, 2015. Final Technical Report, Updating Liquefaction Probability Curves, Seismic Hazard Model, and Urban Seismic Hazard Maps with Public Outreach for Memphis and Shelby County, Tennessee, USGS grant G14AP00099, October 30, 2015, 42 pp (available at http://earthquake.usgs.gov/research/external/reports/G14AP00099.pdf).

Cramer, C.H., R.A. Bauer, J. Chung, J.D. Rogers, L. Pierce, V. Voigt, B. Michell, D. Gaunt, R.A. Williams, D. Hoffman, G.L. Hempen, P.J. Steckel, O.S. Boyd, C.M. Watkins, K. Tucker, and N. McCallister, 2017. St. Louis area earthquake hazards mapping projects: seismic and liquefaction hazard maps, *Seis. Res. Lett.* **88**, 206-223.

Cramer, C.H., M.S. Dhar, and D. Arellano, 2018a. Update of the urban seismic and liquefaction hazard maps for Memphis and Shelby County, Tennessee: liquefaction probability curves and 2015 hazard maps, *Seis. Res. Lett.* **89**, 688-701.

Cramer, C., R. Van Arsdale, D. Arellano, S. Pezeshk, S. Horton, T. Weathers, N. Nazemi, J.A. Jimenez, H. Tohidi,and L.P. Ogweno, 2018b, Seismic and liquefaction hazard maps for Lake County, northwestern Tennessee, (2018 SE-GSA abstract). Geological society of America Abstracts with Programs 50. 10.1130/abs/2018SE-312570.

Cramer, C., R.B. Van Arsdale, V. Harrison, D. Arellano, S. Pezeshk, S.P. Horton, T. Weathers, N. Nazemi, J. Jimenez, H. Tohidi, and L.P. Ogweno, 2019. Lake County seismic and liquefaction hazard maps, CERI Report, 129 pp.

Cramer, C., R.B. Van Arsdale, D. Arellano, H. Tahidi, S. Pezeshk, S.P. Horton, R. Bhattarai, N. Nazemi, and A. Farhadi, 2020. Lauderdale County seismic and liquefaction hazard maps, CERI Report.

Csontos, R., and Van Arsdale, R., 2008. New Madrid seismic zone fault geometry. *Geosphere* **4**, p. 802-813.

Csontos, R., Van Arsdale, R., Cox, R., and Waldron, B., 2008. The Reelfoot Rift and its impact on Quaternary deformation in the central Mississippi River Valley. *Geosphere* **4**, n. 1, p. 145-158, doi: 10.1130/GES00107.1.

Cupples, W., and Van Arsdale, R., 2014. The Preglacial "Pliocene" Mississippi River. *Journal of Geology* **122**, p. 1-15.

Dhar, M.S., and C.H. Cramer, 2018. Probabilistic seismic and liquefaction hazard analysis of the Mississippi embayment incorporating nonlinear effects, *Seis. Res. Lett.* **89**, 253-267, published online 13 December 2017.

Green, R. A., and J.J. Bommer, 2019. What is the smallest earthquake magnitude that needs to be considered in assessing liquefaction hazard?" *Earthquake Spectra* **35**, 1441–1464.

Greenwood, M.L., Woolery, E.W., Van Arsdale, R.B., Stephenson, W.J., and Patterson, G.L., 2016. Continuity of the Reelfoot Fault across the Cottonwood Grove and Ridgely Faults of the New Madrid Seismic Zone. Seismological Society of America Bulletin, v. 106, p. 2674-2685. doi: 10.1785/0120150290.

Hardeman, W.D., 1966, Geologic Map of Tennessee: West Sheet. Scale 1:250,000.

Ishihara, K.,1985. Stability of natural deposits during earthquakes. In: Proceedings of the 11th International Conference on Soil Mechanics and Foundation Engineering. San Francisco, CA, USA,1, pp.321–376.

Iwasaki, T., Tatsuoka, F., Tokida, K. and Yasuda, S., 1978. A practical method for assessing soil liquefaction potential based on case studies at various sites in Japan, Second International Conference on Mierozonation for Safer Construction Research and Application 1978.

Iwasaki, T., Tokida, K., Tatsuoka, F., Watanabe, S., Yasuda, S., and Sato, H., 1982. Microzonation for soil liquefaction potential using simplified methods. Proceedings 3rd International Conference on Microzonation, Seattle, USA. 1319-1330.

Kelson, K.I., Simpson, G.D., Van Arsdale, R.B., Harris, J.B., Haraden, C.C., and Lettis, W.R., 1996, Multiple Late Holocene earthquakes along the Reelfoot fault, central New Madrid seismic zone. Journal of Geophysical Research, v. 101, n. B-3, p. 6151-6170.

Louie, J.N., 2001. Faster, Better: Shear-Wave Velocity to 100 Meters Depth from Refraction Microtremor Arrays. *Bulletin of the Seismological Society of America* **91**, 347–364.

Lumsden, D.N., Cox, R.T., Van Arsdale, R.B., and Cupples, W.B., 2016, Petrology of Pliocene Mississippi River alluvium: provenance implications. *The Journal of Geology* **124**, 501-517.

Markewich, H. H., Wysocki, D. A., Pavich, M. J., Rutledge, E. M., Millard, H. T., Rich, F. J., et al. (1998). Paleopedology plus TL, 10Be, and 14C dating as tools in stratigraphic and paleoclimatic investigations, Mississippi River valley, U.S.A. *Quaternary International* **51**, 143–167. doi: 10.1016/s1040-6182(97)00041-4.

Martin, R.V., and Van Arsdale R.B., 2017, Stratigraphy and structure of the Eocene Memphis Sand above the eastern margin of the Reelfoot rift in Tennessee, Mississippi, and Arkansas, USA. *Geological Society of America Bulletin* **129**, 970-996.

Maurer, B. W., Green, R. A., and Taylor, O.-D. S., 2015. Moving towards an improved index for assessing liquefaction hazard: Lessons from historical data, *Soils and Foundations* **55**, 778–787.

Odum, W., Hofmann, F., Van Arsdale, R., and Granger, D., New ^{26}Al/^{10}Be and (U-Th)/He constraints on the age of the Upland Complex, central Mississippi River Valley. In review with *Geomorphology*.

Parrish, S., and Van Arsdale, R., 2004, Faulting along the southeastern margin of the Reelfoot rift in northwestern Tennessee revealed in deep seismic reflection profiles. Seismological Research Letters, v. 75, p. 782-791.

Petersen, M. D., M. Moschetti, P. Powers, C. Mueller, K. Haller, A. Frankel, Y. Zeng, S. Rezaeian, S. Harmsen, O. Boyed, N. Field, R. Chen, K. Rukstales, N. Luco, R. Wheeler, R. Williams, and A.

Olsen, 2014, *The 2014 update of the United States national seismic hazard models*, U.S. Geological Survey, OFR 2014-X1091, 255 p.

Rittenour, T.M., Blum, M.D., Goble, R.J., 2007, Fluvial evolution of the lower Mississippi River valley during the last 100 k.y. glacial cycle: response to glaciation and sea-level change. *Geological Society of America Bulletin* **119**, 586-608.

Rodbell, D. T., 1996, Subdivision, subsurface stratigraphy, and estimated age of fluvial-terrace deposits in northwestern Tennessee. U.S. Geologic Survey Bulletin, v. 2128, 24 pp.

Romero, S., and G.J. Rix (2001). Regional variations in near surface shear wave velocity in the Greater Memphis area, *Eng. Geol.* **62**, 137-158.

Saucier, R.T., 1994, Geomorphology and Quaternary Geologic History of the Lower Mississippi Valley: Vicksburg, Mississippi. U.S. Army Engineer Waterways Experiment Station, v. 1, 364 p., and v. 2, map plates.

Schrader, T.P., 2008. Potentiometric surface in the Sparta-Memphis aquifer of the Mississippi embayment, Spring 2007, U.S. Geological Survey Scientific Investigations Map 3014.

Schuler, Juerg, 2008. Joint inversion of surface waves and refracted P and S-wave. Masters Science Thesis, Eidgenossische Technische Hochschule Zurich, Swiss Federal Institute of Technology Zurich.

Seed, H. B., and Idriss, I. M., 1971. ''Simplified procedure for evaluating soil liquefaction potential.'' J. Geotech. Engrg. Div., ASCE, 97(9), 1249–1273.

Stokoe II, K.H., and J.C. Santamarina, 2000. Seismic-wave-based testing in geothechnical engineering, International Conference on Geotechnical and Geological Engineering, GeoEng 2000, 1490–1536.

Toprak, S., and Holzer, T. L., 2003. "Liquefaction potential index: Field assessment." Journal of Geotechnical and Geoenvironmental Engineering, ASCE, 129(4), 315-322.

Tuttle, M. P., Schweig, E. S., Sims, J. D., Lafferty, R. H., Wolf, L. W., and Haynes, M. L., 2002. The earthquake potential of the New Madrid seismic zone, *Bulletin Seismological Society of America* **92**, 2080–2089, doi: 10.1785/01200 10227.

Van Arsdale, R.B., Bresnahan, R.P., McCallister, N.S., and Waldron, B., 2007. The Upland Complex of the central Mississippi River Valley: Its origin, denudation, and possible role in reactivation of the New Madrid seismic zone, in Stein, S., and Mazzotti, S., eds., Continental Intraplate Earthquakes: Science, Hazard, and Policy Issues. Geological Society of America Special Paper 425, p. 177-192.

Van Arsdale, R.B., Arellano, D., Stevens, K.C., Hill, A.A., Lester, J.D., Parks, A.G., Csontos, R.M., Rapino, M.A., Deen, T.S., Woolery, E.W., Harris, J.B., 2012. Geology, Geotechnical Engineering, and Natural Hazards of Memphis, Tennessee, USA. *Environmental & Engineering Geoscience* **18**, 113-158, doi:10.2113/gseegeosci.18.2.113.

Weathers, T., and Van Arsdale, R. 2019, Lake County Tennessee: in the Heart of the New Madrid seismic zone. *Frontiers in Earth Science* **7**, 1-20.

Woolery, E.W., Z. Wang, N.S. Carpenter, R. Street, and C. Brengman, 2016. The Central United States Seismic Observatory: site characterization, instrumentation, and recordings, *Seis. Res. Lett.* **87**, 215-228.

Appendices (separate files)